Surface Science Reports 7 (1987) 211–385
North-Holland, Amsterdam

THE INTERACTION OF WATER WITH SOLID SURFACES: FUNDAMENTAL ASPECTS

Patricia A. THIEL *

Department of Chemistry and Ames Laboratory, Iowa State University, Ames, IA 50011, USA

and

Theodore E. MADEY

Surface Science Division, National Bureau of Standards, Gaithersburg, MD 20899, USA

Manuscript received in final form 29 April 1987

The purpose of this review is to compare and discuss recent experimental and theoretical results in the field of H_2O–solid interactions. We emphasize studies of low (submonolayer) coverages of water on well-characterized, single-crystal surfaces of metals, semiconductors and oxides. We discuss the factors which influence dissociative versus associative adsorption pathways When H_2O adsorbs molecularly, it tends to form three-dimensional hydrogen-bonded clusters, even at fractional monolayer coverages, because the strength of the attractive interaction between two molecules is comparable to that of the substrate–H_2O bond The template effect of the substrate is important in determining both the local orientation and long-range order of H_2O molecules in these clusters. The influence of surface additive atoms (e.g., O, Br, Na, K) and also surface imperfections (e.g. steps and defects) on the surface structure and chemistry of H_2O is examined in detail. Some results on single-crystal substrates are compared with earlier measurements of H_2O adsorption on high-area materials.

* National Science Foundation Presidential Young Investigator (1985–1989), Alfred P. Sloan Research Fellow (1984–1986), and Camille and Henry Dreyfus Teacher–Scholar (1986–1990)

0167-5729/87/$61.25 © Elsevier Science Publishers B.V.
(North-Holland Physics Publishing Division)

Contents

1. Introduction

> *"Water is not only rare, not only infinitely precious, it is peculiar, with many oddities in its physical and chemical make-up It is out of this unique nature of water that life originated The ocean is life"*
> *– Jacques-Yves Cousteau [1]*

Water plays a pervasive role in our world, and it has fascinated great scientists from Leonardo da Vinci [2] to Linus Pauling [3]. Consequently, the interaction of water with surfaces is a topic of interest and research in a surprisingly wide variety of scientific disciplines. When one peruses the literature, one finds publications on the subject from a spectrum of fields which includes meteorology, geology, electrochemistry, solar energy conversion, corrosion chemistry, heterogeneous catalysis, and physical chemistry. Meteorologists are interested in the mechanism of ice or water nucleation at surfaces, since this mechanism is exploited whenever cloud-seeding is used to bring about precipitation (e.g. [4,5]). Geologists do a great deal of work related to this topic, since they investigate the forces which produce particular arrangements of water molecules in ice, and the spectroscopic means by which these arrangements can be differentiated, as a means of understanding glacial history (e.g. [6,7]). Electrochemists, of course, postulate the existence of a "double layer" of water molecules near a metal electrode surface. Its characteristics are sufficiently different from those of bulk water that capacitance in, and transport across, this layer plays a key role in electrochemical reactions [8–11]. The dissociation of water at surfaces is important in corrosion and passivation chemistry (e.g. [12,13]), as well as in solar energy conversion processes which split water [14–17].

Numerous heterogeneous catalytic reactions, such as Fischer–Tropsch synthesis of hydrocarbons, involve H_2O as a reactant or product. Even in reactions for which this is not true, traces of H_2O can greatly change the selectivity of the reaction, as in the catalytic hydrogenation of benzene over ruthenium metal [18]. Metal catalysts are also used in the large-scale extraction of heavy water from H_2O, which is then used in nuclear reactors [19]. These are only a few examples of the importance of H_2O at solid catalyst surfaces.

Finally, the structure of small water clusters, and the nature of hydrogen bonding between H_2O molecules, has long been of fundamental interest to physical chemists. The classical matrix isolation experiments of Van Thiel, Becker and Pimentel in 1957 [20] stimulated theoretical efforts to model small groups of H_2O molecules, and also stimulated interest in the infrared absorption coefficient of hydrogen-bonded OH groups. These experiments provided early spectroscopic and structural data about small, neutral water clusters; they illustrated the ability of the matrix isolation experiment to isolate a relatively simple chemical group and study it in detail. In this respect it has

not been surpassed by other techniques until recently, to the authors' knowledge. The recent advance comes with the study of water clusters isolated on well-defined surfaces under ultrahigh vacuum, in which the battery of surface-sensitive spectroscopies available in this area of surface science has begun to yield a wealth of information about the topic.

The purpose of this review, then, is to summarize and generalize the present state of knowledge in the field of water–surface interactions, with *particular* emphasis upon recent studies of single-crystal surfaces of metals, semiconductors, and oxides. We examine the role of substrate composition and structure in determining whether or not adsorption is accompanied by dissociation. When associative (molecular) adsorption takes place, the surface structure is critical in determining the long- and short-range structure of the hydrogen-bonded H_2O aggregates which form. Intermolecular hydrogen bonding can be as important in these systems as the (relatively weak) substrate–water bonds. The influence of surface additives (e.g. O, Br, Na, K) and surface imperfections (e.g. steps and defects) on the surface structure and chemistry of adsorbed water is also discussed.

In closing, we wish to draw the reader's attention to several excellent reviews which concern closely related topics. Norton reviews catalytic hydrogen oxidation over well-characterized metals [21], and Zettlemoyer et al. discuss the thermodynamics of water adsorption at surfaces of high-area solids "in some depth" (their own words) [22]. Other articles review hydroxylation and water adsorption at silica, alumina, and other oxide surfaces. Among these, Knözinger discusses hydrogen bonding in adsorbed layers [23]. Hair [24], Little [25], and Kiselev and Lygin [26] summarize earlier vibrational data for hydroxyl groups and water at surfaces. The text by Bockris and Reddy [9] is a useful introduction to the chemistry and structure of water at electrode surfaces. Together, these articles provide an excellent body of background and supplementary data for the present discussion. This review offers a fresh contribution because it critically examines recent research in water–surface chemistry. The current use of single crystals and careful control of surface composition, combined with the common practice of using several spectroscopies simultaneously, provides far more detailed data about water–surface chemistry *on the molecular scale* than was available even ten years ago. We also compare these recent data with earlier work on more "realistic" and less well-defined surfaces.

2. Surface bonding of water and its dissociation products: an overview

2.1. Introduction

The properties of H_2O which govern its interaction with a surface can be understood qualitatively from an examination of the properties of H_2O in the

gas, liquid and solid phases. Chemical bonding in the isolated molecule is often thought of in terms of a simple Lewis dot construction, where oxygen contributes six valence electrons and each hydrogen contributes one:

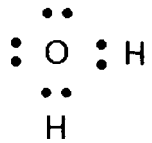

The four valence electrons associated only with the oxygen atom represent the two "lone pairs", and the four valence electrons shared by the hydrogen and oxygen atoms represent the intramolecular bonds. The two lone pairs enable the oxygen to coordinate to other molecules by acting as an electron donor. On a surface, the lone pair density interacts both with the substrate and neighbouring molecules.

Adsorbed H_2O is unique among small molecular adsorbates in that attractive lateral interactions (hydrogen bonds) can be comparable in strength to the molecule–substrate interactions. The molecule–substrate bond can often be understood in terms of a simple Lewis acid–base interaction, with H_2O in the role of the electron donor (Lewis base) and the substrate in the role of the electron acceptor (Lewis acid).

In the following paragraphs we examine the electronic and geometric properties of H_2O which account for its unique chemistry. We introduce many concepts which are used at later points in the text.

2.2. Molecular water

2.2.1 Molecular water: the isolated molecule

The fundamental physical properties of the isolated H_2O molecule (its bond length, hard sphere radius, bond angle, moments of inertia, dipole moment, polarizability, and bond dissociation energy) are shown in table 1. We give a cursory summary of its properties here, but the reader who wishes to obtain a more thorough description is referred to the discussion by Eisenberg and Kauzmann [27].

The isolated water molecule possesses nine degrees of freedom, three of which are translational, three of which are rotational, and three of which are vibrational. The three normal modes of vibration are shown in fig. 1, together with the symmetry of each vibration within the C_{2v} point group [28] and the frequency measured for each $v = 0$ to $v = 1$ transition within the gas-phase molecule [27]. These three vibrational modes are called the symmetric stretch [ν_{sym}(OH)], the asymmetric stretch [ν_{asym}(OH)], and the scissors (also called the bend or the intramolecular deformation) [δ(HOH)].

Table 1
Physical properties of the isolated H_2O molecule

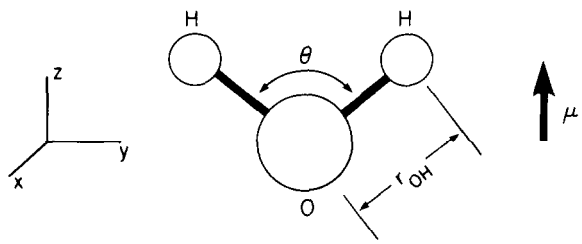

Parameter	Value	Ref
HOH bond angle, θ_{HOH}	104 5°	[27]
OH bond length, r_{OH}	0 957 Å	[27]
Van der Waals (hard-sphere) radius, r_{VdW}	1 45 Å	[28]
Moments of inertia, I		
I_y	$1\ 0220\times10^{-40}$ g^{-1} cm^{-2}	[27]
I_z	$1\ 9187\times10^{-40}$ g^{-1} cm^{-2}	[27]
I_x	$2\ 9376\times10^{-40}$ g^{-1} cm^{-2}	[27]
Dipole moment, μ_z	$1\ 83\times10^{-18}$ esu cm	[27]
Mean polarizability, J	$1\ 444\times10^{-24}$ cm^3	[27]
O–H bond dissociation energy, D_0	498 kJ/mol (5 18 eV)	[28]

The dipole moment of the molecule is a vector which points from the oxygen end toward the hydrogen atoms. This direction is consistent with detailed calculations of charge density distributions for H_2O, examples of which are reproduced in figs. 2 and 3. Such calculations reveal high electron density around the oxygen atom. The value of the dipole moment of water, 1.83×10^{-18} esu cm, is large relative to that of other small molecules commonly studied by surface chemists, such as CO ($\mu = 1.0\times10^{-19}$ esu cm) or NO ($\mu = 1.6\times10^{-19}$ esu cm) [31]. The distribution of charge density is not only manifest in the charge density plots of figs. 2 and 3, but also in the electrostatic potential distribution about the water molecule, shown in fig. 4. There is a strong negative potential about the oxygen atom, in the region of the lone pairs (vide infra).

The binding in H_2O results from interaction of electrons in the $2s^2$ and $2p^4$ atomic orbitals of oxygen with electrons in the $1s^1$ atomic orbitals of the hydrogen atoms. The four electrons which do not participate in the two single O–H bonds are called the "oxygen lone pairs". The linear combinations of the atomic orbitals (LCAO's) which contribute most importantly to the respective molecular orbitals (MO's) of water are listed in table 2, together with the symmetry notation of the resultant MO and a sketch of the main atomic

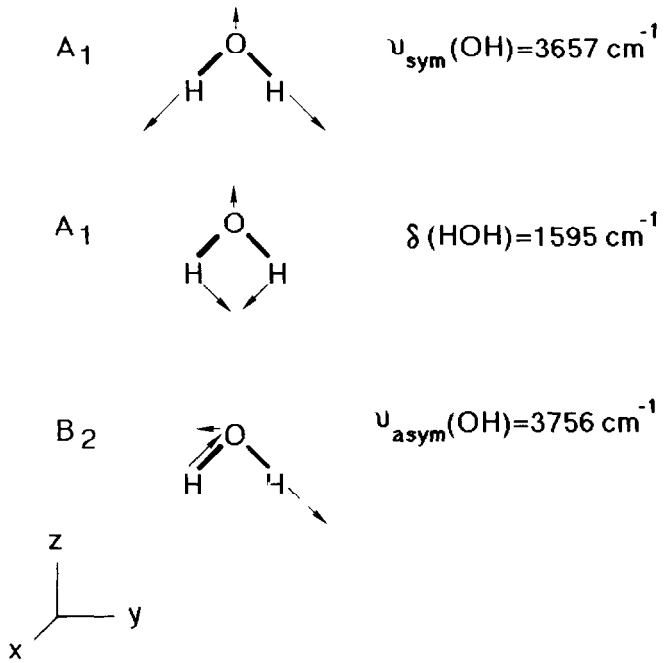

Fig. 1 The three normal modes of vibration of an isolated H_2O molecule The symmetry of each vibration within the C_{2v} point group is also given [28], together with the frequency measured for each fundamental transition [27] The symmetry elements of the C_{2v} point group are defined for the molecule by the coordinate system shown in the lower left corner. For example, the mirror plane $\sigma_v(yz)$ [28] lies within the H–O–H plane

components. Molecular orbitals obtained by solving the Hartree–Fock equations are classified by symmetry and are known as canonical MO's. They are also referred to as delocalized MO's since they must span the entire molecule in order to satisfy symmetry constraints. A set of canonical MO's are shown in fig. 5, after Jorgensen and Salem [34], and their energies are depicted in fig. 6. There is some confusion in the literature about which of these orbitals are bonding, and which are the lone pairs. As reviewed by Levine [35], the $1b_1$ orbital is clearly nonbonding, whereas the $1b_2$ is clearly a bonding orbital. The $2a_1$ and $3a_1$, however, contain both bonding and nonbonding character. It is therefore not possible to say that two of the canonical orbitals represent the lone pairs while two others are clearly bonding orbitals. The $3a_1$ appears to have somewhat more lone-pair character than the $2a_1$ [35] and it is common to refer to the electron density arising from the $1b_1$ and $3a_1$ as the lone pairs, although this is not completely correct since it ignores the mixed character of the $2a_1$.

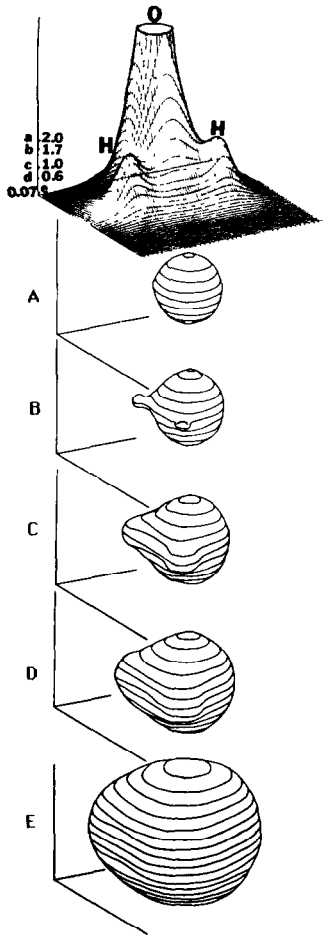

Fig. 2. Comparison of the cross-sectional diagram for the total electron density of water in the molecular plane with five three-dimensional shape plots (a)–(e) constructed from it. The contour surfaces correspond to 2.0, 1.7, 1 0, 0.6 and 0.07 e/(Å)^3, respectively It should be noted that the shape plots are rotated 90° with respect to the density diagram at the top From Smith [29].

The electronic properties of the water molecule are reflected in the experimental photoelectron spectrum, shown in fig. 7 [32]. In the photoelectron experiment, radiation is used to bring about ejection of an electron from a solid or a gas-phase molecule with a kinetic energy which reflects the binding energy of the electron. According to Koopman's theorem [36], the valence electron binding energies may be approximated by the eigenvalues of the canonical MO's of the Hartree–Fock wavefunction. In the free molecule, the

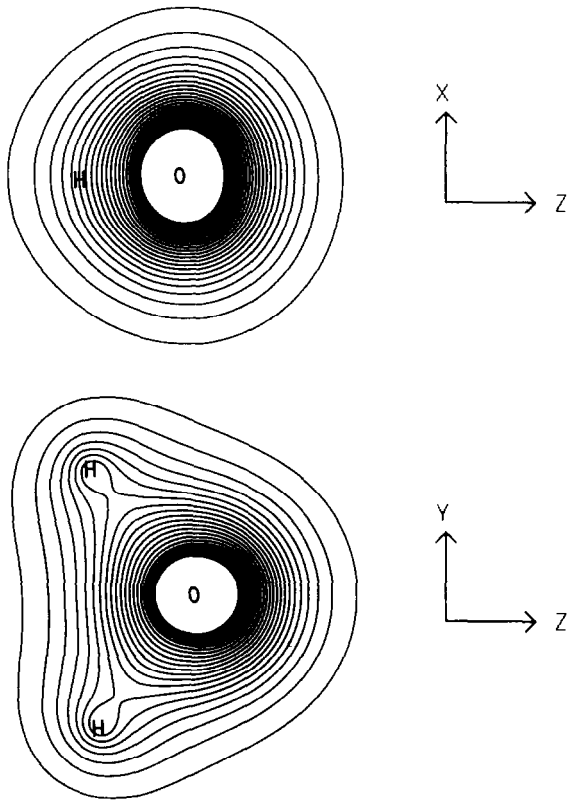

Fig. 3 Contours of the total electron density of water at the experimental equilibrium geometry The electron density is obtained from a Hartree–Fock wavefunction using a double-zeta plus polarization (DZP) basis set. The outermost contour value is 0 05 e/bohr^3 and the increment between successive contours is 0 05 e/bohr^3 Taken from Stevens [30]

three peaks seen in UPS spectra (cf. fig. 7) with He I radiation ($h\nu = 21.2$ eV) correspond to ejection of electrons from the $1b_2$, $3a_1$ and $1b_1$ orbitals, whose ionization potentials are listed in table 2 [32]. The calculated orbital energies are in good agreement with the ionization potentials determined from UPS. In the free molecule, ionization of the highest-energy electron, which comes from the $1b_1$ nonbonding orbital, causes a small decrease both in bending and stretching frequencies, and an increase in the HOH bond angle of $\sim 5°$ [32,37]. In other words, perturbation of the internal bonds of H_2O is small when an electron is removed from this nonbonding orbital. On the other hand, removal of an electron from the strongly bonding $1b_2$ orbital may result in dissociation to H and OH^+ [32,37]. A large change in molecular geometry comes upon ionization from the intermediate $3a_1$ orbital, since the electrons in

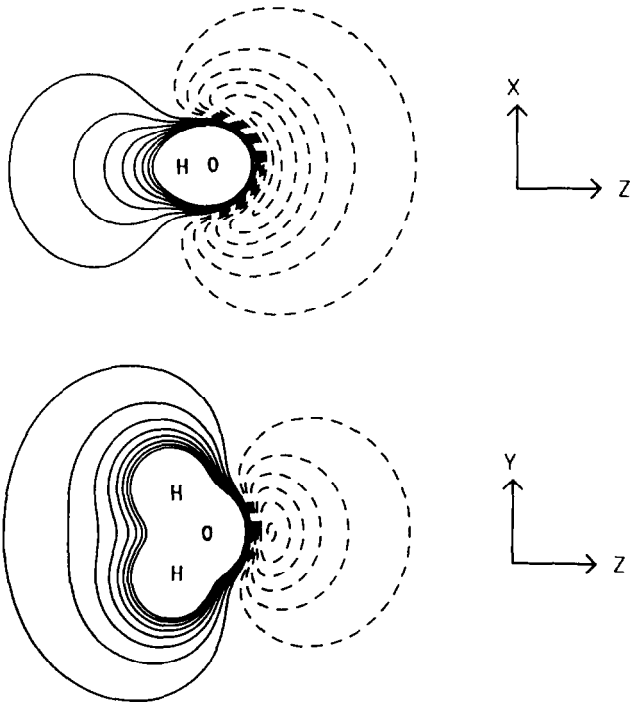

Fig. 4 Contours of the electrostatic potential of the water molecule at the experimental equilibrium geometry. The potential is obtained from a Hartree–Fock wavefunction using a double-zeta plus polarization (DZP) basis set. The dashed contours represent regions of negative potential and the solid contours represent regions of positive potential (as seen by a unit positive charge) The outermost contour value of the positive region is +42 kJ/mol, and the outermost value of the negative region is −42 kJ/mol The increment between successive contours is ±42 kJ/mol in the positive and negative regions, respectively. Taken from Stevens [30]

this orbital serve to screen the two protons from one another. Complete removal of an electron from this orbital causes the HOH bond angle to increase to 180° (which optimizes the bonding geometry of the $1b_2$ orbital) with a concomitant decrease in the bending mode [δ(HOH)] frequency to 975 cm^{-1}. There is no observable change in the O–H stretching vibration frequency [32,37]. These results are useful in the present discussion, since the cases where electrons are completely removed from H_2O orbitals (in photoionization) may help to understand the effects of partial removal of electrons from the same orbitals when H_2O interacts with a surface.

These canonical orbitals can also be recast in terms of localized orbitals [38], which provides a more easily-grasped picture. This leads to the common model of water in which two equivalent MO's exist for the OH bonds and two exist for the lone pairs, according to the known symmetry of the molecule [39].

Table 2
Symmetry-adopted linear combinations of atomic orbitals of H_2O

Orbital	Atomic equivalent	Description	Energy (eV)	Depiction
$(1a_1)^2$	$(1s_O)^2$	Nonbonding (core level)	539 7 (559.6)	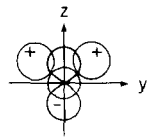
$(2a_1)^2$	$[c_1(2s_O)+c_2(2p_{z,O})+c_3(1s_{H_A}+1s_{H_B})]^2$	Partly bonding and partly nonbonding (lone pair)	32 2 (36 8)	
$(1b_2)^2$	$[c_4(1s_{H_A}-1s_{H_B})+c_5(2p_{y,O})]^2$	Bonding	18 5 (19 5)	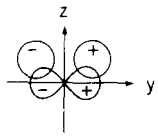
$(3a_1)^2$	$[c_6(1s_{H_A}+1s_{H_B})+c_7(2s_O)+c_8(2p_{z,O})]^2$	Partly bonding and partly nonbonding (lone pair)	14 7 (15 9)	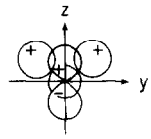
$(1b_1)^2$	$(2p_{x,O})^2$	Nonbonding (lone pair)	12 6 (13 9)	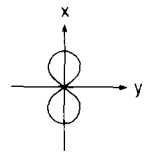

Only those atomic orbitals which contribute significantly to the resultant MO are listed The energies of the orbitals are based on ionization potentials measured with photoelectron spectroscopy [32]. The numbers given in parentheses show the eigenvalues of these molecular orbitals near the Hartree–Fock limit, taken from Dupuis [33].

In water, two equivalent localized orbitals can be formed along the OH bonds by taking a linear combination of the $1b_2$, $2a_1$ and $3a_1$ MO's, while the nonbonding orbitals forming the lone pairs (below the *y*-axis and in the *xz* plane) are made up of contributions from the $1b_1$, $3a_1$ and $2a_1$ orbitals, in that order of importance [35]. The angle between the oxygen lone pairs is calculated to be 114° [40]. The orbital transformation leaves the total energy and density invariant, but the localized orbitals are no longer eigenfunctions of the Hartree–Fock Hamiltonian. The usual picture of bonding in the water molecule, in terms of such localized MO's , is shown qualitatively in fig. 8. The resultant shape of the molecule is described by four doubly-occupied orbitals arranged quasi-tetrahedrally around the oxygen atom, slightly distorted from the ideal tetrahedral angle of 109.5°. The two OH bonds are in the *yz* plane,

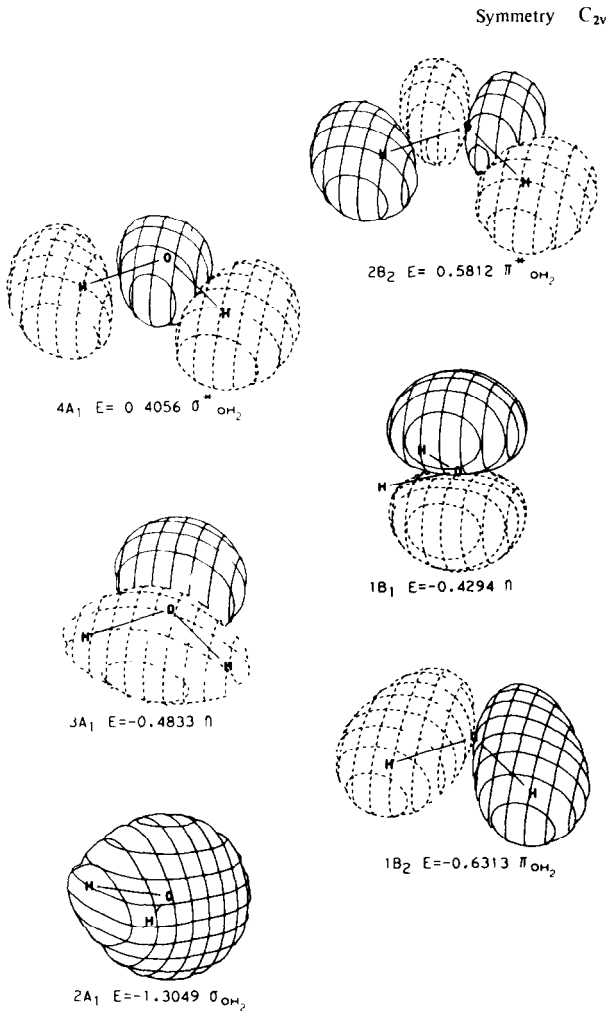

Fig 5 Delocalized molecular orbitals of H_2O, from Jorgensen and Salem [34].

whereas the two lone pairs are in the *xz* plane (figs. 2 and 3). In the language of hybridization, the orbitals surrounding the oxygen atom are approximately sp^3 hybridized. Distortions from the ideal tetrahedral geometry arise because the lone pairs have somewhat more s-character and the bonding pairs have somewhat more p-character [35].

We note that the canonical orbitals are most useful for describing the ionization potentials of the molecule (e.g. in UPS), whereas the localized orbital picture is more compatible with the classical Lewis structure which is

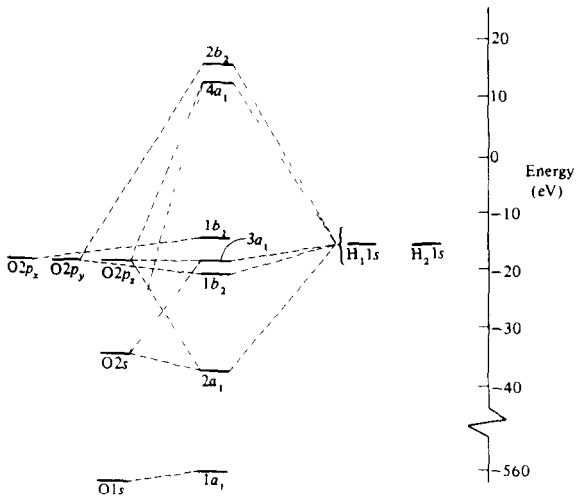

Fig. 6 Molecular orbital energy level diagram of H_2O, from Levine [35]

used to discuss chemical bonding to other molecules. In terms of the total energy or the total charge density distribution of the free water molecule, these two approaches are exactly equivalent; one approach is not "better" than the other for describing physical properties until a perturbation to the free

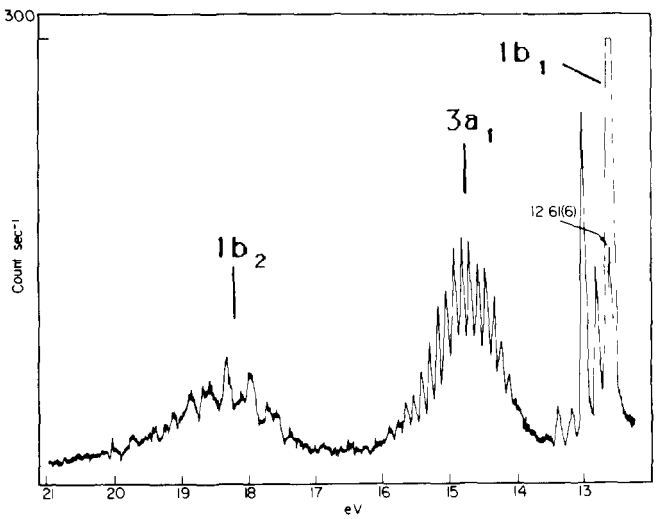

Fig 7 Photoelectron spectrum of gas-phase H_2O, using He I radiation Taken from Turner et al [32]. (Copyright John Wiley and Sons, Ltd., 1970. Reprinted by permission of John Wiley and Sons, Ltd)

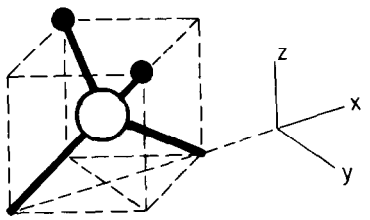

Fig. 8 Schematic representation of the localized molecular orbitals of H_2O. The filled circles represent the hydrogen atoms and the open circle represents the oxygen atom

molecule is considered. In this article, we shall mainly use the localized orbital picture since the perturbation we are addressing is chemical bonding of H_2O to surfaces and other species.

2.2.2. Molecular water: intermolecular hydrogen bonding

A hydrogen bond is formed whenever an AH acidic group engages in a bond of the form A–H · · · B, where the basic group B presents an additional attractive potential to the proton. This so-called "double well" situation is shown schematically in fig. 9, after Novak [41]. The main components of the hydrogen bond are electrostatic forces, charge transfer, covalent forces, dispersion forces, and exchange repulsion [42]. In the case of two hydrogen-bonded water molecules, the acidic group is an OH fragment of one molecule and the basic group is an oxygen lone pair of the other molecule.

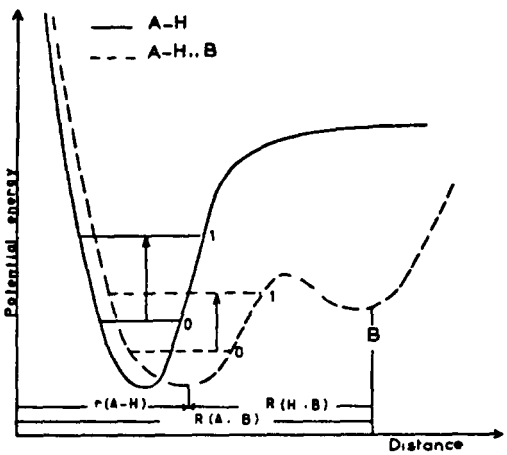

Fig 9. Qualitative potential curves for the free (———) and hydrogen-bonded (- - - - -) AH group, from Novak [41]

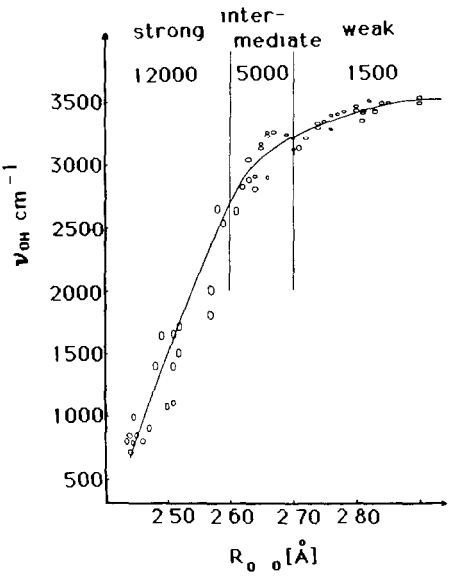

Fig 10. Relation between OH stretching frequency and O–O separation in hydrogen-bonded (O–H · · O) systems, from Novak [41]. The slope ($\Delta\nu/\Delta R$) of a straight line fit to each region is given in units of cm^{-1}/Å. The full-width at half-maximum of ν(OH) increases from ~ 10 cm^{-1} for weak hydrogen bonds, to 10^2 cm^{-1} for intermediate bonds, to 10^3 cm^{-1} for strong O–H O bonds [41]

Hydrogen bonding causes a broadening of the potential energy function near the minimum, as illustrated in fig. 9. An important consequence is that the vibrational energy levels move closer together and, in vibrational spectra, the transitions associated with the A–H stretch shift to lower frequencies. At the same time, it is observed that the distance between the A and B nuclei decreases. In the case of the O–H · · · O bond, in fact, there appears to be a strong experimental correlation between the O–O separation and the frequency of the OH stretch. This has been documented by Novak, and is reproduced in fig. 10 [41]. Hydrogen bonding also causes the FWHM of ν(OH) to broaden; Novak states that weak hydrogen bonds (defined by fig. 10) are associated with full-widths of ~ 10 cm^{-1}; intermediate bonds cause the width to increase to ~ 100 cm^{-1}; and strong O–H · · · O bonds exhibit widths on the order of ~ 1000 cm^{-1} [41].

The strength of the hydrogen bond in ice and water is generally estimated at 15 to 25 kJ per mole of hydrogen bonds, based upon experimental data [27]. The O–H · · · O bonds in ice are approximately linear and are arranged in groups of four (tetrahedrally, or nearly so) about the oxygen atoms [27,43]. This is illustrated in fig. 11 [44]. This is often rationalized as resulting from the

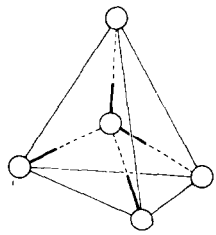

Fig 11 Arrangement of water molecules in ice The open circles represent oxygen atoms, the heavy lines represent O–H bonds, and the dashed lines symbolize hydrogen bonds. From Whalley [44].

classic tetrahedral arrangement around the oxygen atom of lone pair electron donor orbitals and OH bond electron acceptors which was introduced in fig. 8. Diercksen reports that hydrogen bonding causes only small changes in the total charge density contours of H_2O [45], i.e. the contours shown for the free molecule in figs. 2 and 3 still apply. In water, Stillinger [46] has shown that the structure of fig. 11 is not preserved. While hydrogen bonding is still present, the H_2O molecules in the liquid phase tend to form long strings in which each molecule, on average, participates in only two (rather than four) hydrogen bonds [46].

The most common crystalline forms of ice, Ih and Ic, have oxygen atoms situated at sites of C_{3v} and T_d symmetry, respectively. Ice Ih is the only naturally-occurring form, and has a hexagonal unit cell: the Ic form has a cubic unit cell. (The cubic form is obtained by warming a metastable vitreous or crystalline phase to ~ 140 K, or by condensing water directly at this temperature [27]). The structures of these two ices are illustrated in fig. 12. The oxygen–oxygen bond lengths in both forms are 2.76 Å at 273 K and atmospheric pressure (2.74 Å at 90 K) [27]. In forms of ice which can be prepared at higher pressures, the O–O separations do not decrease, but distortion of the O–O bond angles takes place and nonlinear hydrogen bonds may exist [27,43]. Note that, in terms of the classification scheme shown in fig. 10, ice contains relatively *weak* hydrogen bonds.

The arrangement of water molecules in ice can be thought of in terms of the Bernal–Fowler–Pauling (BFP) rules formulated in the 1930's [3,47,48]. Briefly stated, the BFP rules are:

(1) Each oxygen atom has two hydrogen atoms attached at 0.96 Å with an H–O–H bond angle of about 105°.

(2) Each oxygen atom is tetrahedrally bonded to four other oxygen atoms by hydrogen atoms which are on the O–O axes.

(3) There is only one hydrogen atom on each O–O axis.

(4) Non-adjacent molecules do not interact sufficiently to stabilize any structural configurations.

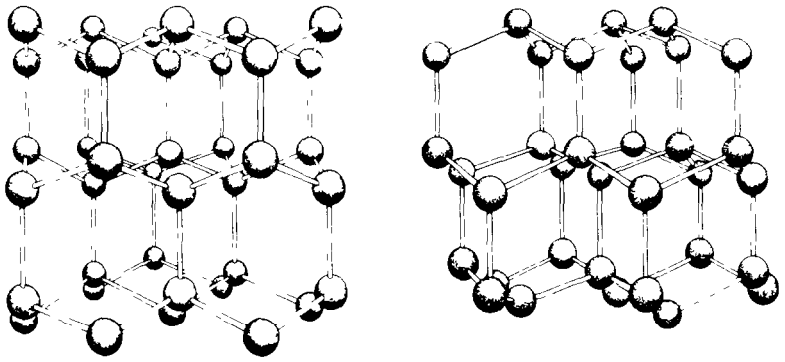

Fig 12 Positions of the oxygen atoms in ice Ic and Ih, from Whalley [44]

The resulting structure consists of water molecules in a given layer which are hydrogen-bonded into hexagonal rings such that alternating molecules are raised or lowered by 0.48 Å relative to the central plane to give the proper tetrahedral bonding angles. This bilayer configuration, which consists of an upper and a lower layer, is often referred to as being "puckered". Successive bilayers are then joined by the raised molecules of one bilayer hydrogen-bonded to the lowered molecules of the next. The two different relative orientations of successive layers comprise the Ic and Ih structures, shown in fig. 12.

The vibrational spectrum of ice is far more complex than that of the isolated molecule, partly because the strong intermolecular interactions perturb the three vibrational modes of the isolated molecule and partly because the free rotations and translations of the isolated molecule are "frustrated" by locking the molecule into the lattice, which transforms them into new vibrational modes. The distinction between the symmetric and asymmetric OH stretch breaks down due to intermolecular coupling; the OH stretch results in absorption of infrared radiation between 3000 and 3600 cm^{-1} [43,44]. The scissoring mode results in a broad infrared absorption feature centered at 1650 cm^{-1}, although this assignment is complicated by possible contributions from the overtones of the frustrated rotations [44,49]. The frustrated rotations (also called librations) occur in the frequency range between 525 and 1040 cm^{-1}, with a broad maximum at 800 to 840 cm^{-1} for ice I [27,43,44]. Finally, a frustrated translation is associated with a spectral feature of 220 to 240 cm^{-1} [27,43,44,47].

In ice the three highest valence orbitals of H_2O ($1b_1$, $3a_1$, $1b_2$) are still observable in the He I UPS spectra [50–53] although the $3a_1$ is severely broadened and reduced in apparent intensity [50–53]. The photoemission spectrum of ice is reproduced in fig. 13.

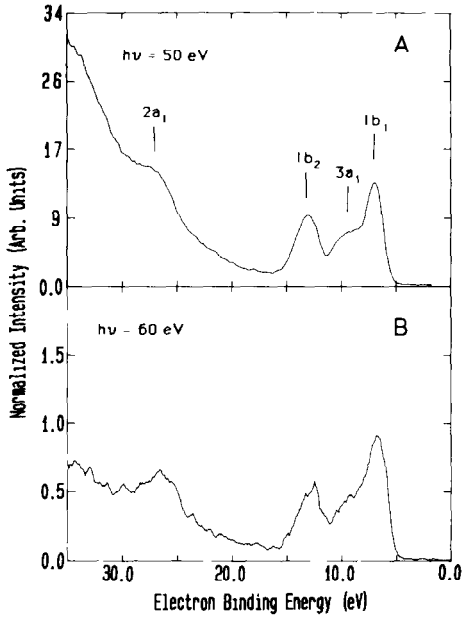

Fig. 13 Photoelectron spectra of ice. The top spectrum is obtained with 50 eV synchrotron radiation. The bottom spectrum is obtained with 60 eV radiation. The zero of energy is at the Fermi edge of the metal substrate. Taken from Stockbauer et al [53]

2.2.3. *Molecular water. bonding to surfaces*

There are several general features which describe the interaction of water with most surfaces. These generalizations, based both upon experimental and theoretical studies, are listed below. In these remarks, we do not consider surfaces at which H_2O dissociates, nor hydroxylated surfaces such as silica. These remarks *do* apply to most well-characterized surfaces of metals, semiconductors, and ionic compounds at which H_2O does not dissociate. (Dissociation of H_2O is considered separately in section 3.)

(1) Water bonds *through the oxygen atom* to the surface. Hydrogen bonds with the surface (O–H $\cdots$ S bonds, where S = surface) are rare. Similarly, water forms bonds to metal atoms in complexes and clusters via the oxygen atom [54,55].

(2) Bonding is accompanied by net *charge transfer to the surface*. Therefore water acts as a *Lewis base*. Charge transfer *to* the surface manifests itself in a *negative* work function change upon adsorption.

(3) The internal bond angle, bond lengths, and vibrational frequencies of the molecule are only *slight perturbed* from the gas phase values by the interaction with the surface.

(4) Formation of *hydrogen-bonded clusters* is common, even at very low coverages, because hydrogen bonding between two or more H_2O molecules is often energetically competitive with the molecule–substrate bond.

Because of the last point, it is difficult experimentally to isolate single water molecules adsorbed on surfaces, and much of our knowledge of the isolated adsorbed molecule must therefore rely upon theoretical work. We are aware of only a few experimental studies which report evidence of isolated monomers on metals. In one, Andersson, Nyberg and Tengstål find that water monomers can be isolated at low coverages on copper and palladium single crystals at 10 K, but warming even to 20 K allows diffusion and clustering [56]. They find that monomeric water is bound through the oxygen atom with its molecular axis tilted by about 57° and 58°, respectively. In a second study, Schmeisser and coworkers report evidence from UPS that, at temperatures near the desorption temperature (~ 160 K), H_2O exists as monomers on Ni and Cu

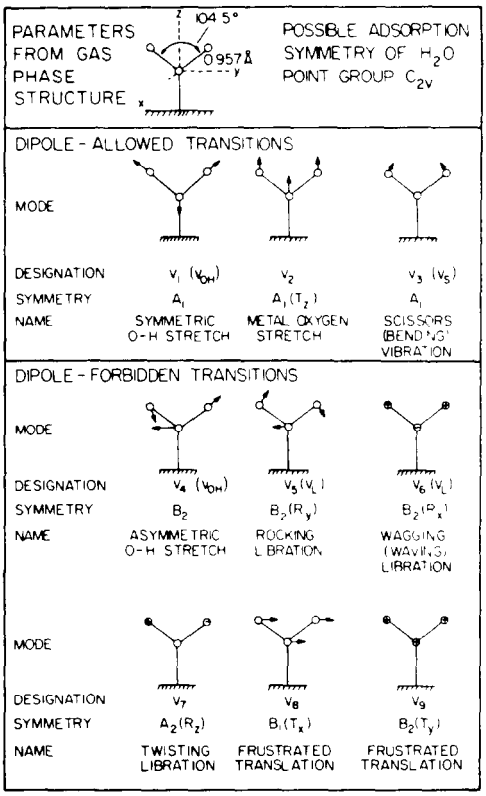

Fig 14 Normal modes of H_2O adsorbed with C_{2v} symmetry on a flat metal substrate Taken from Thiel et al [60]

films [57]. They find that diffusion is rapid enough to allow clustering on the time scale of experimental observations even at 7 K. On the basis of ESDIAD data, Madey and Yates originally suggested that monomeric water exists at low coverages on Ru(001) following adsorption at 80 K [58]; see section 4.4.2 for a discussion of more recent measurements. Thiel, DePaola and Hoffman report spectroscopic evidence of monomeric H_2O on Ru(001) at very low coverages, $\theta \lesssim 0.05$, after annealing to ~ 200 K [59]. However, they suggest that the monomers may be preferentially trapped at defect sites under these experimental conditions.

If we assume that the substrate is flat (i.e. does not contribute to the symmetry of the adsorbed molecule–substrate complex) and infinitely heavy, then an isolated adsorbed molecule possesses the nine normal vibrational modes shown in fig. 14 [60]. As with ice, adsorption on a surface has the effect of frustrating the free molecule's translation and rotations, thereby making them into vibrations. Note that the molecule shown has C_{2v} symmetry, i.e. its molecular plane is perpendicular to the surface, and the modes are labelled according to the irreducible representations within the C_{2v} point group [28]. If the molecular plane adopts a different orientation relative to the substrate, or if the local adsorption site contributes significantly to the overall molecular symmetry, then different point groups result and the vibrational spectrum becomes more complex in its analysis. We show here only the simplest possible case for illustration. The introduction of intermolecular hydrogen bonding within clusters can also complicate interpretation of the spectra, as it does for ice. Nonetheless, certain frequency ranges can be broadly associated with each type of vibration, and these are given in table 3. These values are generalized from data for H_2O chemisorbed at surfaces and coordinated to metal centers, as well as for H_2O in the gas, liquid, and condensed phases. More specific data for H_2O chemisorbed at surfaces is presented in sections 3 and 4.

Many calculations have treated the bonding of H_2O with metal surfaces, clusters, and atoms [61–73]. All predict bonding through the oxygen atom and charge transfer to the metal. The water's $1b_1$ and $3a_1$ orbitals are consistently found to be most important in forming the chemisorption bond. Most calculations are then concerned with predicting the most favorable adsorption sites

Table 3
Typical frequency range for vibrational modes of water

Frequency range (cm^{-1})	Assignment
200–500	Frustrated translations
500–1000	Frustrated rotations, i.e "librations"
1500–1650	H_2O deformation, i e the "scissoring" mode
2500–4000	OH stretch

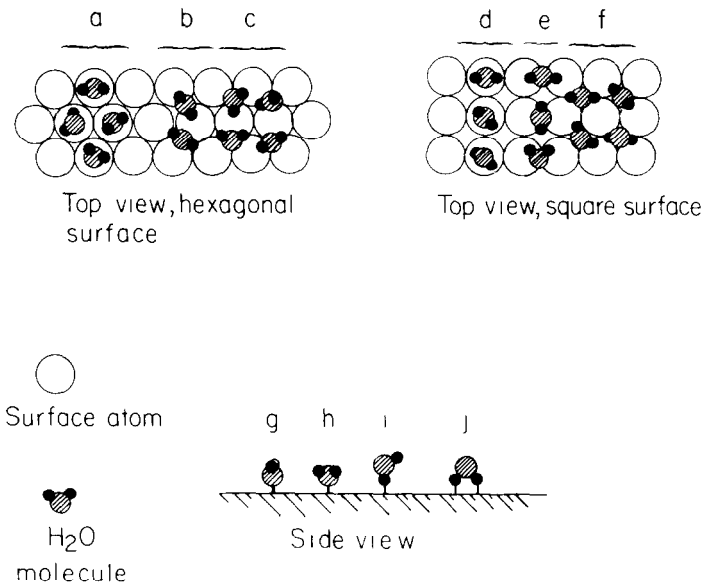

Fig. 15 Selected possible adsorption sites (a–f) and molecular orientations (g–j) of monomeric H_2O adsorbed on a hexagonal and square surface Parts (a) and (d) show occupation of on-top sites, (b) and (e) illustrate two-fold bridge sites, (c) shows H_2O at three-fold hollow sites, and (f) displays adsorption at four-fold hollow sites Orientations (i) and (j) involve hydrogen-bonding to the surface

and adsorption geometries. Some selected possible adsorption sites and geometries are shown in fig. 15.

In discussing preferred adsorption sites, the simplest model is that in which the surface–adsorbate interaction is considered in terms of simple Lewis acid–base chemistry. Stair [74] and Barteau and Madix [75] have applied this model extensively, particularly to metal surfaces. Adsorbed water, acting as the electron donor, is the Lewis base, whereas the metal is the electron acceptor (Lewis acid). On an atomically smooth surface, the on-top adsorption sites [such as sites (a) and (d) in fig. 15] are electron deficient and therefore most acidic. On the basis of this simple argument one would expect water to occupy on-top adsorption sites on metals, which is in agreement with many calculations. Although most experimental data cannot provide a basis to clearly determine the adsorption site, there is one measurement which indicates the nature of the binding site of H_2O on Pd(100) [56,76]. The bending mode of an isolated water molecule on Pd(100) shifts downward in frequency by a factor of 1.2 upon deuteration [56], rather than by a factor of 1.3 to 1.4 as is more often observed (e.g. [60]). Lloyd et al. [76] point out that this may be explained by a harmonic potential energy surface in which the water occupies

either the on-top site or the two-fold bridge site, but not the four-fold site. The exclusion of the electron-rich four-fold hollow site is consistent with the aforementioned expectation that water acts as a Lewis base, while the metal acts as a Lewis acid, in the chemisorption bond. The value of the isotopic frequency shift is also 1.2 for a bending mode of water on Ru(001) at low coverage [60], and the same model may be applicable there as well. Alternatively, anharmonicity in the potential energy surface may also account for these values of the isotopic frequency shifts [69,76], which means that there is unfortunately still some ambiguity in the interpretation of these data.

The next step in sophistication, beyond the Lewis acid–base picture, is to consider the relationship between adsorption geometry and actual adsorbate–surface bonds. Recent calculations with metal clusters by Müller and Harris [69] and Ribarsky, Luedtke and Landman [66] point to an *on-top tilted* geometry as the most favorable [see fig. 15, (a), (d) and (h)], and a *bridge-site perpendicular* geometry as the next most favorable [see fig. 15, (b), (e) and (g)]. In another calculation by Bauschlicher, the second option is comparable in energy to the first [67]. These and other calculations indicate that bonding is mainly due to overlap between the metal's d orbitals and water's lone-pair orbitals. In terms of the canonical orbitals, at the on-top site, the bent geometry results from a competition between the $3a_1$ and $1b_1$ orbitals for optimal overlap; the favorable interaction of the metal with the $3a_1$ orbital is maximized in the perpendicular geometry [fig. 15, (g)] whereas the $1b_1$ overlap is maximized when the molecule lies parallel to the surface. The tilted geometry which results is illustrated by the orbital charge contour maps of fig. 16 [66]. The angle of tilt ranges from 55° to 70° in these three calculations [66,67,69], a range which brackets the experimental observation of 57°–58° by Andersson et al. [56]. For the bridge site, on the other hand, the out-of-plane $1b_1$ orbital has large overlap with surface d-orbitals even in the upright geometry [as in fig. 15, (b), (e) and (g), with the $1b_1$ orbital pointing along the bridge and the H–O–H plane perpendicular to the bridge] and so all three calculations predict that in the bridge site, the H–O–H plane is perpendicular to the surface [66,67,69]. As Müller and Harris point out, to the extent that the overlap depends mainly on the lone-pair characteristics of the H_2O monomer, these arguments should not be metal-specific [69].

The on-top adsorption site is most often predicted theoretically, e.g. for Ru(001) [62], Ni(100) [67], Ni(111) [68], Al(100) [69], Cu(100) [66], and Pt(111) [63]. However, some calculations do not follow this pattern. The three-fold hollow site on Pt(111) is found to be energetically most favorable in the calculation by Leban and Hubbard [72], Anderson's model favors the bridge site on Fe(100) [63], and Bauschlicher finds that the two-fold bridge and on-top sites are effectively indistinguishable on Ni(100) [67].

Models of adsorbed H_2O indicate that the internal molecular bond angle, bond lengths, and force constants are only slightly perturbed upon adsorption,

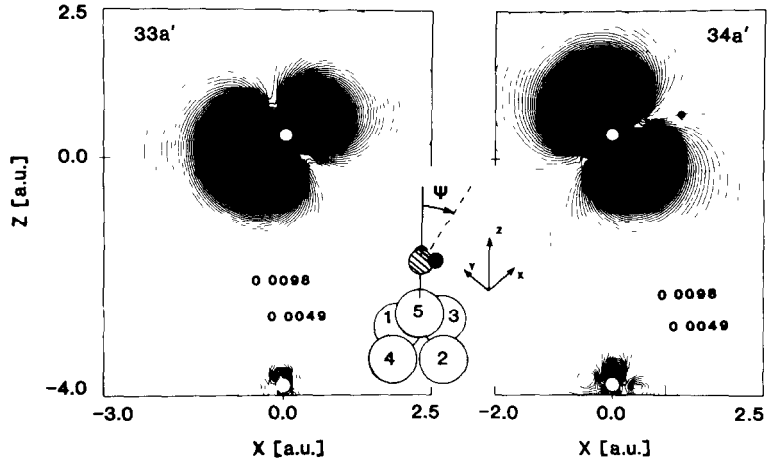

Fig 16 Molecular orbital change density contours for water adsorbed on a five-atom copper cluster The 33a′ orbital corresponds mainly to the $3a_1$ of fig 5 (p. 223), and the 34a′ corresponds mainly to the $1b_1$ of fig 5 (p. 223) The figure is taken from unpublished data generated by the authors of ref [66]

and that the oxygen lone pairs are most important in bonding to the surface [61–72]. This is supported by the experimental evidence to be presented in section 4. On the other hand, Hauge, Kauffman and Margrave [77] propose that electron withdrawal from either the $3a_1$ or $1b_1$ orbitals should at least slightly influence the H–O–H bond angle and the force constant for the in-plane deformation (scissoring mode). They base this proposal on the intramolecular changes which occur when an electron is completely removed from either of these orbitals in photoionization, as discussed in section 2.2.1 These authors use this approach to interpret vibrational spectra of water bonded to Group 3A metals in matrix isolation experiments [77]. They correlate the H_2O–metal bond strength with the "softening" of the frequency of the scissoring mode, arguing that a stronger bond and more extensive transfer from either the $3a_1$ or $1b_1$ orbitals should increase the H–O–H bond angle and decrease the scissoring mode frequency [77]. This effect has been treated theoretically by Blomberg and coworkers [73]. The extent to which this is actually observed on surfaces is discussed in sections 4 through 7.

Charge donation from adsorbed water to the surface causes the work function to *decrease* upon adsorption of H_2O. The dipole moment of the adsorbed molecule can, in principle, be obtained from the experimental value of the work function change in the limit of zero coverage, which is termed the "initial dipole moment". This value is always only 20% to 50% of the dipole moment of the isolated H_2O molecule (1.83×10^{-18} esu cm), based upon data presented in section 3.2 and table 5 (p. 250). This presumably reflects charge

transfer to the surface, as well as the tilting of the molecule relative to the surface normal and depolarization within the hydrogen-bonded aggregates. (See following discussion.)

Most of the foregoing remarks apply to metal surfaces, since the majority of theoretical work has dealt with metal surfaces. If one extends the simple Lewis acid–base picture of bonding to an ionic surface, one expects water to bind via the oxygen atom to the electron-poor cationic sites, and/or (perhaps) to bind via the hydrogen atoms to the electron-rich anionic sites. This is discussed more fully in sections 6 and 7, although we note here that this simple picture is supported by the calculations of Kistenmacher et al. [78].

Finally, the magnitude of the chemical bond which water forms with metal surfaces is typically on the order of 40 to 65 kJ/mol (10 to 15 kcal/mol, or 0.4 to 0.7 eV). The experimental basis for this number is discussed in detail in section 4.2. The strengths of bonds to other types of well-defined surfaces are less-known; heats of adsorption on oxide powders also range from about 40 to 60 kJ/mol [22], which is addressed in section 7.1. Thus, compared with adsorbates such as CO or O_2, H_2O is a weakly chemisorbed species, on the borderline of physisorption.

It is this weak interaction with the surface which makes intermolecular hydrogen bonding energetically favorable. As mentioned in section 2.2.2, hydrogen bond strengths in ice and water are typically 15 to 25 kJ/mol (4 to 6 kcal/mol or 0.2 to 0.3 eV). There is abundant evidence that water forms ice-like clusters on surfaces, similar to those shown in fig. 12 (p. 228), in which some water molecules form direct bonds to the surface and others are only held via hydrogen bonds to the first-layer molecules, forming a three-dimensional network. A possible cluster is shown in fig. 17. It is clear that a molecule which only forms two hydrogen bonds is bound by an energy at least comparable in magnitude to the chemisorption bond energy, so that formation of such clusters is certainly plausible. The tendency of water to form hydrogen-bonded, three-dimensional islands at surfaces is a characteristic property which will recur in many aspects of our discussion. Evidence exists for the formation of hydrogen-bonded clusters on very many substrates, yet most theoretical models of surfaces to date treat *isolated* adsorbed H_2O molecules. (The model of Paul and Rosén is an exception [64].) Intermolecular interaction is clearly very important, and so direct comparison between theoretical and

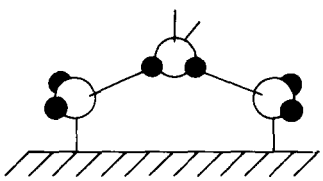

Fig. 17. Possible arrangement of water molecules in a hydrogen-bonded surface cluster

experimental work can, as yet, be made only in rare cases. Hydrogen bonding may be less prevalent for H_2O on ionic surfaces, where the adsorption energy at specific sites is in some cases high enough to prevent clustering (see section 7).

Note that the arrangement of bonds about the oxygen atoms in a surface cluster such as shown in fig. 17 are quasi-tetrahedral, as they are also in ice. In a purely tetrahedral arrangement the H–O–H plane of the first-layer molecules must tilt by 55°, which is close to the most favorable angle predicted for the isolated monomer [66,67,69] and also measured experimentally on Cu(100) and Pd(100) [56]. Therefore little or no distortion is required for the first-layer molecules to go from an energetically-favored monomeric geometry to part of a hydrogen-bonded network. In terms of the localized orbital picture shown in fig. 8 (p. 225), the first-layer molecules use one of the equivalent lone pairs to bond to the surface, while the other points away from the surface to form a hydrogen bond with another (second-layer) molecule.

Doering and Madey [79] propose a systematic basis for the structure of hydrogen-bonded water clusters at metal surfaces by calling attention to the Bernal–Fowler–Pauling (BFP) rules described in section 2.2.2. Although these rules are adequate to describe the general features of bonding and structure in bulk ice, additional constraints must be imposed at the water–metal interface. To accomplish this, the following surface modifications to the BFP rules are proposed for adsorbed water clusters [79]:

(a) Water is bound to the metal surface via an oxygen lone pair orbital.

(b) The tetrahedral bonding configuration is maintained for water bound to the surface even for two-dimensional clusters and incomplete layers. This condition adapts the BFP rules to include structures (e.g., the edges of clusters) where a given oxygen atom is not tetrahedrally surrounded by four other oxygen atoms.

(c) Each water molecule is bound to the system by a minimum of two bonds (either hydrogen bonds to other water molecules or oxygen lone pair bonds to the surface). This is based on the magnitude of the binding energy of adsorbed H_2O, which (as we have discussed) is generally comparable to the energy of two hydrogen bonds per H_2O molecule.

(d) All free oxygen lone pair orbitals are constrained into orientations which are nearly perpendicular to the substrate. This implies that H_2O molecules with free oxygen lone pair orbitals in highly asymmetric orientations relative to the surface or interface will be unstable due to the influence of the substrate on such an orbital.

The application of these rules to specific systems is discussed in section 4.4.

2.3. Dissociation products of water hydroxyl, hydrogen and oxygen

Dissociation of water can lead potentially to a variety of chemical species at surfaces. The simplest of these are adsorbed hydroxyl, atomic oxygen, and

atomic hydrogen. The factors which determine whether water will dissociate, and what the end-products of dissociation might be, are discussed more fully in section 3.1. In this section, we simply describe the main chemical and structural features of these potential dissociation products.

Hydroxyl binds to surfaces and smaller metal centers through the oxygen atom (e.g. [54,55,80]). A variety of surface geometries, from tilted to per-

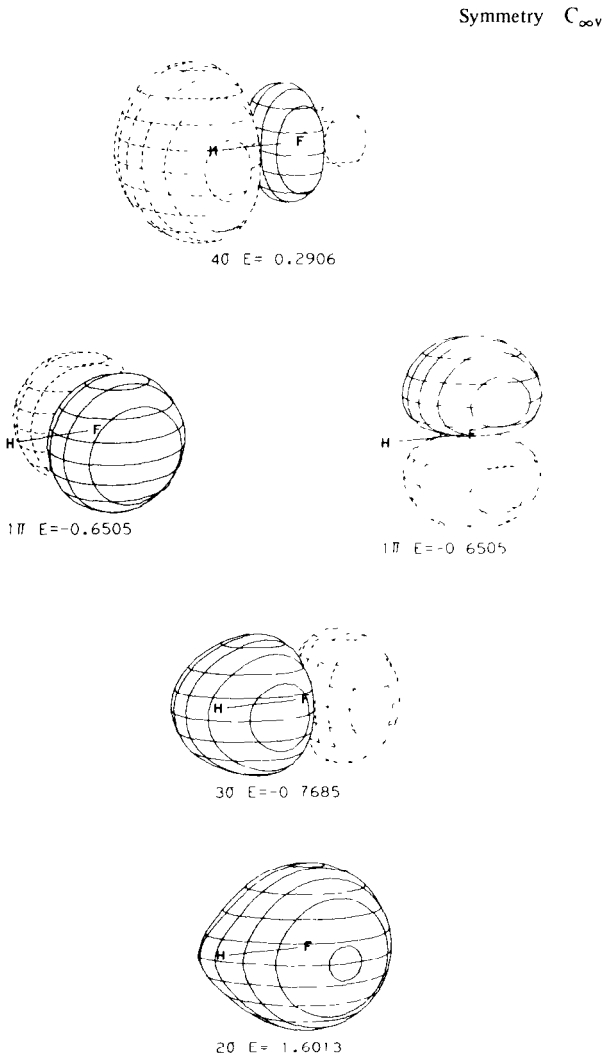

Fig 18. Delocalized molecular orbitals of HF, which is isoelectronic with OH^-, from Jorgensen and Salem [34]

pendicular, have been proposed (e.g. [80–84]). Hydrogen bonding to other surface hydroxyls or water molecules can be important, e.g. for hydroxylated powders [23].

It is well known in chemistry that the hydroxyl radical is electronegative and tends to form hydroxide anion. Hydroxide anion is isoelectronic with HF, and so the molecular orbitals of OH^- can be understood from those of HF, which are illustrated in fig. 18. The energy levels of these orbitals are shown in fig. 19 [85]. In the OH radical, the highest-lying orbital is the antibonding 1π (see figs. 18 and 19), which is partially vacant. It is very probable that bonding of hydroxyl radical to a surface involves a net transfer of electrons from the surface to this partially vacant 1π orbital. This picture is supported by a recent careful measurement of a work function *increase* for chemisorbed OH on Pd(100), in which $\Delta\phi = +0.1$ eV for a partial monolayer [81]. Thus, where water is an electron *donor* (Lewis base), adsorbed hydroxyl is an electron *acceptor* (Lewis acid). One therefore expects that those electronic effects which stabilize adsorbed water can destabilize adsorbed hydroxyl, and vice versa. In the Lewis acid–base picture, it follows that hydroxyl adsorbed on a metal surface tends to occupy the electron-rich hollow or bridging sites; on an ionic surface it may prefer the anionic sites. This general picture of surface bonding of OH is also supported by the calculations of Anderson and coworkers [63,86,87].

The two highest occupied valence orbitals of OH, the 1π and the 3σ, are observable with He I radiation in PES. This is true for the gas-phase species [88] as well as for hydroxyl bound to another atom as in NaOH [89], and for adsorbed hydroxyl (e.g. [80]). The photoemission spectrum of NaOH is shown in fig. 20 [89]. Note that the separation between 3σ and 1π features features of OH^- in NaOH is ~ 3 eV [89]. Experimental differentiation of adsorbed OH from H_2O is discussed in detail in section 3.2.

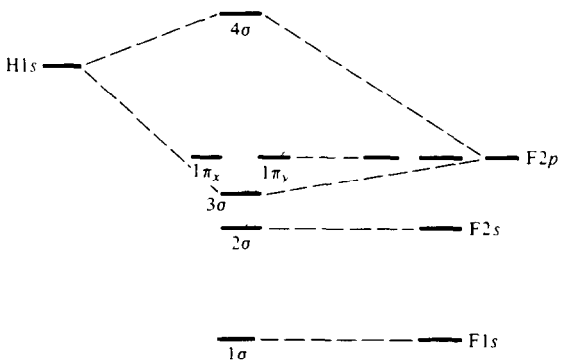

Fig 19 Molecular orbital diagram of HF (not to scale) HF is isoelectronic with OH^- The 1π orbital is the highest occupied orbital and is filled in both species Taken from Levine [85]

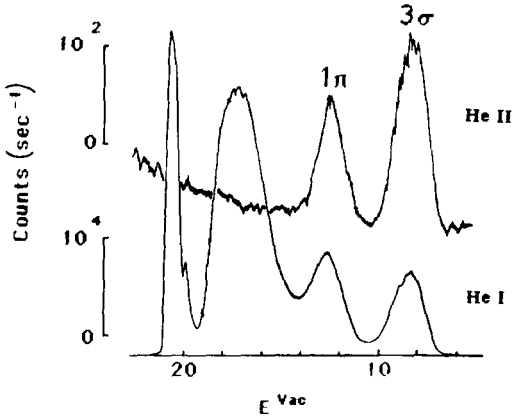

Fig 20 Photoelectron spectrum of solid sodium hydroxide, using He I and He II radiation. The 1π and 3σ orbitals of the hydroxyl group are so labelled. Taken from Connor et al [89]

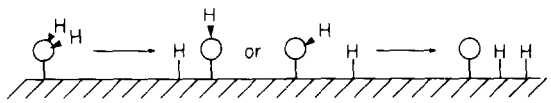

Fig 21 Schematic illustration of possible dissociation reactions of adsorbed water

It is known that both atomic oxygen and hydrogen tend to occupy surface sites of multiple coordination, and are more strongly bound at surfaces than H_2O. Typical surface bond strengths are presented systematically in section 3.1. A full description of these adsorbates, however, is beyond the scope of the present article, and the reader is referred to several excellent reviews available in the literature. Davenport and Estrup [90] discuss surface hydrogen in detail, and Brundle and Broughton [91] review chemisorption of oxygen. Toyoshima and Somorjai [92] compile heats of adsorption for both adsorbates.

3. Considerations of molecular versus dissociative adsorption pathways

3.1. Thermodynamic factors

Adsorbed water can, under some circumstances, dissociate. The simplest products of this reaction, and the only ones thus far encountered experimentally, are adsorbed hydroxyl, atomic oxygen, and atomic hydrogen. The possible dissociation pathways of water are illustrated schematically in fig. 21. As shown, if only one of the internal O–H bonds of the molecule is broken,

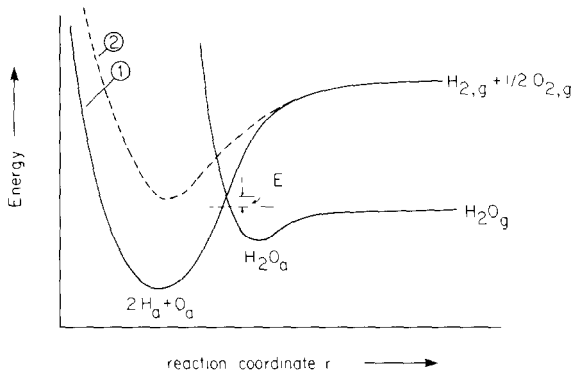

Fig. 22. Potential energy diagram for adsorbed water and its dissociation products

the products are adsorbed hydroxyl and hydrogen; if both of the internal bonds are broken, atomic hydrogen and oxygen will form. The reaction can be visualized using the potential energy diagram of fig. 22, where we have chosen atomic oxygen and hydrogen as the final dissociation products. The same ideas apply if adsorbed hydroxyl and hydrogen are chosen as the final products. The potential energy curve of adsorbed water can have a minimum which is either higher in energy than the dissociation products (curve 1) or lower than adsorbed hydrogen and oxygen (curve 2). In the first case, dissociation is thermodynamically preferred; in the second case, it is not. If the activation barrier to dissociative adsorption from the gas phase, represented by E, is sufficiently high, dissociation may be prevented because of kinetic limitations even though it may be thermodynamically favored.

The most basic questions to a surface chemist are these: what are the products of H_2O adsorption at a surface? Does water adsorb molecularly or does it dissociate, and which conditions can influence this reaction pathway? Simple thermodynamic data can be used to make rough predictions of the answer, as Benziger has shown for diatomic molecules at metal surfaces [93]. Following his treatment, we attempt to predict whether or not dissociation of adsorbed water is thermodynamically favored, for any given surface, in terms of the enthalpy changes diagrammed in fig. 23. The analysis proceeds via determining whether the enthalpy of dissociation, ΔH_d, is larger or smaller than the enthalpy of molecular adsorption, ΔH_m, based upon other enthalpy changes which have been measured or which can be estimated. A value of ΔH_d which is more positive than ΔH_m is taken to suggest nondissociative adsorption, whereas a value which is more negative than ΔH_m supports dissociation.

Note that this treatment cannot predict kinetic rate limitations which may lead to non-equilibrium distributions of reaction products. Coverage effects and entropy contributions to the free energy are ignored as well. As Benziger

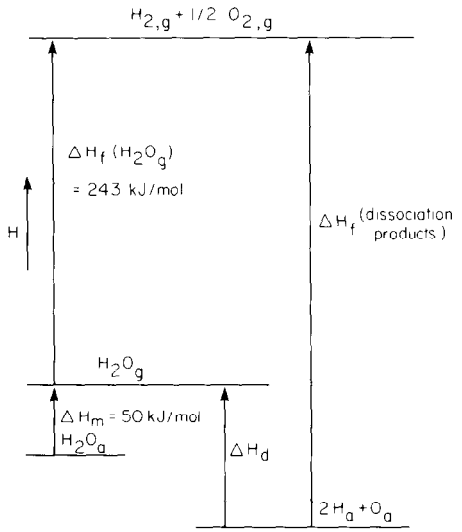

Fig 23 Enthalpy changes which accompany adsorption and dissociation of water, referenced to gas-phase hydrogen and oxygen

emphasizes [93], low coverage and high temperature shift the adsorption equilibrium in favor of dissociation, assuming that thermodynamic quantities are coverage-independent. In summary, all of these effects combine to make this discussion most valid in the limit of high coverage and low temperature, and in the limit where energetic barriers to equilibrium are small.

As in fig. 22 we choose to illustrate the enthalpies involved in adsorption and dissociation in fig. 23 using atomic hydrogen and oxygen as the dissociation products. As shown in fig. 23 the energies are all referenced to the level of gas-phase hydrogen and oxygen. The enthalpy change which accompanies nondissociative H_2O adsorption is simply the negative of the heat of desorption, assuming that there is no barrier to adsorption. As discussed in section 4.2, this value does not vary widely in the metals studied to date, and so we shall assume a constant value for ΔH_m of -50 kJ/mol. The heat of formation of H_2O, $\Delta H_f(H_2O_g)$ in fig. 23, is known to be -243 kJ/mol [94]. The enthalpy levels on the left-hand side of fig. 23 are, therefore, rather well defined.

The heat of dissociative adsorption, ΔH_d, can be expressed as

$$\Delta H_d = \Delta H_f(\text{dissociation products}) - \Delta H_f(H_2O_g).$$

The problem in comparing ΔH_d with ΔH_m now lies in determining ΔH_f for the dissociation products.

The value of ΔH_f(dissociation products) can be obtained in several ways, depending upon the availability of information from any one source. For our

rough predictive purposes, we take bulk values for heats of formation of metal oxides and hydroxides *per* metal–ligand bond, wherever possible, from *The NBS Tables of Chemical Thermodynamic Properties* [94]. For the metal–oxygen bond enthalpy, several types of oxides are sometimes listed; when given a choice, we use the oxide with stoichiometry most nearly 1 : 1. Our qualitative predictions are unchanged (except in some borderline cases) when an alternate source is used for bulk metal oxide enthalpies [93]. For the metal–hydrogen

Table 4
Enthalpy changes which accompany adsorption and dissociation of water, used to predict thermodynamic feasibility of dissociation [a]

Metal, M	ΔH_f (M–O)	ΔH_f (M–H)	ΔH_f (M–OH)	ΔH_d (complete dissociation)	ΔH_d (partial dissociation)	ΔH_m
Ti	−520 [94]	−60 [94]	–	−397		−50
V	−432 [94]	−40		−269		−50
Cr	−383 [94]	−92 [95]	−356 [94]	−324	−205	−50
Mn	−385 [94]	−79 [95]	−347 [94]	−300	−183	−50
Fe	−272 [94]	−67 [96]	−235 [94]	−163	−59	−50
Co	−238 [94]	−59 [95]	−256 [94]	−113	−72	−50
Ni	−240 [94]	−48 [95]	−248 [94]	−93	−53	−50
Cu	−157 [94]	−21 [95]	−212 [94]	−44	+10	−50
Zn	−348 [94]	−48 [95]	−318 [94]	−201	−123	−50
Zr	−550 [94]	−85 [94]	–	−477		−50
Nb	−406 [94]	−63 [96]	–	−289		−50
Mo	−294 [94]	−71 [95]	–	−171		−50
Tc	−159 [94]	−79 [95]	–	−74		−50
Ru	−153 [94]	−38 [97]	–	+14		−50
Rh	−114 [94]	−40 [98]		+49		−50
Pd	−85 [94]	−50 [95]	−198 [94]	+58	−5	−50
Ag	−12 [94]	−50 [95]	−124 [94]	+131	+69	−50
Cd	−248 [94]	−48 [95]	−274 [94]	−111	−79	−50
Hf	−572 [94]	−40	–	−409		−50
Ta	−409 [94]	−33 [94]	–	−232		−50
W	−295 [94]	−73 [95]	–	−198		−50
Re	−202 [94]	−79 [95]	–	−117		−50
Os	−97 [94]	−67 [95]	–	+12		−50
Ir	−137 [94]	−38 [95]	–	+30		−50
Pt	−41 [94]	−42 [95]	−176 [94]	+118	+25	−50
Au	+27 [93]	−50 [95]	−142 [94]	+170	+51	−50
Hg	−90 [94]	−48 [95]	−178 [94]	+57	+17	−50

[a] The enthalpy changes are defined in fig 23, the predicted reaction pathways are summarized in fig 24 The predicted adsorption pathway listed in the eighth column is based upon complete dissociation to $2H_a + O_a$ Note (1) all quantities are given in kJ/mol; (2) where several values exist in ref [94], as in ΔH_f for Fe–OH, the value shown is the average.

and metal–hydroxide bond enthalpies, we also prefer data for the bulk compound which most closely approaches 1 : 1 stoichiometry. When data for a bulk hydride is unavailable in ref. [94], we use the data compiled by Mavroides, Kafalas and Kolesar, or extrapolated from fig. 2a of their publication [95]. Some values for the metal–hydrogen bond enthalpy are also taken from direct surface measurements (Cu, Mo, Ni, Pd, Pt, and W). Effectively, the bulk values are expected to mimic the high-coverage adsorbate behavior.

Predicted adsorption pathway	Observed adsorption pathway		Metal surface(s) studied
Dissociative	Dissociative	[100,101]	(001)
Dissociative			
Dissociative	Dissociative	[101,102,151]	(110), polycr
Dissociative	Dissociative	[102]	polycr.
Dissociative	Dissociative	[103,104,152–154]	(110), (100)
[Borderline]	Face-specific	[105–107]	(001), (110), polycr
[Borderline]	Face-specific	[57,83,107–115]	(111), (110), polycr , (210)
[Borderline]	Controversial	[56,117–123]	(111), (110), (100)
Dissociative	Molecular	[110,124,125]	(001)
Dissociative			
Dissociative			
Dissociative	Dissociative	[126]	Polycr.
[Borderline]			
[Borderline]	Molecular	[58–60,79]	(001)
Molecular	Molecular	[116,127,128]	(111), polycr
Molecular	Molecular	[56,81,130]	(100)
Molecular	Molecular [b]	[84,122,131–137]	(110), (111), (311), (211), (100)
[Borderline]			
Dissociative			
Dissociative			
Dissociative	Dissociative [c]	[138]	(100)
[Borderline]	Step-dependent	[139–142]	(001), polycr
[Borderline]			
Molecular	Molecular	[143]	(110)-(1×2)
Molecular	Molecular	[130,144–150]	(100)-(5×20), (111), (110)-(1×2)
Molecular	Molecular	[126]	Polycr.
Molecular			

[b] Adsorption is reported to be molecular on all faces of silver except the (311), where a very small amount of dissociation to hydroxyl has been reported [133]

[c] Present author's interpretation, based on the apparent absence of a scissoring mode in the vibrational spectrum of ref [138].

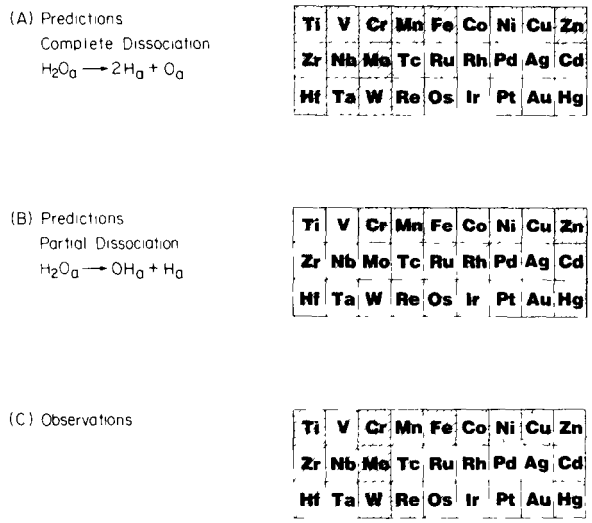

Fig 24 Partial Periodic Tables Panels A and B illustrate the predicted products of H_2O adsorption Panel C shows the actual observed reaction pathways A cross-hatched area indicates dissociation, an unmarked area denotes molecular adsorption, and a dotted area represents a borderline case. A single line indicates that there are insufficient experimental data. The predictions are based upon table 4

The relevant enthalpies are listed in table 4 for the Group VIA–IB metals. Several things are clear from these data. First, the metal–oxygen enthalpy varies widely from metal to metal. The metal–hydroxide enthalpy varies over a narrower range and weakly mimics the trends in metal–oxygen bond strength. Formation of the hydroxide is not favored over complete dissociation in any case where dissociation is predicted, except for Pd and Hg. Comparison with experimental data indicates that a categorical prediction of *whether or not dissociation occurs* is in rather good agreement with experimental observation, independent of the dissociation products The driving force for dissociation is formation of the metal–oxygen or metal–hydroxyl bond, since the other thermodynamic quantities do not vary strongly from metal to metal.

In fig. 24 the results of table 4 are presented in terms of partial periodic tables. Those elements for which dissociation is strongly preferred are cross-hatched; those for which molecular adsorption is favored are not darkened; and elements for which ΔH_m is within 70 kJ/mol of ΔH_d are indicated by dotted areas. (A single line indicates insufficient data.) We consider 70 kJ/mol to be well within the uncertainty of our model. In the top panel we base our predictions upon complete dissociation, whereas in the middle panel we consider only partial dissociation to hydroxyl and hydrogen as the reaction endpoint. In the bottom panel we show *actual observations* of molecular versus

dissociative adsorption for the various clean metal surfaces, with no distinction made between the dissociative reaction products.

The results of table 4 and figs. 24A and 24B are not meant to be taken too exactly, but there are some clear general trends. Dissociation is thermodynamically favored on most surfaces; there is only a small pocket of Group VIII and IB metals for which dissociation is clearly *unfavorable*. Many elements exist on the "borderline", i.e. within the limits of uncertainty of this analysis. In many cases these "borderline" elements are also those for which surface dissociation of water is controversial, or is reportedly face-specific or step-dependent. On Co [105–107] and Ni [57,83,107–115], water dissociates to form hydroxyl on the atomically rough surfaces, whereas it adsorbs molecularly on the close-packed faces. On Re [139–142], H_2O dissociates more readily at the step sites than on the terraces. Finally, the issue of H_2O dissociation on Cu(110) remains controversial [117,118,120] although there is consensus that H_2O adsorbs molecularly on the atomically smooth Cu(111) [120] and Cu(100) [56,119,121] surfaces. In these cases, i.e. for "borderline" metals such as Co, Ni, Re and Cu, surface morphology may be sufficient to tip the balance between molecular and dissociative adsorption, with the rougher surfaces more prone to dissociation.

The cases of observed dissociation shown in table 4 and fig. 24C usually represent *partial* dissociation to form hydroxyl and hydrogen, rather than *complete* dissociation to atomic oxygen and hydrogen. Nonetheless, the predictions of *complete* dissociation (fig. 24A) correlate most closely with the experimental observations (fig. 24C). This may simply show the limitations in accuracy of this type of analysis, due to factors which are not included in our treatment such as entropy changes and coverage dependences of the enthalpy changes discussed earlier. In other words, our approach seems to be more successful at broadly predicting whether or not dissociation occurs than in predicting the identity of the dissociation products. In any case, the general trends outlined here seem valid, and the steadily expanding body of experimental data for H_2O adsorption may, in the future, lead to more sophisticated analyses of the thermodynamics of dissociation.

3.2. Experimental identification of reaction products

The experimental identification of the adsorbed species can be achieved in two basic ways: either by desorption and analysis of the resultant gas-phase species, or via in situ spectroscopic analysis of the surface. Identification is a particularly difficult problem when a mixture of species are adsorbed simultaneously, as is often the case in decomposition of water. No single technique gives an infallible answer, and in the present authors' opinion the least ambiguous results are obtained when several techniques are applied simultaneously to the problem.

In particular, identification of desorbed products may be misleading as to the nature of the adsorbate. Thermal desorption spectroscopy is a widely used method which relies upon measurement of the evolution of gas-phase species as the surface temperature is raised. Dissociation products which are stable at one temperature may recombine and desorb as molecular water as the temperature is raised; products observed in the gas phase are not necessarily the same as the adsorbed species. A common fallacy in this regard arises from the observation of water in the residual gas of a stainless steel vacuum system, particularly when the system is heated (baked) at temperatures of (typically) 450 to 500 K. It is common to assume that the stainless steel walls release water from an adsorbed molecular state at the surface (e.g. [155,156]); in fact, it is known that water dissociates readily at iron and iron oxide surfaces, as discussed in sections 5 and 7.1.8. Molecular water is certainly not chemisorbed in large quantities at room temperature or above on steel surfaces, under high and ultrahigh vacuum conditions. Much of the water which is released into a typical vacuum chamber must result from recombination of atomic oxygen, hydrogen, and/or hydroxyl at the chamber walls. In addition, some molecular water may be trapped in oxide matrices or in pores and crevasses from which it evolves upon heating, but it is certainly not present as a majority species in molecular form on open surfaces. This presents an example of the caution which must be used in relating the identity of gas-phase species to that of adsorbed species.

During thermal desorption from water-treated surfaces, the only gas-phase products which are observed with mass spectrometry are H_2, O_2 and H_2O. (Using laser-induced fluorescence, desorption of OH radical from Pt and Ni is observed under steady-state reaction conditions [157–161], but this is a rather rare type of experiment.) Of these, H_2O presents some ambiguity in its interpretation; it can result from any of several possible reaction pathways, some of which are illustrated below:

$$H_2O_a \rightarrow H_2O_g,$$

$$2\,H_a + O_a \rightarrow [H_2O_a] \rightarrow H_2O_g,$$

$$H_a + OH_a \rightarrow [H_2O_a] \rightarrow H_2O_g,$$

$$2\,OH_a \rightarrow [H_2O_a + O_a] \rightarrow H_2O_g + O_a.$$

As discussed in section 4.2, molecular water often desorbs in a relative low temperature range which clearly distinguishes it from recombination of its dissociation products. This is one (rough) way of using desorption product analysis to determine whether or not water dissociates at a metal surface.

The other approach is to use species which are isotopically labelled prior to adsorption and reaction. For instance, isotopic scrambling between coadsorbed atomic oxygen ($^{18}O_a$) and normal water ($H_2{}^{16}O_a$) appears to be a

consistent indication of H_2O dissociation, based upon confirmatory evidence from other spectroscopies. The appearance of $H_2{}^{18}O$ as a desorption product is generally interpreted as arising from hydrogen abstraction followed by disproportionation:

$$H_2{}^{16}O_a + {}^{18}O_a \rightarrow {}^{16}OH_a + {}^{18}OH_a,$$

$$^{16}OH_a + {}^{18}OH_a \rightarrow H_2{}^{18}O_g + {}^{16}O_a.$$

Another possible reaction pathway (dissociation and recombination) is known to be important in the steady-state production of H_2O_g from reaction between H_a and O_a [21], but is a secondary reaction in several experiments involving OH_a (cf. section 6.2.2). Isotopic exchange of oxygen is observed on Pd(100) [81,129], Ag(110) [134], Ni(110) [83,162], and is due to dissociation followed by recombination, with the existence of OH_a verified by other techniques. Exchange between $^{18}O_a$ and $D_2{}^{16}O_a$ is also observed on polycrystalline Pt, where it is attributed to oxygen–water hydrogen bonding [163]. However, we feel that dissociation followed by recombination is a more likely explanation, particularly in light of recent work which has identified hydroxyl groups under similar conditions on Pt(111) [80]. Another type of isotopic scrambling, i.e. between H_2O_a and D_2O_a, yields more ambiguous results. This is because, in cases where hydrogen bonding between H_2O molecules occurs and protons occupy rather symmetric double-minima potential wells (see section 2.2), isotopic scrambling can take place simply as a result of hydrogen bond formation and cannot be used as evidence of dissociation. Such scrambling has been reported, for instance, when H_2O and D_2O are coadsorbed on Pt(111) [146]. However, there are also difficulties inherent in this type of experiment: one must be certain that any isotopic scrambling takes place *only* on the sample under study, and not on the walls on the gas-handling lines or the vacuum chamber. This experimental problem can be severe [60].

The interpretations of both the isotopic scrambling data and the normal thermal desorption data are greatly strengthened if they are used in conjunction with a technique which can provide direct information about the surface species in situ, such as UPS, EELS and XPS. In UPS [135] the characteristic three-peak H_2O valence spectrum due to photoemission from the $1b_1$, $3a_1$, and $1b_2$ orbitals of adsorbed H_2O is replaced by a two-peak spectrum identified with 1π and 3σ orbitals of adsorbed OH, as discussed in section 2.3. In general, the peaks of OH_a are separated by 3 to 4 eV, with binding energies of 5–7 eV (1π) and 9–11 eV (3σ); see table 12 on p. 328 for a tabulation of binding energies measured for OH_a on various metals. Typical UPS spectra of OH_a and H_2O_a are shown in fig. 25, where the three-feature H_2O spectra shown in the two lower curves (corresponding to H_2O_a) are to be compared with the two adsorbate-induced features present in the two upper curves (corresponding to OH_a) [100]. This technique appears to be quite sensitive to the form of the adsorbed species (see sections 4.3 and 5.1). Some of the first

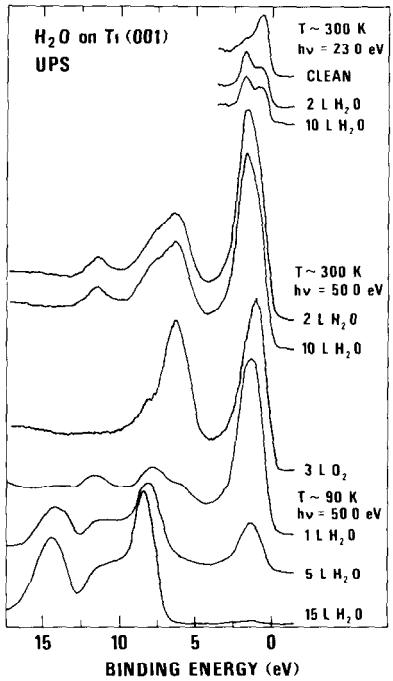

Fig 25. UPS spectra of H_2O adsorbed on a stepped Ti(001) surface at 300 and 90 K The three small curves at top show the H-induced feature at 1.3 eV binding energy The two topmost full curves are UPS spectra for OH_a (together with the other dissociation products, O_a and H_a) produced by exposing the Ti surface to H_2O at 300 K The three bottom curves are UPS spectra of molecular water adsorbed at 90 K. The UPS spectrum of oxygen adsorbed on the same surface at 300 K is shown for comparison Taken from Stockbauer et al [100].

spectroscopic data presented to show the existence of molecular water adsorbed at clean metal surfaces were the UPS data for H_2O on gold published by Atkinson, Brundle and Roberts [126].

Core-level photoelectron spectroscopy via X-ray photoelectron spectroscopy (XPS), can provide a "fingerprint" of OH_a in specific instances [111,135]. For example, on Ni(210) [111], the formation of OH_a is characterized by the appearance of an oxygen 1s (O 1s) feature at ~ 531 eV binding energy, which is intermediate in energy between chemisorbed oxygen (~ 530 eV) and adsorbed molecular H_2O (~ 533 eV). However, Au, Roberts and colleagues [122,164] discuss the difficulty of differentiating between the perturbation of molecularly adsorbed water due to hydrogen bonding and/or the coexistence of OH_a. In many cases, there is sufficient ambiguity in the chemical shifts observed in the O 1s region of XPS spectra of $H_2O_a + O_a$ that the existence of OH_a (particularly at low temperatures) cannot be confirmed. Barteau and Madix [135] also note that the reported binding

energies of OH_a on Ag, Cu and Pt vary by more than 2 eV, rendering the identification of this species on other metals difficult on the basis of binding energies alone.

Another common example of an in situ technique is the work function change measurement, introduced in section 2.3 It should be noted that the work function change due to adsorption of water and the dissociation products contains contributions from two effects, viz. the dipole moment (permanent or induced) of the adsorbed species, and charge transfer between adsorbate and substrate. For adsorbed molecular water, interpretation of these data is usually based upon a simple picture in which an H_2O molecule, bonded to a surface with the oxygen end down, has a positive net dipole oriented away from the surface (see section 2.2.3). This leads to a decrease in the work function, i.e. $\Delta\phi < 0$. Much work has been done by Heras and coworkers (e.g. [106,166,167]) to determine the work function changes of adsorbed water. They and others, whose data are summarized in table 5, always find that a negative work function change is associated with the adsorption of molecular water, indicating that this model for water adsorption is essentially correct. (Note from table 5 that the value of the dipole moment per molecule in the limit of zero coverage, termed the "initial dipole moment" is always only 20% to 50% of the value of the dipole moment of the free molecule. The reasons for this are presented in section 2.2.3.) It appears that associative (molecular) adsorption *does* produce a net negative work function change in every case reported to date. However, associatively adsorbed water often exhibits a rich variety of adsorption geometries to accommodate intermolecular hydrogen bonding, as will be discussed in section 4.4. Some of these geometries may have oxygen atoms pointing away from the surface, which can potentially complicate the simple model outlined above, as discussed in section 2.3.

In principle, molecularly adsorbed H_2O should be distinguishable from adsorbed OH, since OH is expected to cause a work function increase ($\Delta\phi > 0$). However, dissociation may also produce adsorbed atomic oxygen (generally $\Delta\phi > 0$) and hydrogen ($\Delta\phi > 0$ *or* $\Delta\phi < 0$). Therefore, identification of adsorbed hydroxyl based upon work function data *alone* remains ambiguous, in the present authors' opinion.

A powerful class of in situ spectroscopic techniques is that which measures vibrational properties of the adsorbed overlayer. This group, which includes infrared, electron energy loss, and Raman spectroscopies, is presented in section 4.5. The data obtainable from this type of spectroscopy provide the best basis for comparison between single-crystal surface chemistry and chemistry on high-surface-area solids such as oxides or dispersed metals, since much work in the latter field has relied upon infrared techniques [24–26].

The vibrational spectroscopies can, in principle, sense the nine normal modes of an adsorbed water molecule which are depicted in fig. 14 (p. 230)

Table 5
Work function measurements of molecularly adsorbed water at metal surfaces

Metal	Adsorption temperature (K)	Initial dipole moment (D)	$\Delta\phi_{max}$ (eV)	Refs
Fe-polycr	77		-0.97 ± 0.08	[165]
Co-polycr.	77		-1.20 ± 0.02	[106,165]
Co(001)	100		-1.20 ± 0.02	[106]
Co(1120)	100		-1.20 ± 0.02	[106]
Ni-polycr	77	0.56	-1.10 ± 0.15	[165,166]
Ni(110)	150		-1.2	[167]
Ni(110)	20		-1.05	[168]
Ni(100)	110		-1.05	[115]
Cu-polycr	77		-0.73 ± 0.08	[165]
Cu(110)	90		-0.92	[117]
Cu(110)	110	0.87	-1.08	[120,169]
Cu(111)	110	0.5	-1.00	[120]
Cu(100)	90		-0.9	[119]
Ru(001)	90		-0.6	[60]
Pd(100)	110		-0.4	[128]
Ir(110)-(1×2)	130	0.4 ± 0.1	-0.75	[143]
Pt(111)	100	0.6	-1.5	[145]
Pt-polycr	77		-1.02 ± 0.15	[165]
Au-polycr	77		-0.60 ± 0.08	[165]
Isolated H_2O		1.84		

and which are discussed throughout section 2.2. The frequency ranges which are broadly associated with each type of vibration are summarized in table 3 (p. 231), where the values given are generalized from data for H_2O in the gas, liquid, and condensed phases, as well as chemisorbed H_2O and H_2O coordinated to metal centers in inorganic/matrix-isolated complexes. In general, assignments of vibrations of water at metal surfaces are based both upon the observed frequency and the shift in frequency which is measured upon isotopic substitution. In the vibrational spectroscopies, the best basis for differentiation between molecular H_2O and any or all of its dissociation products is the presence or absence, respectively, of the intramolecular deformation mode, δ(HOH). This vibration appears at 1500 to 1650 cm^{-1}. The OH stretch region at ~ 3600 cm^{-1} is not generally as reliable an indicator of dissociative adsorption because of the wide range of OH stretches reported for OH_a on different surfaces (3160 to 3680 cm^{-1}); these overlap the OH stretch region for adsorbed molecular water (see section 4.5). Nyberg and Tengstål [81] point out that the range of OH stretches in metal hydroxo complexes,

Table 6
Comparison of the vibrational frequencies (cm^{-1}) observed for water vapor and ice with those observed upon of water on surfaces

Surface	Hindered translations	$\nu(M-OH_2)$	Mixed translation rotation	Hindered rotations		HOH scissor	$\nu(OH \cdot \cdot M)$	O–H stretch $\nu(OH \cdots O)$	$\nu(OH)$	Refs.
H_2O(solid)	180–300(180–300)	–	–	400 1050 (650)		1620 (1210)	–	3220 (2432) 3400 (2520)	–	[49,54]
Fe(110)	–	–	–	690 (545)	–	1630 (1220)	3070 (2315)	3380 (2595)	–	[103]
Ru(001)	–	–	–	–	–	–	–	3400	–	[170]
Ru(001)	–	390	–	700	920	1520	2935	3400	3565	[59]
Ni(110)	230 (275)	–	–	530	760 (530)	1610 (1110)	3030 (2140)	3350 (2450)	3660 (2670)	[112]
Pd(100)	220 (210)	–	615 (500)	–	805 (615)	1605 (1180)	–	3405 (2500)	–	[81]
Pd(100)	–	–	–	835	–	1645	–	3460	–	[129]
Pd(100)	–	–	335 (282)	–	–	1597 (1186)	–	–	–	[56]
Pt(100)	240 (240)	460 (470)	–	560 (470)	920 (680)	1630 (1210)	2870 (2250)	3380 (2550)	3670 (2710)	[144]
Pt(111)	250 (240)	550 (500)	–	700 (550–700)	–	1625 (1200)	–	3400 (2530)	–	[147]
Pt(111)	–	–	–	–	–	–	(2440)	(2520)	(2570)	[148]
Cu(100)	–	–	230 (198)	–	–	1589 (1178)	–	–	–	[56]
Ag(110)	200	–	–	740	–	1660	–	3410	–	[132]
O/Ag(110)	320 (260)	320 (260)		770 (570)	–	1590 (1190)	–	3230 (2430)	–	[132]
Si(111)-(2×1)	–	–	–	–	–	1575	–	3385	–	[171]
Al(100)	265	–	–	685	–	1655	–	3510	3695	[172]
Al(111)	215–240	660 (660)	–	785 (605)	–	1655 (1225)	–	3445 (2590)	–	[173]

Frequencies for D_2O are given in parentheses; mode assignments are those given by the authors cited. Data for adsorbed species are those compiled by Crowell et al [173].

Table 7
Observed vibrational frequencies (cm^{-1}) for adsorbed hydroxyl species, produced by decomposition of water

Surface	ν(M–O)	δ(OH)	ν(OH)	Ref
Fe(110)	470 (470), 960 (960)	1190	3620 (2715), 3300 (2505)	[103]
Ni(110)	–	950	3580	[112]
O/Ni(100)	–	–	3710	[174]
Pd(100)-p(2×2)O	445 (425)	935 (685)	3160 (2370)	[81]
O/Pd(100)	445 (460)	930 (695)	3250 (2420)	[129]
O/Pt(111)	430	1015 (750)	3480 (2570)	[80]
O/Ag(110)	280 (270)	670 (490)	3380 (2510)	[132]
Si(100)-(2×1)	820 (840)	820 (650)	3700 (2700)	[175]
Si(111)-(7×7)	820 (840)	820 (650)	3700 (2700)	[175]
Si(100)-(2×1)	–	830 (645)	3695 (2700)	[176]
Si(111)-(2×1)	–	805	3630	[171]
Si(100)-(2×1)	–	–	3650	[177]
Si(100)-(2×1)	–	–	3660	[178]
Si(111)	770	770	3710	[179]
Al_2O_3 [a]	–	–	3700 (2730)	[26]
	–	–	3740 (2760)	
	–	–	3790 (2795)	
HAlOH	818	–	3743	[77]
AlOH	810 (795)	–	3790	[77]
Al(111)	765 (765)	–	3745 (2720)	[173]

[a] These frequencies are those of hydroxylated alumina produced by heating an aqueous alumina layer in vacuum

When available, values for OD_a are given in parentheses Data for adsorbed species are those compiled by Crowell et al [173]

3025 to 3680 cm^{-1}, is surprisingly large also. The energies of the vibrational transitions observed for adsorbed H_2O and OH are summarized in tables 6 and 7, respectively. Further discussion of the vibrational spectroscopies is deferred until section 4.5.

A technique known as electron-stimulated desorption ion-angular distribution (ESDIAD) [180,181] is an increasingly useful source of information about the preferred azimuthal and/or polar bond orientations of a water-derived adsorbate. Electron bombardment of an adsorbed layer by electrons having energies greater than about 20 eV causes electronic excitations in the adsorbed species which can lead to the desorption of ions, ground state neutrals, and metastable atoms or molecular fragments. These processes are known as electron stimulated desorption (ESD) effects. The ions which leave the surface often appear as cones of ion emission, in specific directions with respect to the substrate symmetry axes. There is abundant evidence that the direction of a desorbing ion is determined by the orientation of the bond which is ruptured

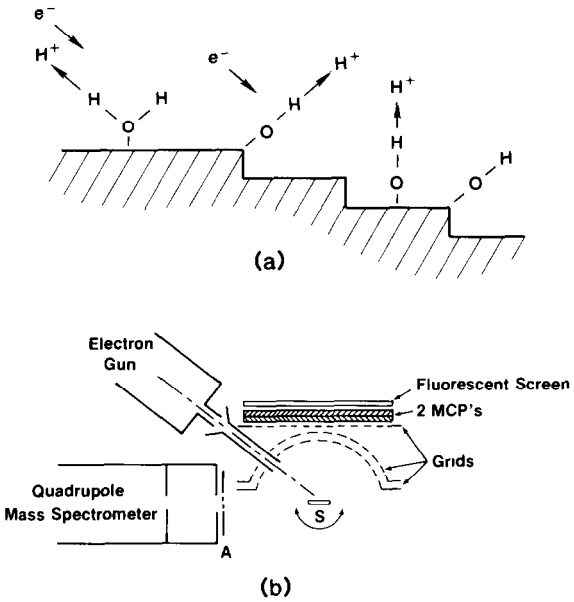

Fig 26 (a) Schematic diagram of H_2O monomer bonded via the O atom yielding an ESD H^+ ion desorbing in a direction determined by the O–H bond (b) Schematic of NBS ESDIAD apparatus ESDIAD patterns are displayed using the grid-microchannel plate fluorescent screen detector array Taken from Madey et al [180]

by the electronic excitation, as illustrated in fig. 26 [180]. That is, *bond angles are directly related to ion desorption angles* in measurements of ESD ion-angular distribution (ESDIAD). Thus, an H_2O monomer bonded via the O atom as shown in fig. 26a will yield an ESD H^+ ion which desorbs in a direction determined by the O–H bond. Similarly, OH bonded perpendicular to a planar surface will give rise to an H^+ ESD signal normal to the surface, whereas "inclined" OH at step sites will yield an H^+ signal in an off-normal direction.

The physical bases of ESD processes and of the relationship between surface bond angle and ion desorption angle are discussed in detail in several recent reviews [180,181] and are not considered extensively here. Two points merit emphasis, however. First, there is a complicating factor which distorts ion trajectories in a polar direction: the electrostatic image force acting on a desorbing ion invariably bends the ion trajectory toward the surface, thereby increasing the polar angle (the image force does not influence the azimuthal angle). The influence of the image force on ion angular distributions is partially compensated by reneutralization effects, but nonetheless, if the O–H bond makes a polar angle greater than about 60° (measured with respect to

the surface normal) an H^+ ESD ion does not escape, but is bent back to the surface. Thus, strongly inclined OH bonds, or OH bonds oriented parallel to the surface, do not yield H^+ ESDIAD signals. Second, long-range order is not necessary to produce a symmetric ESDIAD "pattern" of ions. If a substantial fraction of OH bonds are perpendicular to the surface, a normal H^+ beam will result. If a substantial fraction of OH bonds are inclined along a specific azimuth, an off-normal H^+ beam will be produced. In neither case is long-range order a necessary condition for production of directed ESD ion beams.

ESDIAD patterns from a surface are viewed directly on a fluorescent screen within an ultrahigh vacuum system following image-intensification of the desorbing ion signal using a double-microchannelplate detector in a hemispherical retarding grid analyzer. This is shown in fig 26b [180]. Many of the figures in this article are photographs, schematic drawings, or digitally-processed images of the ESDIAD patterns seen on a fluorescent screen.

Water chemistry at solid surfaces can be rather complex because so many reactions can occur. These include complete or partial dissociation, hydrogen bonding between many different moieties, and simple adsorption. All of these possible reactions must be considered when interpreting experimental data for a water-treated surface.

4. Associative adsorption on clean metals

4.1. Kinetics of adsorption and diffusion

All available evidence indicates that *adsorption* of H_2O on metals is *not* activated; adsorption probabilities are close to unity and are not temperature-dependent below the onset of desorption. The adsorption kinetics of water apparently reflect the fact that it is energetically equivalent to chemisorb directly at the metal or to hydrogen-bond with other water molecules. Effectively, the adsorbing particle cannot distinguish between a filled site and a empty site. Therefore the adsorption probability, S, at low temperatures ($\lesssim 100$ K) is independent of coverage and multilayers can start to form even before the first layer is saturated. It should be noted that this explanation of the coverage-independence of S does *not* rely upon a mobile precursor to adsorption nor upon the water molecule's mobility after adsorption. A representative coverage versus exposure curve is shown in fig. 27, for H_2O on Pt(111) [145]. The linearity of this curve implies a constant first derivative, $S(\theta)$. A coverage-independent value of S is reported also for Cu(100) [182], Ru(001) [60], Rh(111) [127], Pd(100) [130], Ir(110) [143], Pt(111) [145], Pt(100) [144], and as shown in table 8. Most of these measurements are made at adsorption temperatures of 80 to 100 K. In one case, H_2O adsorption on Ni(110), it is reported that S is coverage-dependent [183]. This measurement

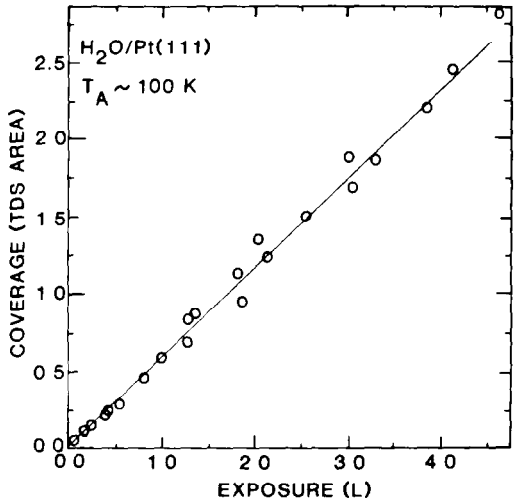

Fig 27. The coverage of water adsorbed on Pt(111) at 100 K versus water exposure The coverage units are relative, with 1 0 corresponding to the coverage where the ice multilayer peak appears in TDS Taken from Fisher [145].

relies upon attenuation of the metal d-band in photoemission, however, which may be sensitive to additional factors besides simple coverage, such as coverage-dependent changes in adsorbate orientation.

Measured values of the initial adsorption probability are always close to unity, as shown in table 8. This is plausible, since a value smaller than unity would probably be sensitive to whether adsorption occurs into the monolayer or into the multilayer, and thus lead to a coverage-dependence in $S(\theta)$.

The kinetics of H_2O diffusion on metal surfaces are most obviously important in those systems where intermolecular hydrogen bonds form. In

Table 8
Adsorption probabilities for H_2O on metals

Metal	Measured or estimated S_0	Coverage-independent?	Ref
Ni(110)	~1	No	[183]
Cu(100)	~1	Yes	[182]
Ru(001)	~1	Yes	[60]
Rh(111)	0 58	Yes	[127]
Pd(100)		Yes	[129]
Ir(110)-(1×2)	~1	Yes	[143]
Pt(111)	0.7	Yes	[145]
Pt(100)	~1	Yes	[144]

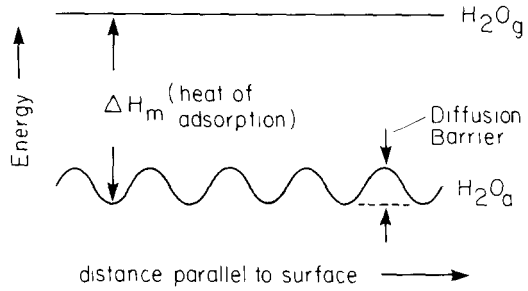

Fig. 28. Simplified view of the energetics of adsorption and diffusion of H_2O

such systems, the kinetics of diffusion can determine the rate at which hydrogen-bonded clusters nucleate and grow following adsorption.

What is the magnitude of the diffusion barrier for adsorbed H_2O? First, the general rule that diffusion barriers for adsorbates are approximately 10% to 40% of the desorption barrier [184] leads to a prediction that diffusion barriers for H_2O_a are roughly 5 to 20 kJ/mol. Most of the theoretical models developed to date also predict site-dependent differences in binding energies of adsorbed water which fall in this same range. (The differences in binding energy between various types of sites should correspond rather closely to the diffusion barrier, as illustrated in fig. 28.) Calculations for H_2O on Pt [63,65] and Fe [63] surfaces indicate only small differences in binding energy for various sites, on the order of ~ 3 kJ/mol. A calculation for H_2O adsorbed on a nine-atom Al cluster predicts a somewhat higher diffusion barrier, based upon a difference in binding energy of 27 kJ/mol between on-top and bridging sites on Al(100) [69].

Experimental data also indicate that the diffusion barrier of H_2O_a is quite low. Water forms hydrogen-bonded aggregates during adsorption on many surfaces (see sections 4.3 and 4.4) even at very low coverages, which requires that the water molecules can travel freely over the metal until they lock themselves into a hydrogen-bonded cluster. Although there is evidence that the degree of order within these clusters improves at higher temperature in some cases (see section 4.4), this probably represents a temperature-dependent barrier to reorientation of H_2O molecules *within* an existing cluster, rather than a barrier to motion of *isolated* H_2O_a across the surface A noteworthy example of this behavior is H_2O on Ru(001) [59,60,79].

Experimental studies of the vibrational spectra of H_2O adsorbed on Cu(100) and Pd(100) indicate that, at 10 K and at coverages below approximately 0.25 monolayers, H_2O monomers can be isolated because surface diffusion is prevented [56]. Slow diffusion and formation of hydrogen-bonded clusters occur if the surface is heated even to 20 K [56], which indicates a very low diffusion barrier.

The diffusion data can be summarized by saying that the energy barrier for *surface diffusion* of H_2O_a on metals is theoretically predicted to fall in the range of about 3 to 27 kJ/mol. Diffusion is rapid on the time scale of typical experimental observations ($\sim$ 1 to 60 min) and at 100 K, which means that water can rapidly form hydrogen-bonded clusters even at low coverage under these conditions.

In conclusion, water generally exhibits a very low barrier to surface diffusion, and an adsorption probability which is independent of coverage. The latter effect is related to the effective energetic homogeneity of the surface during adsorption, as will be discussed in the following section.

4.2. Strength of the H_2O–metal bond

4.2.1. Introduction

The first question to be asked is: how strong is the interaction between water and a metal surface? And how does this compare with the magnitude of the intermolecular hydrogen bond?

The answer is given by results from thermal desorption mass spectroscopy (TDS) experiments. In such experiments, a surface with an adsorbed species is heated in vacuum while the concentration of a particular gas-phase species is monitored with a mass spectrometer. A plot of the mass spectrometer signal versus temperature (time) constitutes the thermal desorption spectrum. When the pumping speed of the system is great enough that readsorption is negligible (and this is generally true), the mass spectrometer measures the rate at which the species leave the surface, either via simple desorption or via a more complex chemical reaction. In the case of (molecularly) nondissociatively adsorbed H_2O, desorption simply involves breaking the metal–H_2O bond and/or any other bonds which hold the molecule at the surface. The integral of the thermal desorption peak area over time is proportional to the total number of particles which desorb.

In general, a multiplicity of thermal desorption states can be observed, following adsorption at $T \lesssim 130$ K and at H_2O pressures $\lesssim 10^{-6}$ Torr, as illustrated in fig. 29. To a first approximation, each state represents a different type of water–metal interaction. For all systems, a TDS peak is observed at $\sim$ 150–160 K which is commonly assigned to sublimation of ice (see section 4.2.2). When this is the only peak in the spectrum, as for Ag(110) (see fig. 29a [185]), the desorption kinetics of H_2O in direct contact with the metal must be degenerate with the desorption kinetics of ice multilayers, i.e. the "chemisorbed" state and the ice state are not physically distinguishable with this method. In many systems, a TDS peak at slightly higher temperatures is resolved and assigned to molecular water which is stabilized by its proximity to the metal surface. Such states are reported in the range of 160–190 K. An example is shown by the desorption spectrum in fig. 29b [145], for Pt(111).

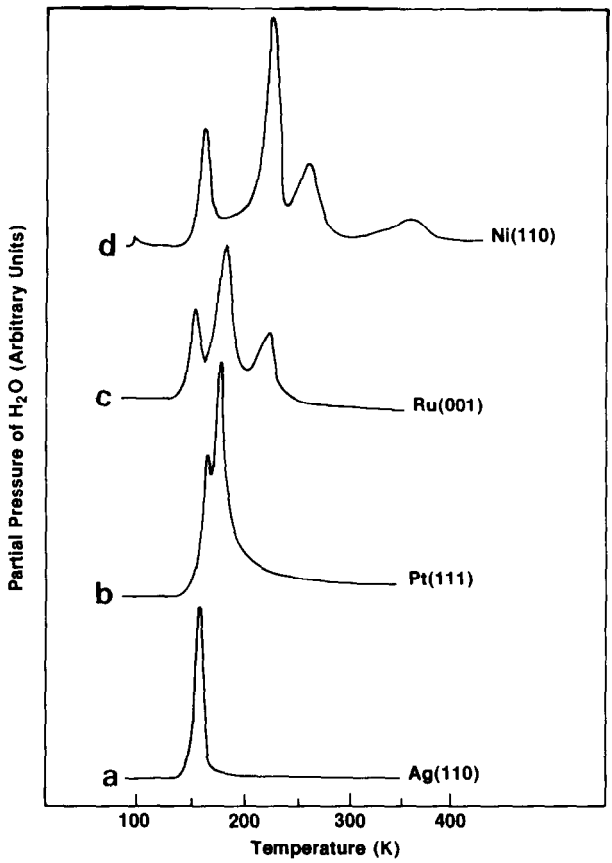

Fig. 29. Thermal desorption spectra of water adsorbed on (a) Ag(110), $\varepsilon = 3.0$ L [185], (b) Pt(111), $\varepsilon = 3.8$ L [146], (c) Ru(001), $\varepsilon \simeq 2.0$ L [79], (d) Ni(110) [162]

Whether the effective "stabilization" results from a relative increase in binding energy or a decrease in the pre-exponential factor in the desorption rate constant cannot be decided conclusively on the basis of the TDS data; measurements of isosteric heats of chemisorbed water, which could in principle provide this information, would be very valuable in this area. In several systems, a third desorption state for molecular, "chemisorbed" water is observed in addition, at still higher temperatures: usually between 200 and 250 K. An example of this behavior is shown in fig. 29c for H_2O on Ru(001) [79]. This third state apparently reflects a yet stronger interaction between H_2O and the metal. The nature of the chemisorbed states will be discussed more fully in sections 4.2.3 and 4.2.4.

Finally, at rather high temperatures, a desorption state for recombination of OH_a is reported on several clean metals (section 5) as well as on modified metal surfaces (section 6). These desorption states vary widely in peak temperature, from 200 K on oxygen predosed Pt(111) [146] to 360 K on Ni(110) [113,162]. Desorption states of *undissociated* water are also reported in the range $T > 250$ K on some metals, including Ir(110) [143], but the trend in desorption temperatures described herein indicates that these assignments are worthy of re-evaluation, and perhaps represent traces of dissociated H_2O. An example of this behavior is shown for H_2O desorption from Ni(110) in fig. 29d. The highest-temperature state at ~ 360 K was originally assigned to molecular H_2O [114], but has been recently re-examined and attributed to OH recombination [113]. In all cases where spectroscopic evidence is available, it appears that the high temperature ($T \gtrsim 250$ K) states of H_2O desorbing from metal surfaces arise from disproportionation of OH_a species via the reaction $2\ OH_a \rightarrow H_2O_g + O_a$, or via the recombinative reaction $2\ H_a + O_a \rightarrow H_2O_g$.

The thermal desorption data are summarized according to crystallographic orientation in table 9. There is a trend to higher desorption peak temperatures and (presumably) higher binding energies as one progresses from the atomically smooth hexagonal and square lattices, to the atomically rough planes, e.g. from the fcc(111) lattices to the fcc(110) lattices. This indicates a trend toward stronger H_2O–metal interactions when the metal is less coordinatively saturated. Therefore, we divide the discussion of H_2O chemisorption states into two parts: smooth surfaces are addressed in section 4.2.3, and rough surfaces are reviewed in section 4.2.4.

4.2.2. Ice sublimation

An example of typical thermal desorption data, for a sequence of initial coverages of H_2O on Ni(111), is shown in fig. 30 [108]. The lowest-temperature state (peak B) always grows continuously, starting from some threshold H_2O exposure, with increasing H_2O exposure; it does not reach a saturation coverage, contrary to the usual observation for other chemisorbed systems. In addition, desorption from this state exhibits zero-order kinetics according to

$$P_{H_2O} \propto d[H_2O_a]/dt = A \exp(-E/RT). \quad (1)$$

In this equation, t is the time, T is the surface temperature, E is the strength of the adsorbate bond, P is the measured pressure at time t, A is the pre-exponential factor in the desorption rate constant, and R is the gas constant. This expression requires, of course, that the rate of desorption at any given temperature is independent of coverage, which is observed. This expression also requires that the peak temperature must increase with increasing coverage, occurring at the temperature where the initial surface coverage is completely depleted. The validity of eq. (1) is demonstrated for a wide range of initial H_2O coverages on Ni(111), as fig. 31 shows [108]. These two

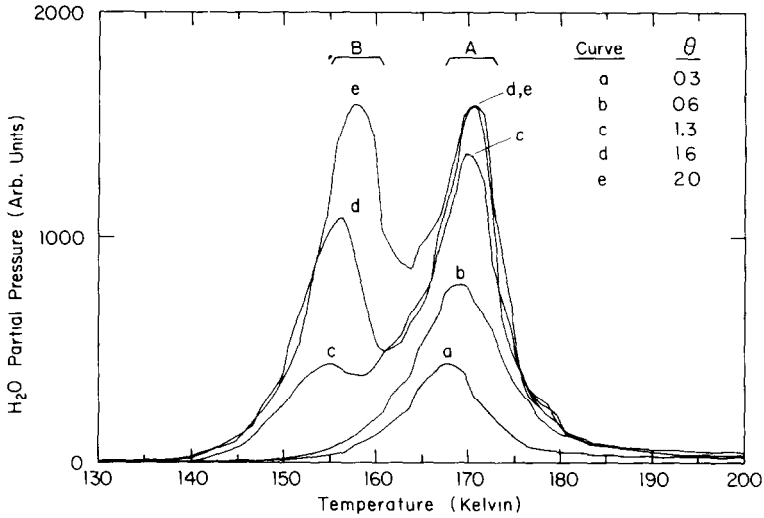

Fig 30. Thermal desorption spectra of H_2O from clean Ni(111) following adsorption at 130 K Taken from Stulen and Thiel [108]

Table 9
Thermal desorption of associatively adsorbed H_2O peak temperatures of chemisorbed states

Metal	Crystal face symmetry							
	Hexagonal faces hcp(001) and fcc(111)		fcc-(100)		fcc-(110)		Stepped or irregular	
Ni	170	[108,82]	–		230	[112–114, 167]		
Cu	{150} [a]	[122]	{150} [a]	[119]	175	[118,123]		
Ru	180–190 and 210–220	[58–60,79]	N/A		N/A			
Rh	190	[127]	–		–			
Pd	–		175	[129, 130]	191	[130]		
Ag	{150} [a]	[131]	{150} [a]	[131]	{150} [a]	[84,123, 132]	{150} [a] on (112) and (311)	[131] [133]
Re	150 and 180	[139]	N/A		N/A			
Pt	170,176	[80,145, 146,150]	165	[144]	204	[130]		

[a] When a desorption temperature is cited in brackets { }, this means it was indistinguishable from the ice sublimation peak

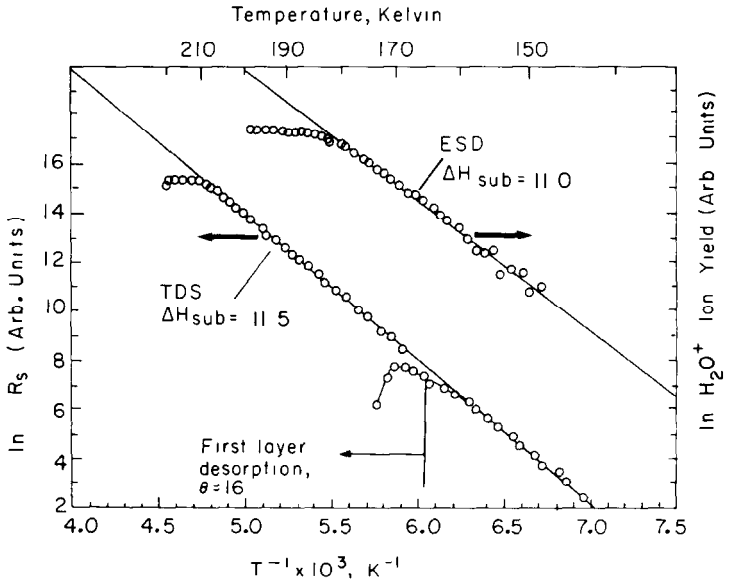

Fig 31 Clausius–Clapeyron plot for ice sublimation from Ni(111), based upon ESD data (upper curve) and thermal desorption data (lower curve) Taken from Stulen and Thiel [108] ·

observations, lack of saturation and zero-order desorption kinetics, both support the assignment of this state as due to ice multilayers, where sublimation is a zero-order process and E in eq. (1) is the heat of sublimation of bulk ice. A graph of ln P_{H_2O} versus $1/T$ then yields a straight line whose slope is E/R and whose intercept is CA, where C is a proportionality constant which depends upon experimental parameters. Using the data of fig. 31, the heat of sublimation of ice is evaluated as 48 kJ/mol [108], in good agreement with the value measured via other techniques, ~ 44 to 48 kJ/mol [27].

Thermal desorption states of ice multilayers are identified under similar conditions on many other metal surfaces as well, including Re(001) [139], Pt(111) [145,146], Pt(100) [144], Pd(100) [129], Ir(110) [143], Ru(001) [58–60,79,170], Rh(111) [127], Ag(110) [132], Ag(111) [131] and Ag(100) [131]. The heat of sublimation is estimated at 48 kJ/mol on Ru(001 [58], 42 kJ/mol on Pt(111) [146], 42 kJ/mol on Ir(110) [143], 43 kJ/mol on Pd(100) [129], and 48 kJ/mol on both Ag(111) and Ag(100) [131].

The heat of sublimation can be taken as a direct indication of the strength of interaction between water molecules in ice or water, since sublimation involves breaking (on the average) two O–H · · · O bonds per molecule, which yields about 21 kJ per mole of O–H · · · O bonds for H_2O on Ni(111) [108]. Other techniques have been used as well; O–H · · · O bond strengths are always estimated at 15 to 25 kJ/mol [27]. (See section 2.2.2.)

4.2 3. Chemisorbed states on atomically smooth surfaces

Thermal desorption data are available for hexagonal surfaces of Ni [108,82], Rh [127], Pt[80,145,146,150], Cu [122], Re [139], Ru [58–60,79] and Ag [131], and for the square surfaces of Pd [129,130], Ag [131] and Cu [119], as shown in table 9. On smooth Ag and Cu surfaces, no state is resolved above the ice feature, reflecting only a very weak interaction with the metal in these cases A single "chemisorbed state", in the range of 165–170 K, is observed on Pt(111) (with traces of a second state at very low coverages [145,146]), reconstructed Pt(100) [144], Pd(100) [129,130], and Rh(111) [127]. Two "chemisorbed states" are observed on Ru(001) [58–60,79] and Re(001) [139] On Ru(001) the highest-temperature state occurs at 210–220 K [58–60,79], whereas it is observed on Re(001) at ~ 180 K [139].

In order to derive quantitative information about the strength of the chemisorption bond from TDS data, one must make assumptions about the kinetics of the desorption process from the "chemisorbed" state(s) The simplest physical assumption is that desorption in the highest-temperature state results from breaking the single metal–H_2O bond, and the desorption rate is first-order in water coverage, with $A \approx 10^{13}$ s^{-1}. In this case, the chemisorption bond strength is about 42 kJ/mol on the hexagonal Pt, Rh and Ni surfaces, and about 50 kJ/mol on Ru(001). Physically, this would indicate that 2–3 hydrogen bonds are (energetically) worth one chemisorption bond. Then one would expect H_2O molecules to form hydrogen-bonded clusters even at low coverages in which some molecules have *no* direct metal–H_2O bond, but only 2–3 hydrogen bonds, given the generally high mobility of an adsorbed H_2O molecule (section 4.1). That this actually occurs may be inferred from data obtained using other techniques.

Interpretation of the thermal desorption spectra is more complex, however, for those surfaces for which detailed information is available. On Rh(111) [127], Ni(111) [82,108] and Ru(001) [60], the highest-temperature state is far too narrow for first-order desorption kinetics with a "normal" pre-exponential factor of 10^{13} s^{-1}; furthermore, first-order kinetics cannot explain the small, but consistently-observed shift to higher peak temperatures with increasing coverage. (Similar qualitative experimental observations have been described for Pd(100) [129].) Such narrow peaks demand pre-exponential rate factors on the order of 10^{20}–10^{22} s^{-1} and desorption energies of 71–88 kJ/mol, if simple first-order kinetics are maintained [60,82,127]. These rate parameters are, in the authors' judgment, improbable; furthermore, the shift to higher peak temperatures is still not explained with this model.

Another approach, which fits the data more successfully, is to assume first-order desorption kinetics, a "normal" value of 10^{13} s^{-1} for A, and attractive interactions between particles on the order of a few kJ per mole. In the case of Ni(111) this explains both the peak shape and position well [82,108], and presumably it could be used to model desorption from other

surfaces also. With this model, a chemisorption energy of about 42 kJ/mol is still obtained for Ni(111). The coverage-dependent attractive lateral interaction term (1.4 kJ/mol) is significantly smaller than single hydrogen bond energies in water (15–25 kJ/mol). If this model is physically correct, then we speculate that the value of 1.4 kJ/mol may instead represent a subtle coverage-dependence in the strength of intermolecular hydrogen bonding. This might occur via dipole reorientation in hydrogen-bonded water clusters as surface coverage increases. In any case, the qualitative similarities of the high-temperature states for the hexagonal surfaces of Rh, Ru and Ni, and the square surface of Pd, suggest that the nature of the desorption process may be similar on all of these smooth metal planes.

Another interpretation of these data is similar to that proposed for water on Pt(111) [146] and discussed for water on Ag(110) [185]. In this model, H_2O diffuses rapidly at low coverages to form hydrogen-bonded clusters (islands) on the surface. Desorption of H_2O from clusters may proceed with a desorption order less than one. (Free sublimation from an ice multilayer, for example, proceeds via zero-order kinetics.) This is consistent with the small shift of T_p as coverage increases. Arthur and Cho [186] show evidence for fractional-order desorption kinetics in desorption of metals (Cu and Au) from islands on a graphite surface, as do Bauer et al. [187] for desorption of Cu and Au from islands on W(110) More detailed data, e.g. isosteric heats of adsorption, would be very valuable before complex models involving coverage-dependent values of A or fractional-order rate processes are approached, however. At present, we feel that the 42–50 kJ/mol values are probably correct for the chemisorption bond strengths on the smooth surfaces, especially in view of the propensity for adsorbed H_2O to form hydrogen-bonded clusters in these and other systems

For the hexagonal surfaces, it is tempting to draw a correlation between the existence of multiple molecular desorption states and the existence of well-ordered hydrogen-bonded clusters, which are presumably favored by a particularly good match between the lattice constant of the metal and the ice-like cluster [60,79]. For this reason, in fig. 32 the highest TDS peak temperature is shown as a function of the difference between the metal lattice constant and the corresponding ice lattice constant. (Note that this does not correspond to the *nearest*-neighbor distance in ice, but to the *next-nearest*-neighbor distance – the reasons for this choice are discussed more fully in sections 4.3 and 4.4.) The most interesting group is the cluster of Re, Ru and Rh (shown with filled circles), which fall within -0.26 to -0.15 Å of ice. Two of these three metals also show strong evidence for both short-range and long-range structure (sections 4.3 and 4.4) while the third (Rh) exhibits long-range structure but its short-range order has not been studied [127]. These three metals have the three highest-temperature molecular states of all the hexagonal surfaces studied to date. In contrast, on Ni(111), the water clusters do not form in short-range

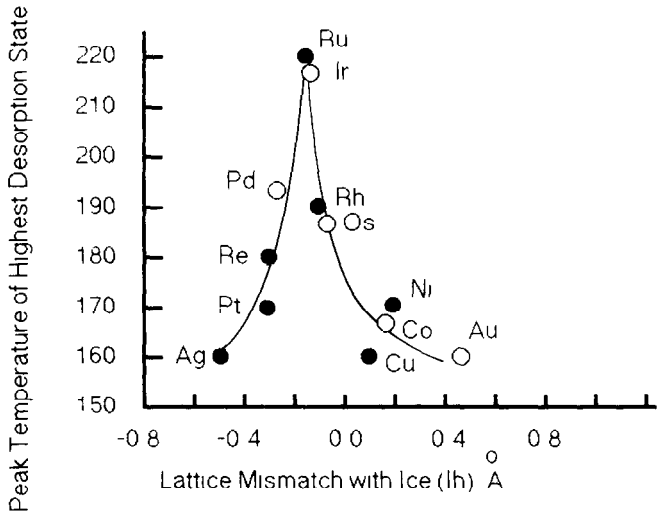

Fig 32 Peak temperature of highest desorption state of molecular H_2O on hexagonal transition metal surfaces, shown as a function of lattice mismatch between the metal and crystalline ice Darkened symbols represent experimental measurements, as described in text, open symbols represent predicted experimental outcomes The reader should keep in mind that exact peak temperature depends slightly on heating rate and coverage

ordered arrays [82]; also, only a single desorption state at 168–171 K is resolved from the ice feature [82,108]. For purposes of future predictions, metals for which TDS have not yet been measured are shown with open circles. If the rough correlation shown in fig. 32 between TDS peak temperature and lattice mismatch extends to other metals, one might expect that Ir(111), Pd(111) and Os(001) all behave similarly to Ru and Re with respect to molecular adsorption characteristics, particularly multiplicity of TDS chemisorption states and short-range order. These rough predictions must await refinement based upon results of future experiments, however.

The identification of the multiple desorption states on Ru(001) is discussed in section 4.4.2. We note here that the highest-temperature state is associated with small hydrogen-bonded clusters which form by *conversion* from larger clusters. Conversion is much slower for D_2O than for H_2O (isotope effect), so that the high-temperature state is suppressed in D_2O desorption from Ru(001) [188].

4.2.4. Chemisorbed states on atomically rough surfaces

Water on the rougher, more "open" (110) surfaces of Pt, Pd, Ni, and Cu exhibits desorption states at significantly higher temperatures than the corresponding smooth (100) and (111) surfaces, whereas Ag(110), Ag(112) and

Ag(311) do not show any state in thermal desorption distinguishable from the ice multilayers observed on Ag(111). The heats of adsorption on the atomically rough surfaces are generally about 10–20 kJ/mol higher than on the smoother surfaces, assuming first-order desorption kinetics with $A = 10^{13}$ s^{-1}. It appears that when the metal–H_2O interaction is extremely weak, as for Ag, the surface morphology cannot exert enough influence to change the bond strength measurably, but for slightly stronger interactions (as for Cu, Pt or Ni) the influence of surface morphology is apparent. The reasons why a rougher surface presents an effectively stronger interaction should probably be thought of in terms of the nature of H_2O bonding to a single metal atom versus a large metal cluster. The calculation of Ribarsky, Luedtke and Landman [66] shows that the binding energy of an H_2O–Cu complex is just twice that of an H_2O–Cu_5 complex. This is apparently explained by a rather simple picture of H_2O–metal bonding: since bond formation only involves electron transfer from H_2O to the metal, the H_2O effectively acts as a Lewis base (section 2). Coordinative unsaturation increases the acidity (electron deficiency) of the metal, which increases its ability to accept electrons from the H_2O ligand. This leads to the conclusion that H_2O molecules on a stepped or corrugated surface probably occupy positions at the tops of the ridges or steps, where the metal atoms are most exposed. It should be remembered that this is an extremely simple picture. It provides a plausibility argument, however, for the slight face-specificity of bond strengths illustrated in table 9. Furthermore, it is supported by a structural study of H_2O dimers on Ni(110) [113], which indicates that at low coverages the H_2O molecules preferentially occupy sites *atop* the (110) ridges (see section 4.4.3).

4.3. Long-range structure of the H_2O lattice

Years ago, meteorologists observed that there was a correlation between the type of nuclei used to seed clouds, and the effectiveness of the nuclei in stimulating precipitation. (This is discussed at length in section 7.) The surface morphology of the nucleation particles was thought to be important. Indeed, silver iodide is believed to be particularly efficient, at least in part, because its lattice constant matches very closely that of ice [4,5]. However, in a comparative study of various ionic substances as nucleation materials, Mason concludes that the strength of the water–substrate interaction is also critical [4]. These basic ideas regarding surface lattice structure and ice overlayer growth, proposed by meteorologists over forty years ago [4], are being rediscovered today for metal substrates.

In some cases, H_2O adsorbed on metal surfaces forms ice-like structures which have long-range order; this two-dimensional periodicity is observable with the technique of low-energy electron diffraction (LEED), which can also measure the two-dimensional periodicity of the metal lattice. This type of long-range structure is reported, for instance, by Firment and Somorjai [189],

who observe hexagonal patterns for epitaxial ice grown on Pt(111) and Ag(111) surfaces for adsorption temperatures between 120 and 150 K. They further observe that the hexagonal structure can be either parallel to, or rotated by 30° from, the Ag(111) unit cell, whereas only the 30°-rotated structure is observed for the Pt(111) substrate. They interpret this in terms of the mismatch between a hexagonal crystalline ice lattice and the metal substrate. The mismatch is about equal for both types of superstructures which exist on Ag, but on Pt it is smaller by 0.4 Å for the lattice which is rotated 30° [189]. It is obvious from these data that the metal surface acts as a template for the overlying ice layers, which try to remain in registry with the substrate as closely as possible while maintaining the intermolecular separation of ice. [The LEED data are taken to reflect only the positions of the oxygen atoms, not the hydrogen atoms, for two reasons. First, intensities of fractional-order spots due to ordered arrays of hydrogen atoms on metal surfaces are generally quite weak [190,191], weaker than the spots of the (1×1) pattern. Fractional-order beams due to oxygen, however, can be quite intense. Second, the positions of hydrogen atoms in fig. 33 cannot be reconciled with a simple $(\sqrt{3} \times \sqrt{3})R30°$ superlattice, whereas the positions of the oxygen atoms can be easily explained with this model.] Long-range structure is also observed for H_2O/Ru(001) [60], where a similar $(\sqrt{3} \times \sqrt{3})R30°$ superstructure exists even at *low* coverages of H_2O during adsorption at ~ 120 K. Using other data which show that intermolecular hydrogen bonds form at these coverages, a model is proposed in which the H_2O forms ice-like clusters even at low coverage [60]. In this model, the H_2O can form three-dimensional structures in which a "first layer" of water molecules is bound by direct chemisorption bonds, and molecules in the second layer are held by two or three hydrogen bonds to the first-layer molecules. Together, these two layers are termed a "bilayer". The $(\sqrt{3} \times \sqrt{3})R30°$ structure, then, is a nonprimitive lattice with an absolute ideal coverage of $\theta = 2/3$ for the first two layers. In each unit cell, one H_2O molecule is in the first layer and one is in the second. ($\theta = 1$ monolayer is herein defined as 1 adsorbed particle per surface metal atom.) Vibrational spectra indicate that the properties of the first two layers are indeed distinct from ice multilayers [60]. As noted elsewhere in this article, the thermal desorption experiments support the general thermodynamic feasibility of cluster formation in this manner [60]. A continuous, coverage-dependent splitting of the spots of the $(\sqrt{3} \times \sqrt{3})R30°$ LEED pattern on Ru(001) [79] is examined in some detail by Williams and Doering [192]. They propose a model in which antiphase domains of bilayer islands cause the spot splitting [192]. In this model also, the first-layer H_2O molecules maintain specific adsorption sites at the expense of some small strain in the ice lattice: this strain effectively limits the bilayer domain size. A schematic depiction of a perfect extended bilayer, with the $(\sqrt{3} \times \sqrt{3})R30°$ unit cell outlined, is shown in fig. 33.

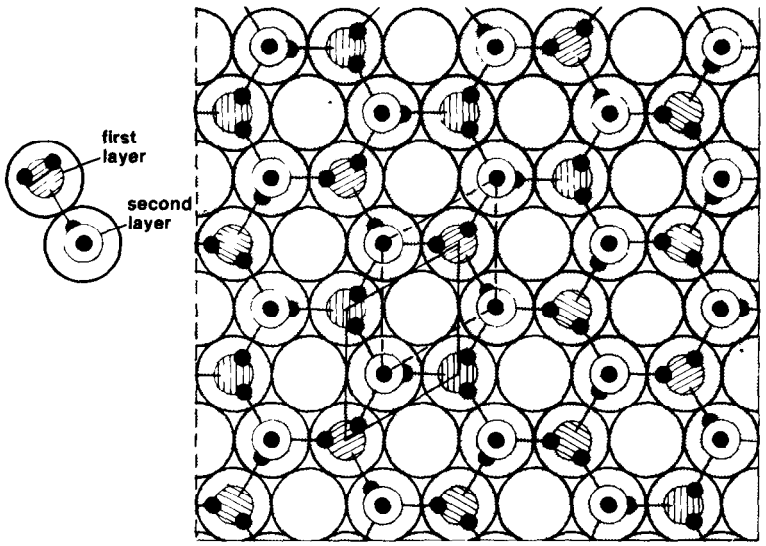

Fig 33. Schematic diagram of a perfect, infinite, adsorbed, water bilayer Taken from Doering and Madey [79].

LEED patterns have now been reported also for several other hexagonal H_2O–metal systems at even low H_2O coverages, as listed in table 10. Interestingly enough, the data indicate that, for the hexagonal surfaces, the goodness of fit between the metal surface and bulk ice lattices is the main factor which determines whether a periodic H_2O lattice will form at H_2O coverages which are below that required for the ice multilayer. For Ag(111) [131], the $\sqrt{3}\,a$ parameter of the metal unit cell is evidently too large to accommodate a hydrogen-bonded lattice readily while maintaining specific adsorption sites for the first layer of H_2O molecules. In turn, this implies that chemisorbed H_2O is at least somewhat site-sensitive; to build a long-range periodic lattice, the first layer of chemisorbed H_2O is not willing to sacrifice specific adsorption sites, in spite of the weakness of the chemisorption bond. Empirically, we can conclude that a $(\sqrt{3} \times \sqrt{3})$R30° H_2O overlayer will form on those hexagonal substrates for which the nearest-neighbor distance between water molecules is greater than about 4.31 Å (Ni), but less than 5.01 Å (Ag). These limits may change as new data are accumulated.

On the square lattices, no evidence for long-range structure has yet been observed, though there is strong evidence for intermolecular hydrogen bonding even at low coverages (e.g. [81,129]).

On the (110) lattices, a c(2 × 2) pattern is reported for Cu and Ni [113,117,118]. This is interpreted by several authors in terms of a slightly distorted hexagonal ice-like bilayer, as shown in fig. 34, where the c(2 × 2) unit

Table 10
Summary of long-range ordered structures (observed with LEED) and preferred molecular orientations (observed with ESDIAD) at low H_2O coverages on metal surfaces

Metal surface	Related lattice parameter (Å)	LEED pattern of adsorbed H_2O, *low* θ	Evidence of preferred molecular orientation at low coverage?	Adsorption temperature (K)	Refs
(i) Hexagonal $\sqrt{3}\,a$					
Ag(111)	5.009	None	No	80	[131]
Ni(111)	4.31	None at lower coverages, $(\sqrt{3}\times\sqrt{3})R30°$ at $\theta\approx 1$	Poor	80	[82]
Ice I	4.48–4.52	N/A	N/A	90	[46]
Rh(111)	4.66	$(\sqrt{3}\times\sqrt{3})R30°$	–	Not reported	[127]
Ru(001)	4.69	$(\sqrt{3}\times\sqrt{3})R30°$	Yes	80	[60,79,192]
		split $(\sqrt{3}\times\sqrt{3})R30°$		$150 \leqslant T \leqslant 200$	[79,192]
Re(001	4.78	$(\sqrt{3}\times\sqrt{3})R30°$	Yes	80	[139]
		$c(2\times 2)$		>150	
Pt(111)	4.80	$(\sqrt{3}\times\sqrt{3})R30°$	–	100	[145,146, 148,189]
Pt(100)-(5×20)	?	Unidentified	–	150	[144]
(ii) Square N/A					
Ag(100)		None	–	80	[131]
Pd(100)		None	–	110	[81,129]
(iii) Corrugated 2a					
Ag(110)		None	Poor to none	100	[84,123,132]
Cu(110)		$c(2\times 2)$	Yes	90	[117–119,123, 193,194]
Ag(112)	N/A	None	–	80	[131]
Ag(311)	N/A	None	Yes	95	[133]
Ni(110)		$c(2\times 2)$	Yes	$\leqslant 150$	[112,113]

cell is outlined. The similarity between this type of H_2O lattice, and the one shown in fig. 33, is apparent.

In summary, studies of the long-range structure of H_2O layers rely upon LEED. They consistently indicate that H_2O forms three-dimensional ice-like layers in which the first-layer H_2O molecules tend to occupy specific adsorption sites and the second-layer molecules are hydrogen-bonded to the first layer. Thus, the first layer or two mainly feel the template effect of the substrate and subsequent layers mainly feel the forces which are present in bulk ice. The hexagonal surfaces generally form nonprimitive $(\sqrt{3}\times\sqrt{3})R30°$ lattices (fig. 33) when the lattice mismatch between the metal and bulk ice is

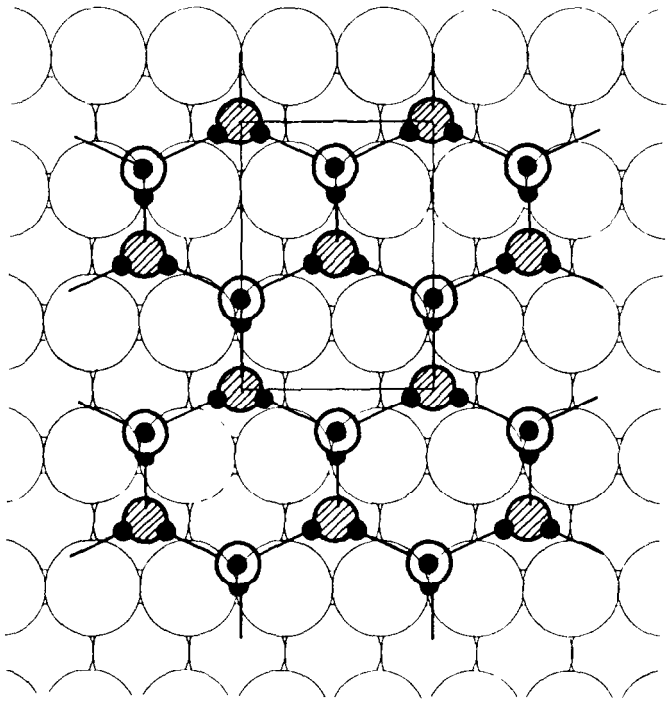

Fig 34 Schematic diagram of a compressed H_2O bilayer giving a c(2×2) LEED pattern on an fcc(110) surface [113,117,118]

not too great, while the ridged (110) surfaces of the fcc metals tend to form c(2 × 2) lattices (fig. 34).

This entire discussion, of course, assumes that the electronic differences between metals as dissimilar as Re and Ag are unimportant. As we have seen in section 3.1, this is simply not true in terms of how easily H_2O dissociates at a metal surface; but it *does* appear to be a reasonable working hypothesis for predicting the long-range periodicity of H_2O on metal surfaces at low temperatures (~ 80 K) and low coverage, in those cases where dissociation does not occur.

4.4. Orientations of adsorbed H_2O molecules

4.4.1. Background

The long-range order observed in LEED studies of H_2O is a manifestation of the positions of the O atoms in the molecular layer; even if the H atoms were ordered in a long-range sense, the scattering by H is too weak to contribute significantly to LEED intensity measurements. Molecules in the

adsorbed layer may preferentially adopt a particular azimuthal and polar orientation, even in the absence of any long-range (LEED) order. In this review, we examine the orientation of OH bonds: we define preferential orientation to exist in an assembly of adsorbed H_2O molecules when a substantial fraction of the molecules have OH bonds oriented along specific polar and/or azimuthal directions with respect to the substrate symmetry directions.

Solid but indirect evidence for the existence of such preferred orientation in adsorbed H_2O is based on the long-range order seen in LEED coupled with the well-documented occurrence of hydrogen bonding in the adsorbed layer. If the O atoms are fixed with respect to substrate atoms and hydrogen-bonded complexes are formed, it follows that some sort of polar and/or azimuthal registry of OH bonds must occur. The question is, what are the preferred orientations of OH bonds in specific cases?

Direct evidence for the orientation of adsorbed molecular H_2O is found using the ESDIAD method, which is described in section 3.2. Based upon data from this technique, which is sensitive to the angular orientation of OH bonds, a number of instances are presented in which OH bonds adopt specific azimuthal and/or polar registries with the substrate, and models of adsorbed H_2O clusters are developed. Several examples are discussed in the following sections.

4.4.2. Models for H_2O orientation on hexagonal substrates ice-like clusters

As discussed in section 4.3, the adsorption of H_2O on the hcp Ru(001) basal plane is accompanied by an interesting series of LEED patterns as a function of water coverage and temperature, indicative of complex long-range order [79,192]. The H^+ ESDIAD from H_2O on clean Ru(001) at 80 K provides direct evidence for preferred molecular orientation also [58,79]. At coverages less than 0.1 monolayer, a dim halo-like ESDIAD pattern is observed, with virtually no emission normal to the surface (fig. 35b [79]). At H_2O coverages greater than 0.1 monolayer, a hexagonal pattern of distinct spots is formed; the hexagon is rotated by 30° relative to the Ru(1 × 1) LEED pattern (fig. 35c [79]). Further increase in H_2O coverage leads to the development of normal emission, giving a central spot within the hexagon. As the H_2O coverage exceeds 0.67 monolayers, the hexagonal ordering of the ESDIAD pattern disappears, and a broad, random H^+ ESDIAD pattern appears. Detailed discussion of the "source structures" for the ESDIAD patterns in fig. 35 is given in the following paragraphs.

A sequence of ESDIAD patterns similar to fig. 35 is reported also for H_2O adsorbed on the hcp Re(001) surface at 80 K [142]. H_2O adsorbs molecularly on the smooth Re(001) surface at 80 K, but dissociates on a stepped Re(001) surface at this temperature [139]. Above 250 K, adsorption is dissociative on

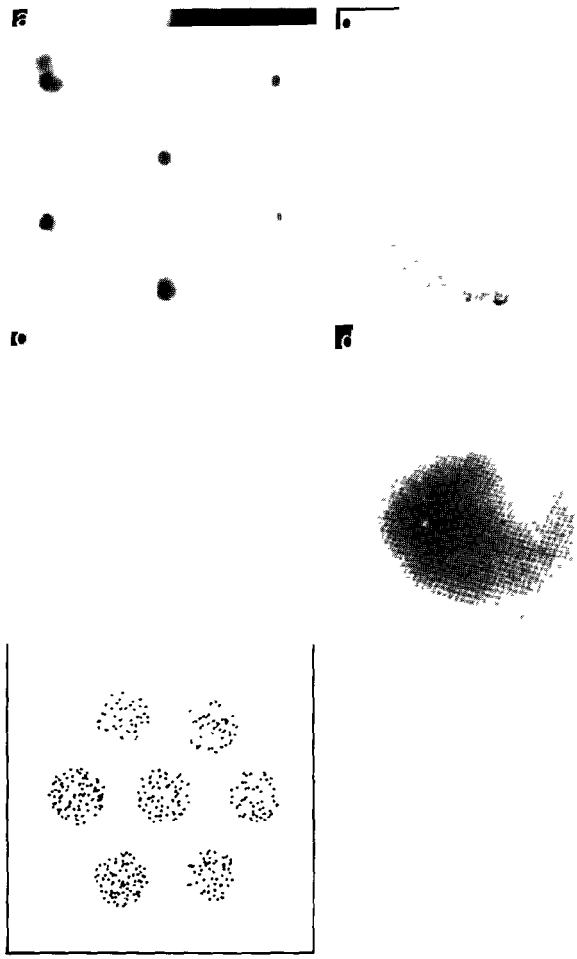

Fig. 35 (a) Ru(001)-(1×1) LEED pattern demonstrating the crystal orientation. (b)–(d) ESDIAD patterns of H_2O adsorbed on Ru(001) at 80 K with various coverages. (b) $\theta_{H_2O} < 0.1$, (c) $\theta_{H_2O} \simeq 0.33$, (d) $\theta_{H_2O} > 0.67$. A schematic representation of pattern (c) is provided for clarity. Taken from Doering and Madey [79]

both Re surfaces, and the LEED and ESDIAD are more complex than for Ru(001).

Hydrogen-bonded H_2O structures which have varying degrees of consistency with the data of fig. 35 are proposed by several groups [58,60,170]. Doering and Madey [79] propose, however, that the modified Bernal–Fowler–Pauling rules, described in section 2.2.2 may be particularly appropriate to

the interaction of water with Ru(001) because of the close match of the ice and Ru lattice spacings and the strength of the H_2O–metal interaction (cf. discussion in section 4.3). In bulk ice, the oxygen–oxygen nearest-neighbor distance varies from 2.74 to 2.76 Å between 90 and 270 K [27]. The distance of closest approach of two non-hydrogen-bonded H_2O molecules is 4.52 Å [27]. This distance can be compared with the next-nearest-neighbor distance in the metal lattice; for the hexagonal Ru(001) and Re(001) substrates, these distances are 4.68 and 4.78 Å, respectively. Epitaxial ordering of a hexagonal ice lattice thus is slightly more favored on Ru(001) than on Re(001), although the similarity of ESDIAD patterns for the two surfaces [79,139] suggests that the ice-like adsorbed layer grows in the same way on both substrates.

Now we examine the structures predicted for the adsorption of H_2O on Ru(001) based on the BFP rules and their surface modifications (cf. sections 2.2.2 and 2.2.3), and we follow with an interpretation of the ESDIAD data of fig. 35 based on these structures.

Based on BFP rules, combined with EELS and LEED data [60], H_2O forms three-dimensional structures in which a "first layer" of H_2O molecules is bound to the substrate by chemisorption bonds and a "second layer" of molecules is bound by two or three hydrogen bonds to the first layer molecules. Together, these two layers form a "bilayer" with an ideal H_2O density of 1.0×10^{15} molecules/cm^2, i.e., 2/3 monolayers of H_2O on Ru(001). A model of the ideal bilayer is shown in fig. 33 (p. 267).

The electric dipole moment of the water molecule lies along the C_{2v} symmetry axis with the negative end toward the O atom. If the molecule has a component of the dipole moment away from the metal, it is referred to as a "flip-up" molecule and one with a component of the dipole moment toward the surface is referred to as a "flop-down" molecule. From surface modification (a) of the BFP rules (cf. section 2.2.3), all molecules of the first layer are "flip-up". For the perfect bilayer of fig. 33, all of the second-layer molecules are also "flip-up", oriented with OH bonds perpendicular to the surface.

If the surface coverage is less than 2/3 monolayers, the modified BFP rules predict that finite bilayer clusters form, as shown in fig. 36c. Note that there are non-hydrogen-bonded OH ligands at the edges of the cluster, and that the second layer contains both flip-up and flop-down molecules. The fraction of flop-down second-layer molecules increases with decreasing cluster size (fig. 36b). A small cluster which satisfies all of the BFP rules and surface modifications is shown in fig. 36a. (Note that the nine-molecule cluster of fig. 36b has been incorrectly identified in ref. [79] as the smallest cluster consistent with the rules.)

Now, we are in a position to relate the ESDIAD patterns of fig. 35 to structures predicted by the BFP rules and surface modifications, as shown in table 11. The dim halo-like H^+ pattern (fig. 35b) seen at very low H_2O coverages ($\theta < 0.1$) may be due in part to isolated water molecules which are

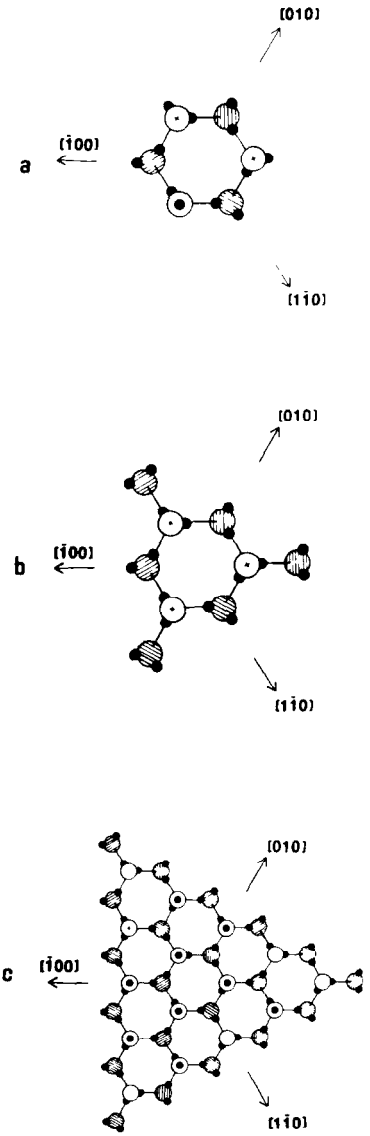

Fig. 36 (a) Schematic diagram of the smallest bilayer cluster which obeys the BFP rules and surface modifications (b) A nine-molecular water cluster. (c) A finite bilayer cluster consistent with the modified BFP rules, which may exist as the surface coverage approaches saturation of the bilayer (0 67 monolayers). Taken from Doering and Madey [79].

Table 11
Schematic drawings of ESDIAD patterns for H_2O on Ru(001), and their interpretation (from Doering and Madey [79])

ESDIAD pattern		Source structure
I Halo-like		Isolated water molecules, rotating or randomly oriented, small, poorly ordered clusters
II Hexagonal		Edges of finite water bilayer clusters with three-fold symmetry of the oxygen positions in two equally probable orientations
III Normal		Second layer flip-up water molecules in the bilayer, intensity increases with cluster area Over a wide coverage range ($0\,1 < \theta < 0\,67$) a combination of II and III is seen (as in fig 35c)
IV Random		Water multilayers which are either liquid-like or rocking

either randomly oriented azimuthally, or freely rotating. Disordered clusters smaller than the stable six-molecule structure of fig. 36a may also contribute to the halo. Note that hydrogen atoms involved in hydrogen bonding are not believed to contribute to the ESDIAD pattern.

As discussed in section 4.5, there is strong evidence from vibrational spectroscopies that an increasing degree of water cluster formation occurs with increasing coverage on this surface, especially for coverages $\theta_{H_2O} > 0.1$ [59,60]. Since this water overlayer eventually develops a $(\sqrt{3} \times \sqrt{3})R30°$ LEED pattern [59,60,79], the ice clusters of fig. 36 are assumed to be in registry with the Ru substrate. Then, H atoms within a cluster are always in positions of three-fold symmetry with respect to the O atoms (fig. 36). The hydrogen atoms involved in hydrogen bonding are not thought to contribute to the ESDIAD pattern [79], so that H ligands at the edges of a given cluster should give rise to three-fold symmetric ESD ion emission (the off-normal beams of fig. 35c). The six-fold symmetry of the ESDIAD pattern (fig. 35c) from these clusters probably results from the two possible orientations of the clusters on the hexagonal Ru(001) surface. The central beam in fig. 35c is due to second-layer

flip-up molecules, which produce H^+ ESD ion emission intensity normal to the surface. Since the fraction of the second-layer molecules in the flip-up orientation increases with increasing cluster area, the intensity of the normal ESDIAD beam increases with increasing fractional bilayer coverage (fig. 36).

Near saturation of a perfect bilayer, the hexagonal emission pattern from the cluster edges fades out, leaving primarily H^+ ESD emission normal to the surface and additional random H^+ emission from water multilayers which also form at fractional bilayer coverages. Water layers not directly bound to the Ru substrate may not be strongly bound in a regular structure, giving rise to a high intensity of random H^+ emission from multilayers (fig. 35d).

Thus, the ESDIAD data provide a "fingerprint" for a series of water structures having preferred local orientations of molecules, even at coverages below which the ordered $(\sqrt{3} \times \sqrt{3})R30°$ LEED structure is formed. During thermal desorption, starting from $\theta \approx 0.67$, one observes evidence in ESDIAD that the two desorption features associated with the chemisorbed layer are due to the breaking up of hydrogen-bonded clusters such as shown in fig. 36c at high coverage, followed by the dissolution of hydrogen-bonded clusters such as shown in fig. 36b at lower coverages (higher temperatures) [79]. The smaller clusters are created by conversion from the larger clusters [59,188], and this conversion step is much slower for D_2O than for H_2O [188]. Experimentally, one observes that the high-temperature state is suppressed for D_2O. The suppression is thought to occur because rotation of a water molecule within the cluster is the rate-limiting step for conversion between the two structures, and this rotation is much slower for the heavier isotope of water [188].

4.4.3. Models for H_2O orientation on fcc(110) surfaces: stable dimers

Based on the above discussions (section 4.4.2 and section 4.3), there is a clear rationale for the existence both of local preferred orientations and long-range order (observable in LEED) for H_2O on substrates having hexagonal symmetry [i.e., hcp(001) surfaces and fcc(111) surfaces]. LEED patterns are also reported for H_2O on two-fold symmetric Cu(110) and Ni(110) surfaces, and are thought to represent strained, quasi-hexagonal H_2O bilayers [113,118]. Evidence also exists that a stable cluster at low coverages on a Ni(110) surface may be the smallest of all possible clusters, the H_2O dimer [113], and that the dimers exhibit preferred azimuthal and polar orientations of OH bonds.

Nöbl et al. [113] suggest that oriented H_2O dimers form at fractional monolayer coverages, $\theta_{H_2O} = 0.2$ to 0.5, on Ni(110) at $T < 150$ K. This conclusion is founded primarily on angle-resolved UPS (ARUPS) measurements, and is supported by EELS data [112]. The UPS data exhibit a characteristic splitting of the adsorbate-induced peaks, similar to the data of Schmeisser et al. [57] for H_2O on uranium nitride. Based on the molecular orbital calculations of Morokuma and Umeyama [195,196], this splitting is

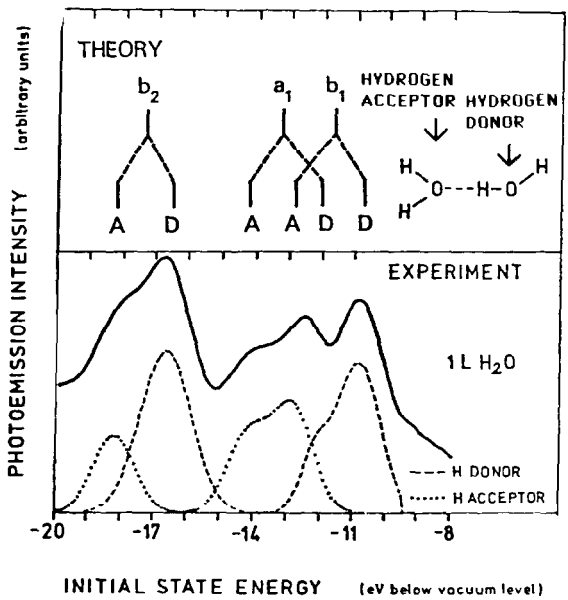

Fig 37. Analysis of the photoemission spectrum following a 1 L exposure of water on uranium nitride at 41 eV photon energy The observed splitting of the three molecular orbitals is explained by comparison with the calculated binding energies [196] of the proton-acceptor (A) and the proton-donor (D) levels for the linear water dimer (schematic sketch) Taken from Schmeisser et al. [57].

associated with H_2O dimer species containing one H-donor and one H-acceptor molecule. (See fig. 37 for a schematic of the splitting, and the UPS data of Schmeisser et al. [57].) The splitting of the three H_2O features ($1b_1$, $3a_1$, $1b_2$) is absent for larger hydrogen-bonded clusters on Ni(110) because each H_2O molecule acts as a H-donor and H-acceptor at the same time.

Evidence that the dimers have specific orientations on the Ni(110) substrate is provided by ARUPS and ESDIAD [113]: both methods lead to the identical conclusion that the dimers are oriented along [001] directions. Fig. 38 contains LEED and ESDIAD patterns for H_2O on Ni(110), together with a model of the dimer structure. The LEED pattern of the clean surface (fig. 38a) provides the basis for identifying the azimuthal orientation of the "four-spot" H^+ ESDIAD pattern (fig. 38b) characteristic of H_2O at low coverages. This pattern is consistent with the dimer model of fig 38c in which three H atoms and one oxygen lone pair from the proton donor molecule point away from the surface in specific azimuthal directions. These four directions are suggested to be active for H^+ ESD emission. (Note that the lone pair is not perpendicular to the surface, which is a slight relaxation of the surface modifications to the BFP rules.) The direction of the oxygen lone pair becomes equivalent to an

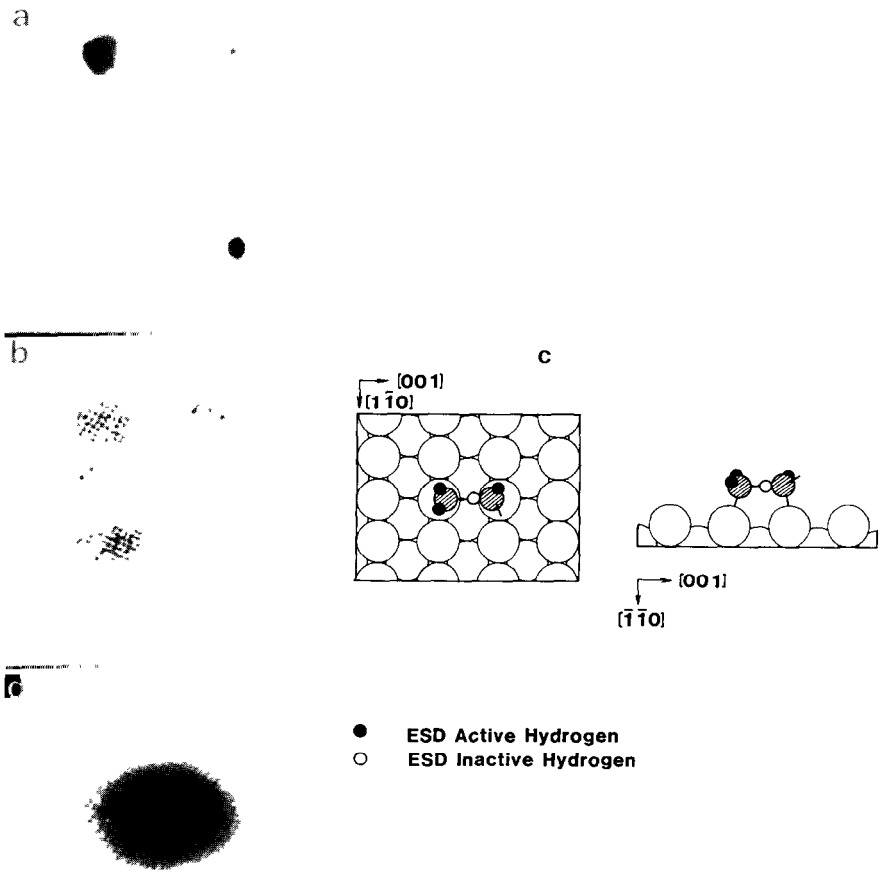

Fig. 38 LEED (a) and H^+ ESDIAD (b,d) patterns for H_2O on Ni(110) Primary electron energy, E_p, for LEED is 70 eV and for ESDIAD 350 eV In (b), ESDIAD is dominated by a "four-spot" pattern due to H_2O dimers in addition, two weak spots in the [001] azimuthal direction are observed, caused by electron beam damage (c) Model for H_2O dimer orientation on Ni(110) A model for pattern (d) is given in fig 34 (p. 269) Taken from Nobl et al. [113]

H^+ active O–H direction by rotating the dimer 180°. If we assume that the azimuthal directions of the H^+ emission are determined by these four bond directions, a "four-spot" ESDIAD pattern results.

UPS studies of H_2O on other metal surfaces [e.g., Ni(111) [147], Cu(100) [117] and Pt(111) [145]] do not reveal evidence for dimer formation. Due to the high mobility of H_2O at low coverages (section 4.1) as well as the strong

attractive hydrogen-bonding interaction, larger two-dimensional clusters probably form immediately upon adsorption.

Why, then, do dimers form on Ni(110)? The dimer appears to be the stable form at low H_2O coverages due to a moderately strong H_2O–metal bond (table 9), combined with a good geometrical match between the oxygen lone pairs of the dimer and the Ni(110) substrate: the structure of the gas-phase dimer must be perturbed only slightly to achieve the configuration shown in fig. 38c. Moreover, the existence of ordered LEED structures at low coverages on Ni(110) [113,162] indicates that the net dimer–dimer interaction is repulsive. However, as the H_2O coverage increases beyond $\theta_{H_2O} \approx 0.5$, the interaction between neighboring molecules forces some of the H_2O dimer molecules into second-layer position, and a distorted quasi-hexagonal bilayer forms (see fig. 34, p. 269). This bilayer is discussed more fully in section 4.3, and is observed also on Cu(110).

ESDIAD data for H_2O on Cu(110) [193,194], Ag(110) [185] and Pd(110) [130] also reveal "four-spot" ESDIAD patterns at low H_2O coverages but the molecular structures giving rise to these patterns are not verified using other surface-sensitive techniques, nor is it clear whether the structures always form in the absence of impurities Irrespective of the details of the adsorbate structures, however, it appears that H_2O adopts preferred orientations when it is adsorbed on the (110) surfaces of several fcc metals, including Ni, Ag, Cu, and Pd. The local atomic roughness of these ridged surfaces apparently results in unique orientations of H_2O, which are not found on smoother surfaces of the same metals (Ni(111) [82], Ag(100), Ag(111) [131]).

4.4.4 Summary of data on molecular orientation

When we consider the range of metal surfaces on which water adsorption has been studied using ESDIAD and LEED, several general conclusions can be reached. H_2O exhibits little or no azimuthal or polar orientation for substrates on which the chemisorption bond is weak [Cu(100), Ag(100), Ag(111)]; exceptions are two atomically-rough surfaces, Ag(110) [185] and Ag(311) [133]. For Ni(111) [82], on which H_2O is slightly more strongly bound, there is no clearly-defined azimuthal H_2O orientation revealed by ESDIAD, presumably due to the lattice mismatch. There is, however, evidence of preferred ion desorption along non-normal directions on Ni(110), suggesting that there are few "flip-up" molecules at fractional-monolayer coverages. On surfaces which bind molecular H_2O relatively strongly [Ni(110), Ru(001), Re(001)], the evidence for preferred orientations is strong and clear. Thus, on surfaces where H_2O is strongly bound and/or atomically rough, the surface acts to induce preferred orientations in the adsorbed layer, even at fractional-monolayer coverages. Much more work is necessary to broaden these generalizations, including studies on surfaces of four-fold symmetry and surfaces having widely different lattice parameters.

In closing this section, we note that the data on molecular orientations are included, for comparison with LEED measurements, in table 10 (p. 268).

4.5. Vibrational spectra of H_2O

In 1967, Propst and Piper were the first to study the vibrational spectra of H_2O (probably dissociated) on a surface using electron energy loss spectroscopy (EELS) [138]. This technique has proven to be our most generally useful probe of vibrational properties of water at surfaces, mainly because of the wide spectral range which is routinely accessible to it ($\nu \gtrsim 100$ cm^{-1}) and the ability to isolate cleanly the water–metal interface in ultrahigh vacuum. The vibrational spectra of molecularly adsorbed H_2O have been obtained, using electron energy loss spectroscopy, for the following surfaces: Rh(111) [197], Ni(110) [112], Ru(001) [59,60], Pd(100) [81,129], Pt(111) [146], Pt(100) [144], Cu(100) [56, 198], Ag(110) [132] and Ag(100) [137]. In addition, H_2O on Ru(001) and Pt(111) has been studied with infrared reflectance-absorbance spectroscopy (IRAS) [148,170]. Some work has also been done with surface enhanced Raman scattering (SERS) (e.g. [199]), but, as discussed by Blatchford et al. [200], this technique has not proven as sensitive in detecting the O–H fundamental mode as it has in detecting lower-frequency vibrational modes, and this seems to place a major constraint on its usefulness. A second major drawback is the necessity of using roughened Ag, Au, or Cu surfaces in order to gain an enhancement of 10^3 or greater. Finally, even with enhancement, this technique does not seem promising for the study of water at surfaces immersed in aqueous solution due to the large competitive signal from the solvent [199,200], although some very nice work has been done using SERS in ultrahigh vacuum [199].

As discussed in sections 2 and 3.2, the vibrational spectrum of H_2O in the gas phase consists of bands due to the O–H stretch, ν(OH), and the intramolecular deformation, or scissoring mode, δ(HOH). Upon adsorption at a metal surface, the translational and rotational degrees of freedom become frustrated (cf. fig. 26), giving rise to additional bands in the vibrational spectrum. A frustrated rotation is also known as a libration, and the frustrated translation perpendicular to the surface is usually referred to as the metal–admolecule (in this case, metal–H_2O) stretch. In bulk ice, an analogous frustrated H_2O–H_2O translation at very low frequency is also observed [27,44]. The frequency ranges which are broadly associated with each type of vibration are listed in table 3 (p. 231). Frequencies obtained in specific studies of surfaces are listed in tables 6 and 7 (pp. 251 and 252). We first examine the EEL spectrum of ice multilayers; with this as a reference, we then turn our attention to the EEL spectra of chemisorbed H_2O, to see what information each type of vibrational feature provides about the H_2O–metal system.

The EEL spectrum of ice multilayers on Ag(110) is shown in fig. 39 [132];

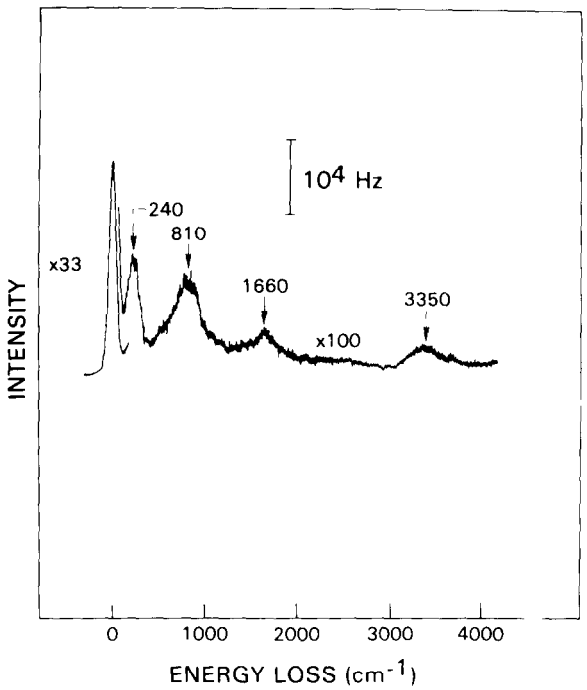

Fig 39 EEL spectrum of H_2O adsorbed on clean Ag(110) at 100 K, after an exposure of approximately 2×10^{15} molecules cm^{-2} Taken from Stuve et al [132]

this spectrum is not sensitive to the metal substrate, and very similar spectra are reported also for ice on Cu(100) [56], Pt(111) [147], Pt(100) [144], Ru(001) [59,60], and Fe(100) [103]. SER spectra of ice on polycrystalline Ag [199] also show essential agreement with these data. As fig. 39 shows, the frustrated H_2O–H_2O translation appears at 240 cm^{-1}, a broad feature due to frustrated rotations (librations) has maximum intensity at 810 cm^{-1}, the scissoring mode (intramolecular deformation) occurs at 1660 cm^{-1}, and the O–H stretch causes a broad loss feature centered at 3350 cm^{-1}. These frequencies and assignments are in agreement with the infrared spectra of bulk ice at ~ 90 K [27,44]. Both ν(OH) and δ(HOH) are strongly perturbed relative to the gas-phase spectrum, due to the formation of hydrogen bonds. As discussed in section 2.2.2, hydrogen-bond formation causes the FWHM of ν(OH) to increase while its maximum frequency decreases, relative to the gas phase; it also induces an *upward* frequency shift in δ(HOH) of about 50 cm^{-1}.

The frequency and broad width of the ν(OH) feature are usually similar for lower coverages of water, providing the clearest evidence that hydrogen bonding occurs even at low coverage on metal surfaces (e.g. [59,81,137]). This is illustrated also in the data of fig. 39 [132]. In such systems, hydrogen

bonding typically results in peak maxima between 3200 and 3400 cm^{-1} and FWHM as high as 500 cm^{-1}, to be compared with gas-phase frequencies of 3660 and 3760 cm^{-1} for the asymmetric and symmetric O–H stretches, respectively, and corresponding line widths which are below 1 cm^{-1} for the isolated molecules [27].

In addition to hydrogen-bonded moieties, it is believed that in some cases different types of OH groups can exist on the surface, whose natures can be deduced from the vibrational spectra. The simplest of these is the *non-hydrogen-bonded OH group* of an undissociated H_2O molecule. One can also make the following distinction: either the second OH unit of the molecule forms a bond elsewhere (to another H_2O molecule, or to the surface), or it is also free. In the latter case, there should be only the asymmetric and symmetric components of the ν(OH) peak in the spectrum of this molecule. [Note that of these two, only the symmetric O–H stretch is dipole-allowed under simple C_{2v} symmetry (cf. fig. 14, p. 230), or under any symmetry wherein the molecule–surface complex retains a C_2 axis.] In the former case features at other frequencies will be observed as well. The latter type is usually called an H_2O monomer, to distinguish it from H_2O in hydrogen-bonded aggregates. (In principle one *could* have isolated H_2O molecules with one free OH group and one bonding to the surface, but this is usually not expected. In the absence of secondary influences, theory predicts surface bonding through the oxygen atom's "lone pair" orbitals and a high degree of symmetry in the chemisorbed state. This is discussed more fully in section 2.)

Evidence for a non-hydrogen-bonded OH group is reported by Ibach and Lehwald on Pt(100) [144], where a relative narrow band at 3670 cm^{-1} occurs, surprisingly close to the gas-phase frequency. However, this feature is never observed without the hydrogen-bonded OH stretch also, i.e. isolated H_2O monomers alone cannot be prepared at the adsorption temperature (100 K). Therefore this feature may be due only to the O–H stretch of nonbonded OH groups at the peripheries of hydrogen-bonded aggregates, or to coexistent monomers and aggregates [144]. Stuve, Madix and Sexton prepare a Ag(110) surface with oxygen and H_2O coadsorbed, in which a narrow ν(OH) peak appears in EELS at 3600–3670 cm^{-1} [132]. This is assigned to the H_2O molecules isolated in the metal "troughs", with hydrogen-bonding somehow prevented by the oxygen adatoms. Ollé, Salmeron and Baró have assigned an O–H stretching vibration at 3610 cm^{-1} to non-hydrogen-bonded OH groups on Ni(110) [112]. On Ru(001), a feature at 3500–3565 cm^{-1} has been assigned to single OH groups at the borders and surfaces of hydrogen-bonded clusters [59]; because of the extensive supporting data from ESDIAD studies [79], this is a firm assignment. Furthermore, at very low coverages, isolated H_2O molecules are identified at 80 K on this surface, with ν(OH) at 3600 cm^{-1} [59]. In short, non-hydrogen-bonded OH groups at metal surfaces tend to have rather high vibrational frequencies between 3500 and 3670 cm^{-1}, with narrow

peaks whose FWHM approach the limiting resolution of the typical EEL spectrometer (~ 50–$100\ cm^{-1}$).

A third basic type of OH group is one which forms a *bond to the metal surface*. Evidence for such types of bonds is reported on Pt(100) [144], and Ru(001) [59]. These groups always cause relatively weak features in the vibrational spectra, indicating that they are minority species. Their frequencies fall in the range of 2850–2935 cm^{-1}, representing a "softening" of the OH fundamental. An interesting analog exists for several cyclic hydrocarbons, most notably chemisorbed cyclohexane on hexagonal Pt, Ni, and Ru surfaces, where some C–H bonds of the molecule point into the surface and are "softened" by the resultant strong interaction (e.g. [201,202]). Some other possibilities for the assignment of these features in chemisorbed H_2O *do* exist, most important of which are a Fermi resonance between $2[\delta(HOH)]$ and $\nu(OH)$, well-known in the liquid state [203], and a strongly distorted intermolecular hydrogen bond [41]. However, the experimental isotopic frequency shift [144], the coverage-dependent behavior, and the intensities with respect to other vibrational features [144,59] appear to preclude such alternative explanations for the features in this frequency range.

If they are in the minority, why do such bonds form at all? One possible answer is that they are structurally necessary to the larger hydrogen-bonded cluster, perhaps existing only at its periphery, or that they exist only in very small clusters of two or three molecules [204]. A similar concept is proposed by Ibach and Lehwald for H_2O on Pt(100) [144].

It should be kept in mind that *not all* types of OH groups exist on every surface; but it does appear that the existing data now provide a predictive basis for future assignment of OH vibrational features to certain types of OH groups. The amount of data upon which this conclusion rests is already much larger than the early matrix isolation experiments on H_2O clusters which prompted such interest on the part of physical chemists [20].

The *scissoring mode* is also a potentially good source of information about chemisorbed water. The information which can be obtained is of two types: (1) With some caution about experimental sensitivity, the presence or absence of this feature can be taken to indicate nondissociative or dissociative adsorption, respectively, since the vibration involves all three atoms of the molecule; and (2) the frequency of the vibration may reflect the relative strength of the metal–H_2O bond, unless hydrogen bonding competes and interferes.

Based on matrix isolation work [77,205,206] and infrared studies of metal–H_2O complexes [207], it is postulated that the frequency of the scissoring mode *decreases* from its gas-phase value as the extent of charge transfer to the metal center *increases* [77,205–207]. Some insight into why this might happen is provided by the discussion of section 2.2.3 and table 2 (p. 222). As shown there, the chemisorption bond of H_2O (via the oxygen atom) may involve electron donation from the $3a_1$ orbital, or the $1b_1$ orbital, or both. In

any case, a decrease in the scissoring mode force constant is expected [73,77]. This is easily visualized for the $3a_1$ orbital, where removal of electrons reduces the screening between protons; complete removal of the electrons results in a linear ion [208] (see section 2). In aquo–metal–sulfate complexes, δ(HOH) frequencies as low as 1498 cm^{-1} are reported. Interaction with the metal therefore causes a shift to *lower* frequencies relative to the gas-phase value (1595 cm^{-1}), whereas it is well known that intermolecular hydrogen bonding causes a shift to *higher* frequencies [203].

In the vibrational studies to date, the scissoring mode frequencies of chemisorbed H_2O fall both below and above gas-phase values. At even *low coverages* of H_2O on clean Ag(110) [132], Pt(100) [144], Pd(100) [81,129], and Pt(111) [146], δ(HOH) is observed between 1630 and 1660 cm^{-1}, comparable to the value of *bulk* ice, ~ 1620–1640 cm^{-1}. This reflects a relatively weak interaction with the metal and the predominance of intermolecular hydrogen bonding. In contrast, on clean Ru(001), at low coverages the scissoring mode frequency falls at 1500–1520 cm^{-1} [59,60]. Also, for oxygen-dosed Ag(110), δ(HOH) is slightly lower than otherwise, ~ 1590 cm^{-1} [132]; this is true as well for H_2O on clean Ni(110) [112]. In the latter three cases, δ(HOH) indicates a somewhat stronger interaction with the surface; it is probably not coincidental that in these cases desorption states of molecular H_2O are observed at $T > 200$ K, with binding energies $\gtrsim 50$ kJ/mol [60,132]. When δ(HOH) appears at higher frequency, as for clean Ag(110), Pd(100), Pt(111) and Pt(100), only desorption states at $T \lesssim 180$ K are present. It appears that the temperature of the thermal desorption peaks and the frequency of δ(HOH) at low θ may be parallel indicators of the strength of the metal–H_2O interaction. It would be interesting if this prediction regarding δ(HOH) were borne out, for instance, in the vibrational spectra of H_2O on Ir(110), where desorption states at $T > 200$ K also appear for the clean surface (see table 5, p. 250). In summary, for chemisorbed H_2O at metal surfaces, *values of δ(HOH) both above and below the gas-phase frequency are observed.* It is proposed that shifts to lower frequency reflect a relatively strong H_2O–metal interaction, whereas higher frequencies are due to hydrogen bond formation *and* only weak metal–H_2O bonds. These qualitative predictions and experimental trends regarding softening in the scissoring mode frequency are not borne out in theoretical calculations to date, however (section 2).

The *librational modes* are frustrated rotations which, in the EELS experiments, would not be observed if the molecule maintained perfect C_{2v} symmetry with respect to the surface, as one early model proposed [58]. (This statement would not be true if nondipolar scattering were important, but the evidence indicates that for these modes, scattering is largely dipolar [60].) However, the librations invariably account for the most intense features in the EEL spectra, for both low and high H_2O coverages. The necessary conclusion is that the symmetry of the molecule must be lowered in such a way that at

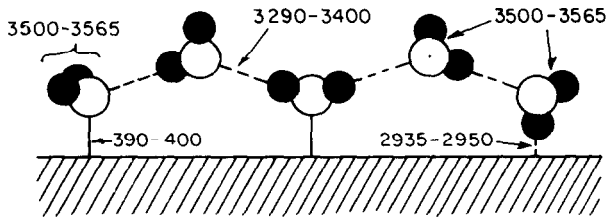

Fig 40 Schematic representation of types of H_2O molecules present in the bilayer For more detailed depictions see refs [79,192] Taken from Thiel et al [59]

least one of the librational modes becomes dipole-active. One explanation for their observation, supported in general by other data, is that hydrogen-bonded clusters form in which the molecular planes of many of the H_2O molecules are not perpendicular to the metal surface, due to tetrahedral bonding at the oxygen atom, as shown in figs. 36 (p. 273), 38 (p. 277), and 40. The selection rules which operate in dipolar scattering are thus particularly useful in obtaining structural information from the frustrated rotations.

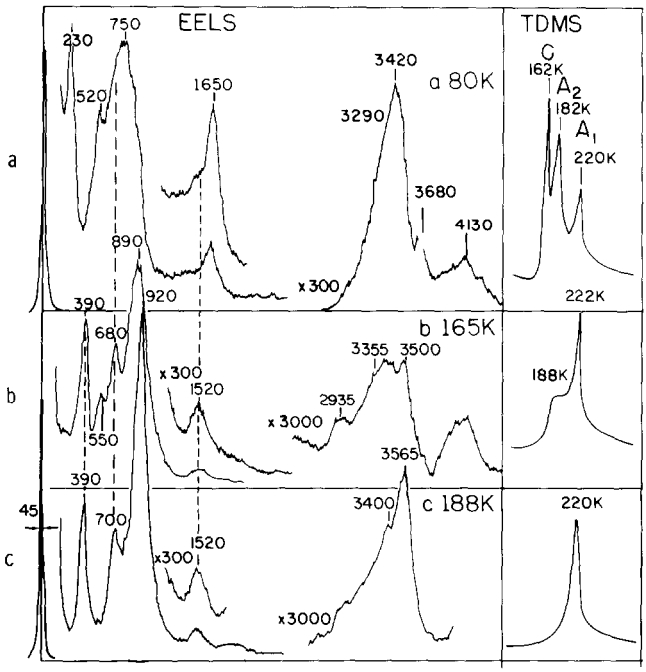

Fig 41 EELS and TDS data obtained after adsorption of ice multilayers on Ru(001) and annealing to the temperatures indicated. Taken from Thiel et al [59]

In several cases, more than one librational mode appears. For a single chemisorbed H_2O molecule, it is easy to visualize three different types of frustrated rotations, one about each of the molecular axes, commonly referred to as the rocking, twisting, and wagging motions. These are shown in fig. 14, p. 230. However, the assignment of the librational features to distinct rocking, twisting, or wagging motions is not straightforward, particularly when coupling to the other molecules via hydrogen bonding comes into play. Such simple assignments are controversial even in the simpler cases of metal–aquo complexes [54,55]. The librational modes of a well-ordered bilayer of H_2O on Ru(001) are visible in figs. 41b at 680–700 and 890–920 cm^{-1} [59]. In bulk ice, a single broad feature at $\sim$ 780–820 cm^{-1} is always observed (cf. fig. 41a). In figs. 41b and 41c, the sharp peak at 890–920 cm^{-1} seems to be uniquely associated with a well-ordered bilayer, an observation whose significance may be clarified by future comparisons with other systems.

5. Dissociative adsorption on clean metals

5.1. Equilibrium considerations: a survey of the Periodic Table

In this section we briefly review the cases in which dissociation of H_2O is reported to occur at transition metal surfaces. We then present a similar review of several nontransition groups: Group 1 (the alkali metals), Group 2 (the alkaline earths), Group 3A and 4A metals, and the rare earths.

In section 3.1. and fig. 24 (p. 244), we use thermodynamic arguments to show that dissociation of water is driven by enthalpy on many transition metal surfaces. The driving force is provided by the heats of formation of the chemisorption bonds of the dissociation fragments (OH_a, H_a, O_a) relative to the chemisorption bond of molecular water. This simple picture can only be used to predict the state of adsorbed water which is favored *in equilibrium*, but in fact this picture is surprisingly accurate in most cases (see fig. 24).

What controls the enthalpy changes which accompany dissociation? As pointed out in section 3.1, the metal–oxygen bond of atomic oxygen varies more strongly from metal to metal than does the metal–hydrogen bond strength, so this is the most important factor. The trends in stability of the metal oxides are mimicked by the metal hydroxides, since the same factors which stabilize the electronegative oxygen atom also tend to stabilize the electronegative hydroxyl fragment. Therefore, the same overall pattern is followed across the periodic table for both partial and complete dissociation of the water molecule. As shown in fig. 24 and table 4, dissociation is enthalpically favored for most of the transition metals, with only a small pocket of relatively inert metals among the Group VIII elements. The main reason why these metals are predicted to be inert toward H_2O is because they do not form

strong metal–oxygen bonds, i.e. ΔH_f of the oxides is not large and negative [94], and table 4).

Among the transition metals, it is noteworthy that there is good evidence for dissociation of water even at $T < 100$ K on Ti(001) [100], Cr(110) [101,151], Mn films [102], Mo films [126] and Fe(100) [103]. Studies on other transition metals, carried out at room temperature, show that water dissociates also under these conditions on W(100) [138], Fe(110) [104], Fe(100) [152,153,209], Re(001) [139], and Re films [140]. Transition metals for which the dissociation reaction is sensitive to surface morphology are discussed in section 5.3.

The non-transition metals have been (thus far) less exhaustively studied than the transition metals. In section 6, we discuss adsorption of water at surfaces which have been modified by *traces* of non-transition metals, such as the alkali metals, but here we are concerned with adsorption at surfaces of bulk or bulk-like samples of the non-transition metals themselves.

An analysis similar to that reported in table 4 (pp. 242–243) indicates that water dissociation is favored by the net enthalpy change on Li, Na, K, Rb and Cs surfaces. (There is not sufficient data to discuss francium, although it presumably follows the same trend.) This is based upon calculation of ΔH_d for partial dissociation to OH_a and H_a. We have chosen this pathway instead of complete dissociation to O_a and $2H_a$ because thermodynamic data for the hydroxides of the alkali metals are more readily available and self-consistent than the corresponding data for the oxides. The value of ΔH_d then varies from -332 kJ/mol for Li, to -240 kJ/mol for Na and K, to -227 kJ/mol for Rb and Cs [94]. (It is noteworthy that these metals all form stable hydrides as well as hydroxides [94].)

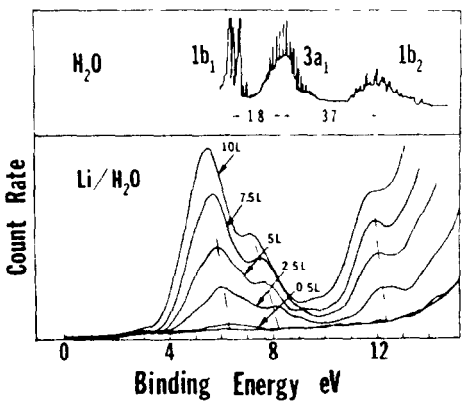

Fig 42. UPS of lithium exposed to H_2O The energy zero is the Fermi edge of clean lithium Upper H_2O_g taken from Turner et al [32], centroid of first peak arbitrarily placed over (extrapolated) zero coverage peak of H_2O on lithium, two strong vibronic members in $1b_1$ have been truncated for this graph Taken from McLean et al [71]

Photoemission data, shown in fig. 42, indicate that exposing a thick Li film to H_2O at room temperature results in *associative* adsorption [71]. The positions of the three photoemission features, assigned as the $1b_1$, $3a_1$, and $1b_2$ orbitals of H_2O, are extrapolated to binding energies of 6.3, 8.3 and 12.4 eV below E_F at zero coverage. The interpretation of the UPS data is supported by cluster calculations, which indicate that water forms a stable molecular complex with the alkali metal rather than forming hydroxide and hydrogen [71]. This is an unusual result, given the thermodynamic arguments advanced previously and the data for the other alkali metals which are presented in the following paragraphs. It is not impossible that the UPS spectra are due to a mixture of OH_a and O_a on Li, since similar data are reported for water

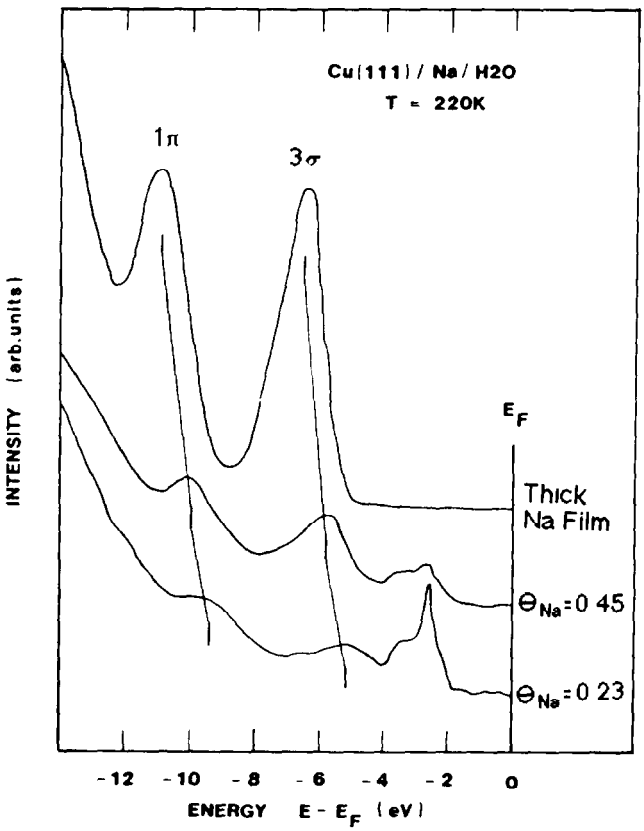

Fig. 43 He I (21 2 eV) UPS spectra of Cu(111)/Na/H_2O. Each different Cu(111)/Na surface is saturated with H_2O at 100 K The temperature is flashed to 220 K and recooled to 100 K before measuring spectra. The 1π and 3σ features show the presence of OH_a. No undissociated H_2O is observed $\theta_{Na} = 0\,46$ equals one full layer Taken from Paul [210]

dissociation products on Ti (see fig. 25, p. 248). Matrix isolation experiments also indicate that a water molecule does not dissociate when it interacts with a single Li atom [205,206], although the temperature in such experiments is very low relative to most surface adsorption studies, ~ 15 K [205,206].

For sodium, there are two studies of the alkali metal's interaction with water [154,210]. Relying primarily upon ESDIAD and TDS, Doering et al. show that H_2O dissociates very readily (even at 80 K) on top of a dense, two-dimensional Na layer deposited on a Ru(001) substrate [154]. Such a layer presumably possesses electronic properties approaching those of the bulk metal [154]. Dissociation at 80 K yields a maximum of two OH groups and two H atoms per surface Na atom [154]. The hydroxide decomposes above 350 K, and hydrogen desorbs at 350 to 600 K [154]. No H_2O desorbs. Paul reports on the reaction of water with thicker Na films on a Cu(111) substrate [210]. He finds that three-dimensional NaOH forms upon exposure of a Na film to H_2O. He identifies the reaction product on the basis of the very clear and distinctive NaOH spectrum shown in the upper curve of fig. 43 [210].

The picture is similar for bulk-like samples of potassium. For a full, dense layer of the alkali metal, dissociation occurs upon adsorption at 80 K on a Ru(001) substrate [211], and upon adsorption at 100 to 125 K on Pt(111) [212–214]. The products are OH_a and H_a. This reaction takes place also for multilayers of potassium, up to ten layers deep on Ru [211] or 110 Å thick on Pt [212,214]. In both cases, reaction is not limited to the *surface* of the alkali metal film upon adsorption, but instead the dissociation products penetrate the *bulk* of the film and form a three-dimensional mixture of K and OH. In the work with the Pt(111) substrate, it is further reported that water of hydration permeates the K film at 125 K [212,214]. The water of hydration is driven off between 250 and 300 K, i.e. at higher temperatures than normal chemisorbed water [211,212,214]. Both studies agree that, upon heating, the KOH layer decomposes at approximately the same temperature: 570 to 580 K [211,212,214]. In the work with the Ru(001) substrate, thermal desorption studies further show that decomposition of the hydroxide is accompanied by simultaneous evolution of K and H_2O in the gas phase [211]. Formation of the hydroxide must stabilize the entire potassium multilayer against desorption, since clean potassium multilayers begin to sublime at much lower temperatures, ~ 300 K [211]. This is illustrated in fig. 44, where thermal desorption of H_2O and K from the KOH multilayer is compared with thermal desorption of K from K multilayers [211]. At higher temperatures, a complex mixture of potassium, oxygen, and (possibly) hydrogen remains on the water-treated surface [211].

The ability of water to react with many layers of an alkali metal sample is somewhat reminiscent of the results of Connell and Dumesic [254], in which the mobility of potassium on iron and alumina surfaces is shown to be greatly enhanced by exposure to water vapor. They attribute this to the formation of

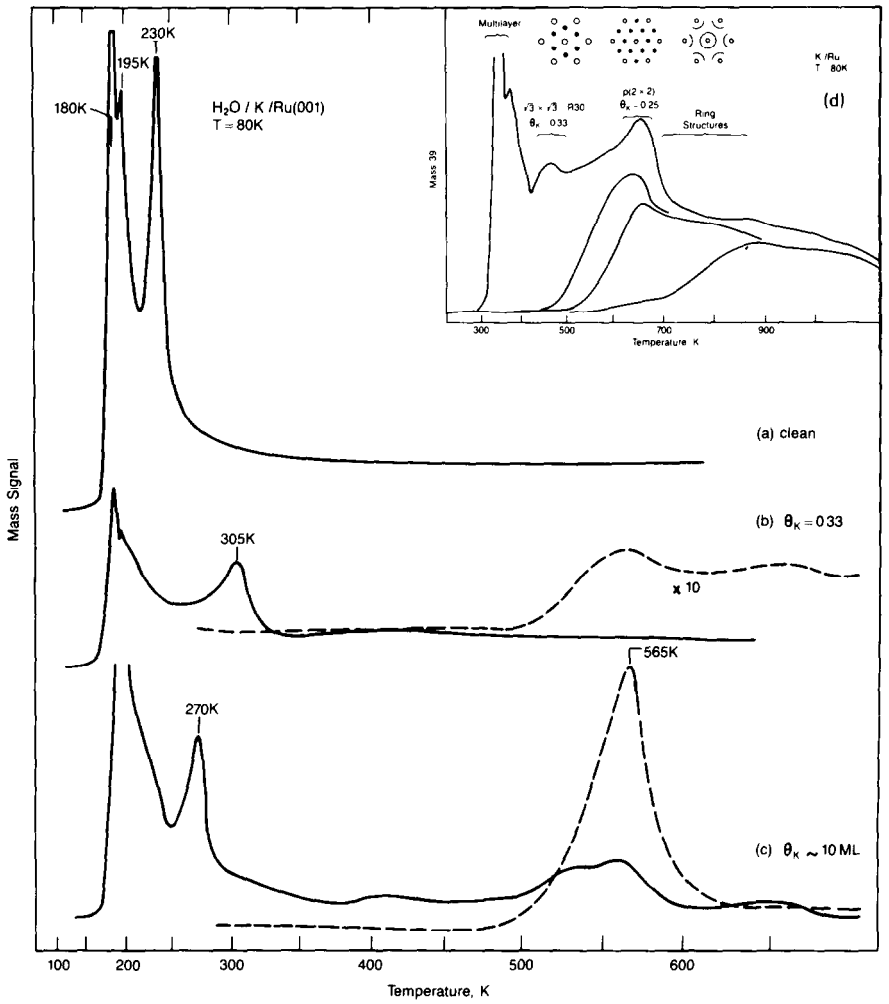

Fig 44 Thermal desorption spectra of H_2O (mass 18, solid line) and K (mass 39, broken line) after exposure of water to Ru(001). (a) clean; (b) precovered with one monolayer of potassium ($\theta_K = 1/3$); (c) precovered with potassium multilayer The inset (d) shows desorption of potassium alone from Ru(001) at various coverages Taken from Thiel et al. [211]

hydroxylated or hydrated forms of potassium in which the potassium–surface bond is weakened and the adsorbed complex more readily migrates from surface site to site [254]. This same model may qualitatively explain the lack of a barrier to surface penetration of bulk samples of potassium by H_2O, discussed above.

It is noteworthy that Thiel et al. [211] and Kiskinova et al. [215] both report

that multilayers of K on Ru and Pt do *not* react at room temperature with gas-phase H_2O, despite the strong thermodynamic driving force to KOH formation. This is presumably an example of a kinetic barrier to water dissociation which arises from its short lifetime in the adsorbed state at 300 K, as discussed in the following section. The interaction of water with bulk rubidium and cesium has not yet been studied experimentally.

Water dissociation on the alkaline earths is favored to about the same degree as on the alkali metals: ΔH_d for dissociation to OH_a and H_a varies from -228 kJ/mol for Be to -343 kJ/mol for Ca [94]. The values for the other alkaline earths fall within this range. These metals also form stable hydrides [94]. Data on the surface chemistry of the alkaline earths is scarce. Fuggle and coworkers [102] use XPS to show that H_2O dissociates on Mg at room temperature, resulting in slow oxidation of the metal; at lower temperature, hydroxides appear to be stable. Their XPS data are shown in fig. 45. They assign the feature at 531.0 eV binding energy to magnesium oxide, the feature at 535.1 eV to oxygen in water, and the peak at 533.5 eV to oxygen in $Mg(OH)_2$ [102]. The data show that the effect of warming the sample from 77 to 390 K is (first) to drive off the molecular condensed H_2O, and (second) to decompose the hydroxide to the oxide [102]. The second step, they report, occurs already at about room temperature, in contrast to the hydroxides of the alkali metals – which, we have seen, are stable up to 570–580 K [211,212,214]. Schultz et al. report, however, that water dissociates *at room temperature* on Mg to form $Mg(OH)_2$ species [216].

The Group 3A metals (B, Al, Ga, In, Tl) form stable oxides and hydroxides, but a complete set of thermodynamic data is available only for Al [94]. We estimate that ΔH_d for partial and complete dissociation of H_2O by Al is -198 and -343 kJ/mol, respectively, i.e., dissociation is favored over molecular adsorption [94]. Indeed, there are several reports that water dissociates even at 150 K on clean Al surfaces [102,173,217,218]. These studies generally agree that dissociation on clean Al is accompanied or followed by desorption of hydrogen, as illustrated in fig. 47. On the other hand, in the presence of oxygen, less hydrogen is evolved and the dissociation mechanism is believed to involve mainly hydrogen abstraction:

$$H_2O_a + O_a \rightarrow 2\ OH_a.$$

Several authors note that, at low water coverages and at low temperatures on *clean* Al, some water dissociates while some adsorbs molecularly and reversibly [102,173,218]. On Al(111), Netzer and Madey report that reversible molecular adsorption is competitive with dissociation to a significant extent [218]. In agreement with Netzer and Madey, Crowell et al. find that adsorption is partly dissociative (but predominantly molecular) on clean Al(111) at 130 K; they report complete dissociation upon adsorption at 300 K [173]. Supporting data from the latter study are shown in fig. 46. There are two studies

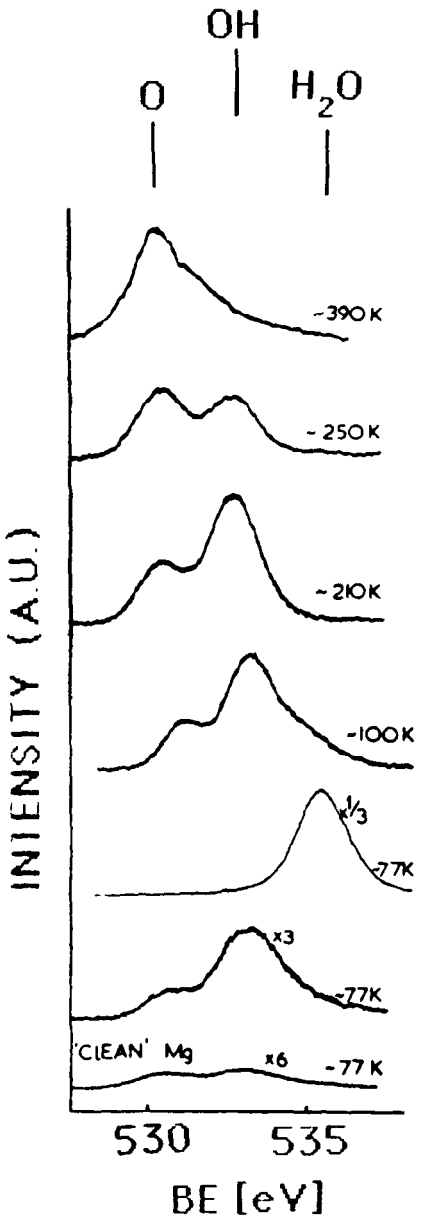

Fig 45 Reaction of H_2O with clean magnesium at 77 K, and upon warming. The 100, 210, 250 and 300 K spectra are derived directly from the 77 K curve by successive heatings. Taken from Fuggle et al [102]

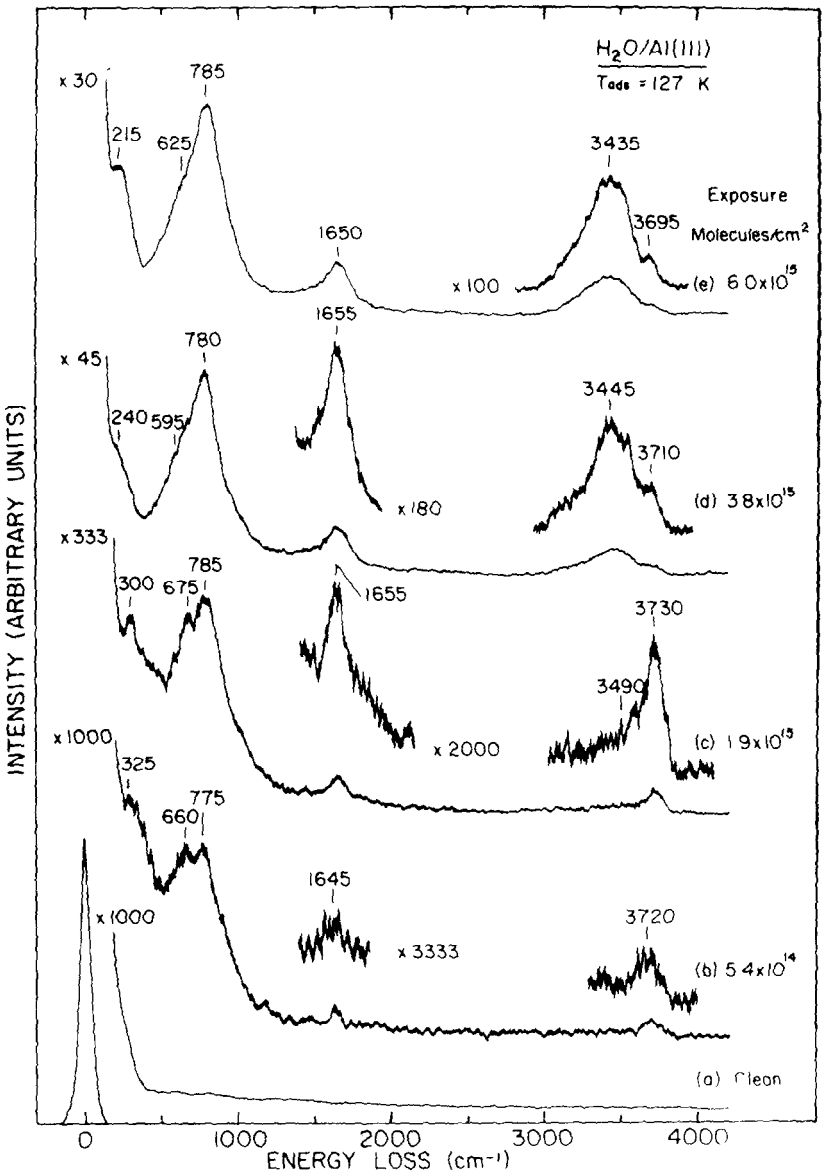

Fig 46 Vibrational spectra recorded using EELS as a function of exposure for H_2O adsorption on clean Al(111) at 127 K Taken from Crowell et al [173]

dealing with Al(100) both of which agree that adsorption is *entirely* molecular at 80 to 100 K [172,217]. Dissociation to hydroxyl begins at 150 K [217], as shown in fig. 47, and at 300 K an oxide-stabilized OH species is present [172,217]. The extent of dissociation in the chemisorbed layer at $T \leqslant 130$ K may be face-specific on Al, based on this comparison between the results for Al(100) [172,217] and Al(111) [173,218].

Lead, a metal of the 4A group, is reportedly inert toward water dissociation (cf. fig. 74) [111]. This is reasonable, since lead forms a relatively weak bond to oxygen in bulk oxides, and does not form a stable hydride [94].

Finally, work on the rare earths (which form very stable oxides [94]) generally indicates that oxidation by water yields different products than does oxidation by O_2, with stable hydroxyl species playing an important role as

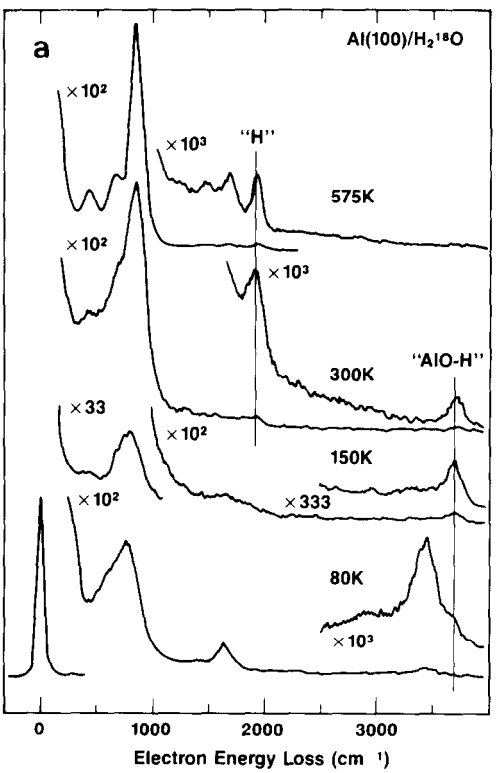

Fig. 47. (a, b) EEL spectra following adsorption of (a) $H_2{}^{18}O$ or (b) $D_2{}^{16}O$ onto Al(100) at 80 K, and heated to the temperatures indicated. Each surface is exposed to ~ 2 L of water. (c) TDS spectra following the adsorption of ~1 L of H_2O (D_2O) on Al(100) at 80 K Note the change of the scale on the horizontal axis at ~ 325 K Taken from Paul and Hoffmann [217].

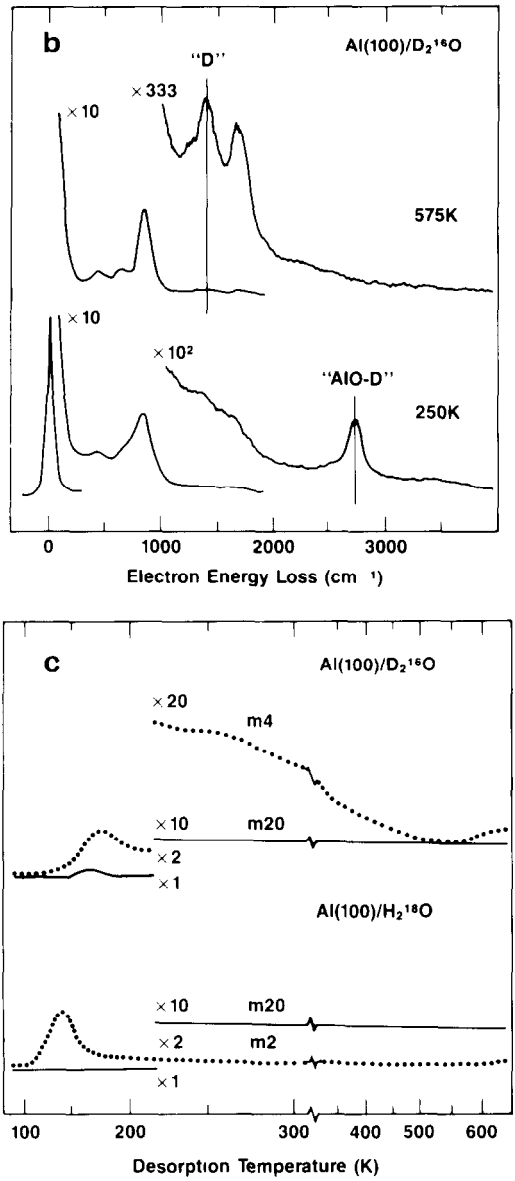

Fig 47 continued

intermediates or end-products in the reaction [219–221]. This is based on studies of lanthanum [220,221], cerium [220], thorium [219] and uranium [219], mostly at room temperature.

5.2. Kinetic barriers

Adsorbed water may be *kinetically prevented* from reaching the equilibrium states discussed in the previous section, even when dissociation is favored, if the activation barrier to dissociation is sufficiently large and/or the pre-exponential rate factor for dissociation is sufficient small. If one or both of these factors make the rate constant for dissociation much smaller than the rate constant for desorption (i.e., if it is easier to break the metal–water bond than to break any of the internal molecular bonds), then water desorbs into vacuum before it can dissociate, and dissociation is not observed under the conditions of typical UHV experiments. Experiments performed under conditions of adsorption–desorption equilibrium can populate the adsorbed phase at higher temperature; however, the residence time of the adsorbed molecule (which can be calculated directly from the Frenkel equation [222]), may still be too short ($\lesssim 10^{-13}$ s) to allow dissociation under these conditions.

The first O–H bond of the free water molecule has a dissociation energy of 498 kJ/mol (5.2 eV) [31]. The barriers to water dissociation on metals are certainly much lower than this, as indicated below. This implies that the metal surface exerts a strong influence on the transition state as the first O–H bond is being broken. The transition state can be stabilized by a strengthening of the metal–oxygen bond, and/or partial formation of the metal–hydrogen bond, as the O–H bond breaks. As illustrated in fig. 48, breaking the O–H bond of the adsorbed water molecule can occur, in principle, with or without this stabilization of the transition state by the surface Fig. 48a illustrates a hypothetical case in which the metal surface does not help to stabilize the

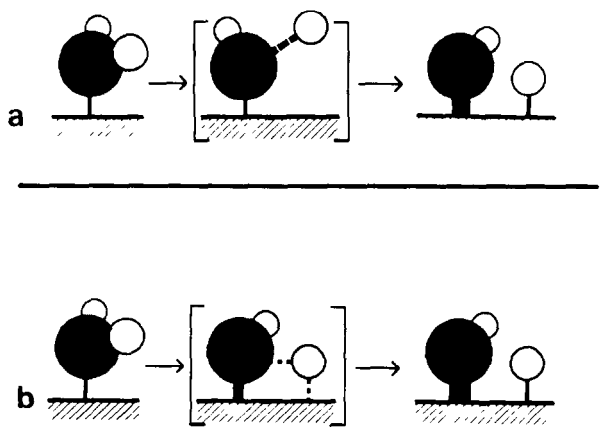

Fig 48 Schematic depiction of possible transition states in H_2O dissociation to OH_a and H_a (a) A transition state which is not strongly affected by the surface (b) A transition state in which the metal–oxygen bond is strengthened, and the metal–hydrogen bond is partly formed

transition state, whereas fig. 48b illustrates a case in which the metal assists the hydrogen atom and also strengthens the metal–oxygen bond as the OH bond breaks. The barrier to dissociation in the former case is probably close to the gas-phase value of ~ 500 kJ/mol, since the internal molecular bonds of H_2O are only slightly perturbed upon chemisorption (as discussed in section 2.2). In the latter case, however, the barrier will be lower due to the catalytic effect of the surface.

The latter type of transition state, shown in fig. 48b, is proposed by Anderson based on theoretical models of water dissociation over Pt_4 and Fe_5 clusters [63]. He calculates a barrier for O–H bond breaking of 40 kJ/mol on the Fe_4 cluster, but a much higher barrier (close to the gas-phase value) on the Pt_5 cluster [63]. These results are consistent with experimental data, which show extensive dissociation on Fe but no dissociation on Pt (table 4, pp. 242–243). Anderson finds that a major contribution to the dissociation barrier consists of simply bringing the OH bond parallel to the surface [63]. This is not reported to be a stable configuration in most calculations (cf. section 2.2.3). However, a periodic tilting of the molecule may occur via large amplitude vibrational modes, such as rocking librations or frustrated translations (cf. fig. 14, p. 230).

The temperatures at which water dissociates in real systems are relatively low. Experimentally, 80–100 K is frequently an effective lower limit on the range of sample temperatures which generally are achieved. (This is because many samples are cooled with liquid nitrogen, which boils at 77 K at atmospheric pressure.) Several metals dissociate water upon adsorption already in this temperature range, including Ti(001) [100], Cr(110) [151] and stepped Re(001) [139]. Others adsorb water without dissociation at this temperature, but cause the chemisorbed water to dissociate when the sample is heated between 100 and 350 K. Examples of metals which fall into this category are Ni(110) and Ni(210) [111,112,162], Re(001) [139], Fe(110) [104], Al(100) [172,217] and Co(110) [106].

If we assume that the rate of dissociation follows a simple Arrhenius first-order rate law, then we can estimate the barriers to dissociation on these surfaces. In order to do so, we choose a value for the pre-exponential rate factor, A, of $10^{13\pm2}$ s^{-1}. In a typical experiment, a sample is heated to a given temperature for one or two seconds, then recooled to low temperature and examined to see whether dissociation has occurred, using a spectroscopic technique such as EELS, XPS, or ESDIAD. We assume that the initial coverage of water, N_a, which dissociates during heating in a 1 s period is $10^{14\pm1}$ molecules cm^{-2}. The rate of dissociation at a given temperature, $-dN_a/dt$, is $10^{14\pm1}$ molecules cm^{-2} s^{-1}. The activation barrier to dissociation can be calculated from

$$dN_a/dt = N_a A \exp(-E_{diss}/kT_{diss}).$$

Substituting, we find

$$-10^{14\pm1} \text{ molecules cm}^{-2}\text{ s}^{-1} = (10^{14\pm1} \text{ molecules cm}^{-2}) \times (10^{13\pm2}\text{ s}^{-1}) \times \exp(-E_{diss}/kT_{diss}),$$

or

$$E_{diss} = (0.17 \text{ to } 0.32)T_{diss},$$

where T_{diss} is the temperature in K at which dissociation occurs, and E_{diss} is the energy barrier to dissociation in kJ/mol.

For example, if the dissociation reaction occurs upon heating a water-covered surface to 300 K, then the dissociation barrier is roughly 53 to 94 kJ/mol, according to this analysis. On the other hand, if dissociation is observed already at the lowest attainable temperature – say 80 K – then it is only possible to estimate an *upper limit* for the dissociation barrier, which would be 14 to 25 kJ/mol. The barrier could be estimated more accurately in this case only if the sample could be cooled to lower temperature for adsorption, then heated to see the temperature at which the dissociation reaction begins.

Since dissociation actually occurs on many metal surfaces between 80 and 350 K, the upper limit of the dissociation barrier is about 110 kJ/mol – far less than the barrier to breaking an OH bond in the free water molecule, 500 kJ/mol. Therefore the surface must stabilize the dissociation fragments *during* OH bond breaking, as shown in fig. 48b.

5.3. *Examples of preferential dissociation on atomically rough surfaces*

In section 3.1, our simple attempt to predict whether dissociation occurs on a given metal surface, based on thermodynamic arguments, leaves many metals in a "borderline" category. For a given metal within this category, it often happens that the adsorption pathway (associative versus dissociative) depends upon surface morphology, with atomically rough surfaces more active for H_2O dissociation than atomically smooth surfaces.

A good example is nickel. While there is no evidence that water dissociates under any conditions on the clean, atomically smooth (100) and (111) planes (section 4), there *is* evidence that dissociation takes place at about 200 K on the atomically rough (110) face [112]. This reaction produces OH_a and H_a. Adsorbed water is undissociated at 80–150 K on this surface, and adopts the coverage-dependent configurations shown in section 4. Dissociation at 200 K corresponds to an activation barrier of 34 to 64 kJ/mol. The vibrational spectra which give evidence for dissociation on Ni(110) are shown in fig. 49 [112]. The Ni–OH species is associated with the O–H stretch at 3580 cm^{-1}, and the Ni–OH bend and/or the Ni–H stretch, at 950 cm^{-1} [112].

On the clean, atomically rough Ni(210) surface, about 2×10^{14} water molecules cm^{-2} can dissociate [111]. XPS data have been decomposed as

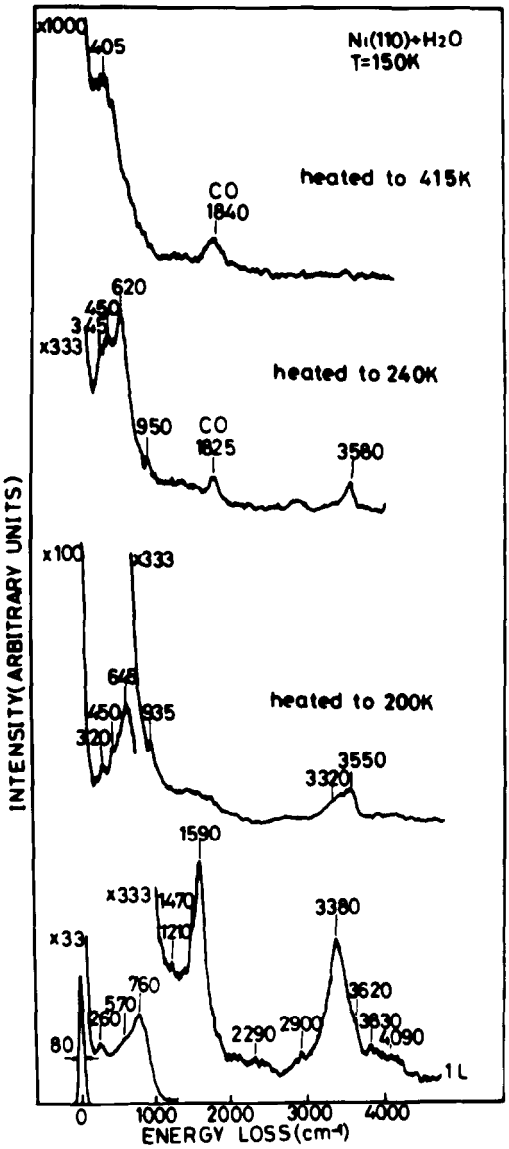

Fig. 49. EEL spectra obtained at 150 K after an exposure of 1 L H_2O and flashing to 200, 240, and 415 K Taken from Ollé et al [112]

shown in fig. 50 [111], to show that OH groups form at ~ 150 K. This corresponds to a dissociation barrier of 26–48 kJ/mol, slightly lower than for the (110) face, where no dissociation is detected during adsorption at 150 K

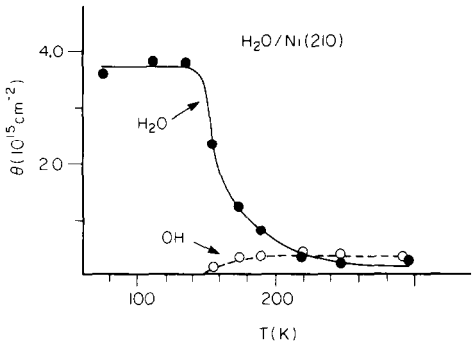

Fig. 50 Variation of surface concentration θ with temperature for Ni(210)–H_2O, based on O 1s XPS data Taken from Carley et al [111]

[112]. In short, there appears to be a slightly lower dissociation barrier for the rougher of these two Ni surfaces.

Rhenium also exhibits this trend. Jupille, Pareja and Fusy compare water adsorption on the (001) and stepped-(001) surface of rhenium, using ESDIAD, TDS, AES and LEED [139] (fig. 51). They find that dissociation occurs upon adsorption at 80 K on the Re steps, whereas water does not dissociate on the atomically smooth (001) terraces until about 190 K; adsorption at 250 K is

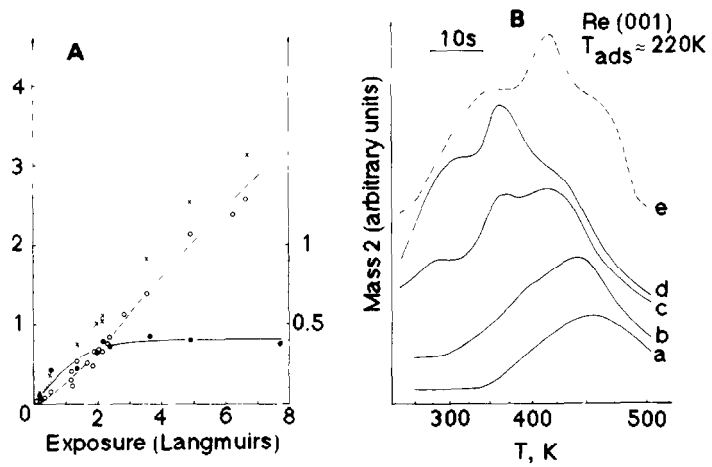

Fig. 51 (A) H_2O adsorption on Re(001) at 80 K variation versus exposure of (●) quantity of desorbed hydrogen; (○) quantity of desorbed water; (×) sum of the two previous quantities (B) H_2 desorption spectra from Re(001) following different H_2O exposures at 80 K· (a) 0.22 L, (b) 0 45 L; (c) 1 32 L; (d) 6 2 L and (e) following H_2 exposure at ~ 80 K. Taken from Jupille et al [139].

entirely dissociative in both cases [139]. In other words, the activation barrier for dissociation on a Re surface is lower at atomically rough areas, i.e steps (with an upper limit of 14–25 kJ/mol) than at atomically-smooth areas ($\sim$ 32–61 kJ/mol).

Alnot et al. [142] and Schulze et al. [140] use XPS to study adsorption of water on polycrystalline Re Upon exposure of 5 L D_2O or H_2O at 135 K, both groups observe evidence for only molecular water. However, it may be that this high exposure is sufficient to form a thick ice multilayer and thereby attenuate photoelectrons emitted from the surface layer. They do not report XPS data at lower water exposures, at 135 K [140,142], and so their data are not directly comparable to those of Jupille et al. [139,141]. Such a comparison would be interesting, since the polycrystalline surface must have a higher distribution of grain boundaries and crystallite orientations than the single crystal, and so might dissociate water as easily as a stepped Re(001) surface [111].

Cobalt is a third example of a metal on which water chemisorption is sensitive to surface morphology. Water adsorbs dissociatively on polycrystalline cobalt samples, even at temperatures as low as 77 K [105,107]. This conclusion is based upon data from XPS and work function measurements. The dissociation products consist of adsorbed hydroxyl groups, and possibly some atomic oxygen and hydrogen, up to at least room temperature [105,107]. Heras et al. determine that the adsorption pathway of water is a strong function of cobalt surface structure: the atomically smooth Co(001) plane is completely inert toward water dissociation, but the rougher (110) and polycrystalline surfaces are active catalysts for this reaction [106]. They base this conclusion on combined data from LEED, UPS, work function, and TDS [106]. Photoemission data from their work are shown in fig. 52, where the dissociation of water on Co(110) gives rise to hydroxyl-related features at about 6 and 10 eV, and some emission at 6 eV may also be due to atomic oxygen [106].

In summary, the dissociation of water at clean metal surfaces appears to occur more readily at atomically rough areas, such as fcc(110) faces or steps, than at atomically smooth areas. But what does one mean by "more readily"? In some cases, such as Re, dissociation can occur on both smooth and rough regions, but the *energy barrier* to dissociation is lower at the steps [139]. On other metals, such as Co and Ni, dissociation occurs only at rough areas, e.g Co(110), Ni(110) or Ni(210) surfaces; dissociation does not take place at all on the smoother planes, such as Co(001) and Ni(111) [106,112]. In this case, one cannot tell from the experimental data whether lack of dissociation on the smooth metal faces is due to a higher energy barrier to dissociation, so that water simply desorbs before it dissociates, or due to a shift in the *equilibrium distribution* between dissociated and undissociated water. The latter interpretation would be consistent with our observation, in section 3, that both Co and

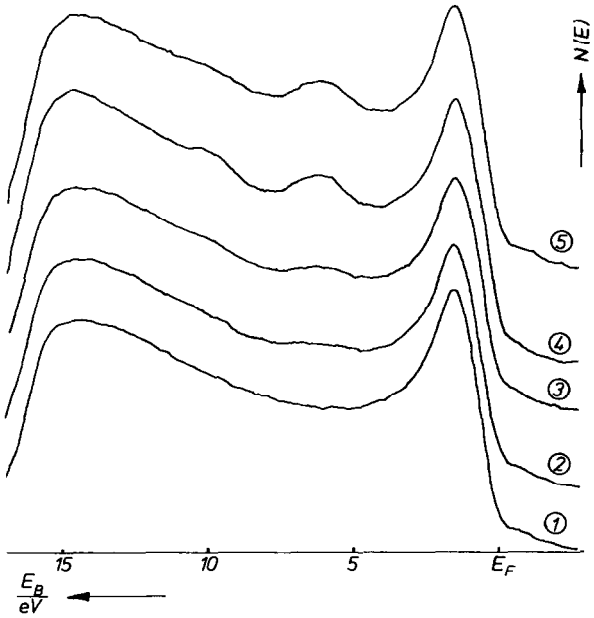

Fig. 52 Influence of H_2O admission on the He I UP spectrum of Co(110) at 298 K (1) clean surface: (2) 2 42 L H_2O· (3) 9.9 L H_2O; (4) $P_{H_2O} = 4\,5 \times 10^{-7}$ Torr, (5) $P_{H_2O} = 3\,75 \times 10^{-8}$ Torr. Taken from Heras et al [106]

Ni are "borderline" metals, i.e. thermodynamic considerations do not weigh heavily either for or against dissociation. A small perturbation, such as surface morphology, may tip the balance in such cases.

5.4. Reactions of dissociation products: recombination, desorption, and metal oxidation

5.4.1. Reaction pathways

There are three main thermally activated reactions which the dissociation products of water can undergo. The first is recombination followed by desorption of molecular water, which can be represented in a general way as:

$$H_2O_a \rightarrow \text{dissociation products} \longrightarrow [H_2O_a] \rightarrow H_2O_g.$$

The second is recombination to yield molecular hydrogen and/or oxygen, which can be written as:

$$H_2O_a \rightarrow \text{dissociation products} \longrightarrow H_{2,g} + \tfrac{1}{2}O_{2,g}.$$

The third is reaction with the metal to form a stable bulk oxide, hydroxide, and/or hydride, which can be represented as:

$$H_2O_a \rightarrow \text{dissociation products} \longrightarrow M_xO_y,\ M_n(OH)_m,\ M_rH_s.$$

While the first reaction is most commonly observed in studies of water dissociation over modified surfaces of the Group VIIIB transition metals (cf. section 6.2), the latter two types of reaction appear to dominate over the rest of the Periodic Table. In some cases, of course, these three reactions or some combination thereof can occur sequentially or competitively. Potassium, for instance, forms a bulk hydroxide which is stable up to ~ 580 K, but then the hydroxide decomposes to yield H_2O_g and bulk potassium oxide [211,212,214]. In this case, the adsorbed water essentially undergoes the third reaction (bulk hydroxide formation) followed by a combination of the first reaction (water desorption) and the third reaction (bulk oxide formation) above 580 K.

We shall now discuss and give examples of the three reactions individually.

5.4.2. Recombination and desorption of H_2O

A possible mechanism for thermally activated recombination of water on metal surfaces appears to be disproportionation of adsorbed hydroxyl.

$$OH_a + OH_a \rightarrow [H_2O_a + O_a] \rightarrow H_2O_g + O_a.$$

The end result of the reaction after H_2O desorption is an oxygen-covered surface, since oxygen desorbs from metal surfaces at much higher temperatures than does water. Water evolution from recombination of dissociation products is typically complete by at least 350 K [83].

The disproportionation reaction is proposed to be the source of recombinative water in the gas phase, rather than an alternative mechanism such as the one outlined below, based on two types of evidence: oxygen remains on the surface after water desorbs, and OH_a is stable up to the point of H_2O desorption. Furthermore, disproportionation is well documented in the presence of pre-adsorbed oxygen on Pd [81,129], as discussed in section 6.2.2. The disproportionation reaction has been proposed to take place (following dissociation of H_2O) on two clean metal surfaces: Fe(100) [103] and Ni(110) [83]

Another possible reaction scheme is:

$$H_2O_a \rightarrow OH_a + H_a \rightarrow O_a + 2\ H_a \rightarrow H_2O_g.$$

Adsorbed oxygen could remain at the end if the overall reaction is non-stoichiometric. In support of this mechanism, it must be noted that adsorbed atomic oxygen is known to react with adsorbed atomic hydrogen to produce water over many surfaces. This topic has been treated extensively by Norton [21]. A careful study of isotopic exchange between labelled OH_a and H_a is necessary to differentiate between disproportionation of hydroxyl and reaction between atomic oxygen and hydrogen on the clean metals. Such a study has

been carried out for the O/Pd(100) surface, and provides clear proof of hydroxyl disproportionation in that system [81,129].

5.4.3. Recombination and desorption of H_2 or O_2

On several surfaces, dissociative adsorption is accompanied by, or followed by, liberation of hydrogen. Perhaps the most notable example of this reaction is provided when Al is exposed to H_2O. Oxidation of the metal proceeds at room temperature, and excess hydrogen is evolved [223]. (Some of the hydrogen may be incorporated as a bulk hydride or hydroxide as well [102,217,224,225].) Hydrogen evolution is also reported to occur following dissociation of H_2O to hydroxide over sodium [154] and iron [104], as well as during H_2O adsorption at 250–300 K on Re(001) [139].

Desorption of $O_{2,g}$ as a result of water dissociation has not been reported, to the authors' knowledge.

5.4.4 Formation of bulk metal oxides, surface passivation, and corrosion

It is not surprising that many metals can form bulk compounds as a result of reaction with water. Most commonly, bulk oxides are formed. An interesting point is that the oxidation products are sometimes different than those obtained from reaction with oxygen, as Strasser et al. show in their studies of Ce(001) [220]. Heavy oxidation with $O_{2,g}$ yields CeO_2, whereas oxidation with H_2O_g yields only Ce_2O_3 in which the terminal groups are surface hydroxyl species [220]. Oxidation with water often proceeds less efficiently than does oxidation with O_2, and in some cases oxidation by water forms a passivating layer at the surface which *protects* the bulk against further oxidation. Notable examples of the latter effect include titanium, iron, and aluminum, where the tendency to form a passive layer upon normal atmospheric exposure gives these metals valuable resistance to corrosion [12,13,104,209].

Recent work with samples in ultrahigh vacuum indicates that surface hydroxyl species are important in forming the passive layer. On Al, bulk oxidation is enhanced by an incident beam of 300 eV [226]. Data which support this hypothesis are shown in fig. 53, where the AES feature and ESD yield of the species associated with the oxide increase slowly during electron bombardment [226]. Ding and Williams attribute this development to electron-beam-induced dissociation of OH and concomitant desorption of hydrogen, leaving oxygen to react with the metal [226]. Baer and Thomas also find that an electron beam incident on an iron surface during H_2O exposure enhances the rate of oxidation and breaks down the stable passive surface layer which would otherwise form [227]. Unlike the case of H_2O/Al [226], they do not attribute this to beam damage of a surface *hydroxide*, but rather to the electron beam's effect on a surface *oxide* layer which uniquely results from H_2O exposure [227]. In either case, both studies indicate that electron beams can enhance the rate of metal oxidation by water vapor.

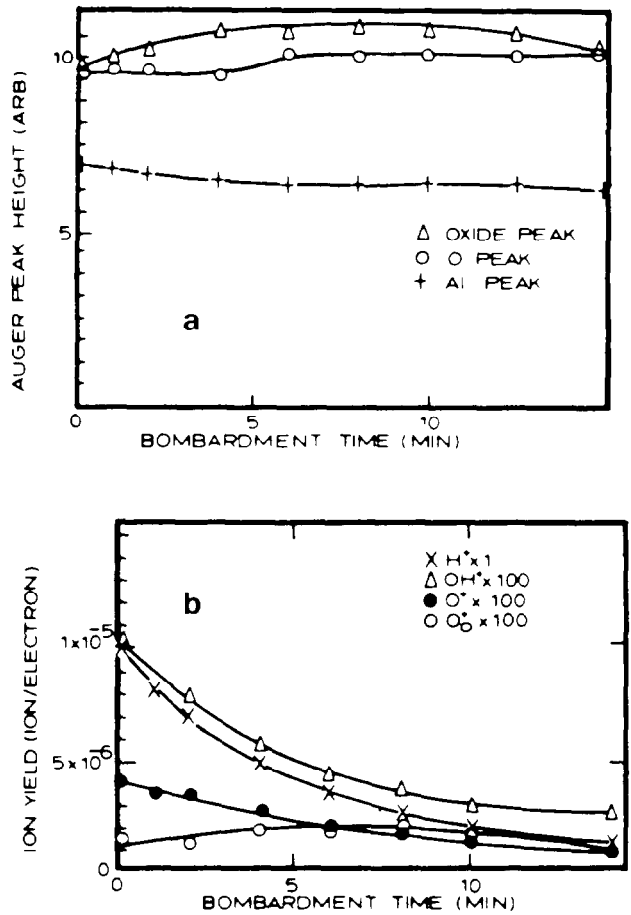

Fig 53 Desorption studies with (a) AES and (b) ESD. The Al(100) surface is exposed to 150 L H_2O at room temperature, then bombarded with 300 eV electrons at current density equal to 150 $\mu A/cm^2$ During bombardment, the evolution of surface composition is followed with both techniques. The ESD data indicate that surface hydroxyls are removed by electron bombardment The Auger data indicate that this is accompanied by enhanced surface oxidation Taken from Ding and Williams [226]

In closing this section, we note that electrochemical effects due to the presence of moisture and other contaminants can be extremely important in the reliability of electronic materials and devices. Moisture in the atmosphere can affect the rate of corrosive oxidation of a material, the composition and structure of its oxidation product, and its electrical properties [228,229]. An extensive discussion of the important subject of corrosion by H_2O is beyond the scope of this review, however.

6. Adsorption of water on chemically modified metal surfaces

6.1. Introduction

It is well known in surface chemistry and catalysis [230] that the presence of adsorbed additive atoms on metal surfaces have a profound influence on surface reactivity. Modification of surface properties by addition of promoters or poisons (either deliberately or via impurity adsorption) can lead to changes in reaction rates, reaction pathways, and product distributions in surface reactions. Moreover, a major area of interest in electrochemistry [231] concerns the influence of additive ions in aqueous solution on the microscopic structure of the double layer at the electrode–solvent interface. In the following pages, we examine the way in which adsorbed impurity atoms (or molecules) on metal surfaces influence the chemistry of adsorbed H_2O. Additive atoms can induce dramatic changes in the geometrical and electronic properties of H_2O_a, and in many cases, cause dissociation to form OH_a.

Before discussing the details of the H_2O–additive interactions on different surfaces, it is appropriate to consider what types of interactions may be expected between the adsorbed polar molecule, H_2O, and various electronegative and electropositive additive atoms. Simply speaking, an additive atom can block specific binding or reaction sites, or it can alter the bonding of H_2O to specific sites due to electronic effects which operate "through the surface", or "through space". Several different models have been developed during the last few years which provide useful physical insights into adatom–molecule interactions. As introduced in section 2.2, Stair [74] and Barteau and Madix [75] have applied the concept of Lewis acids and bases to metal surfaces. In particular, they show how chemical modifiers (additive atoms) can influence the surface acid–base character through an inductive effect. In general, a metal surface is an electron acceptor in bonding H_2O, i.e., the surface acts as a Lewis acid (section 2). Adsorption of a electronegative impurity (e.g., oxygen) increases the acidity of the neighboring substrate atom, while an electropositive impurity (e.g., Na) makes the surface more basic. In either case, the electronic inductive effect introduced by the impurity atoms is expected to modify the heat of adsorption of H_2O; this is in fact observed, as discussed below. Nørskov, Holloway and Lang [232] have shown further that the presence of additive atoms is expected to alter the bonding energies of a polar molecule such as H_2O via a through-space electrostatic interaction.

There are a number of calculations [78,219,233] and measurements [234–236] of the interaction between gaseous or liquid H_2O and positive or negative ions that provide useful concepts relevant to this discussion. In an elegant series of experiments, Castleman and coworkers [234] and Kebarle and coworkers [235,236] measure the heats of formation of various cluster ions, $[M^+(H_2O)_n]$ and $[X^-(H_2O)_n]$, where $n = 1, 2, 3, \ldots$ and $M^+ = Na^+, K^+, \ldots; X^- = Cl^-,$

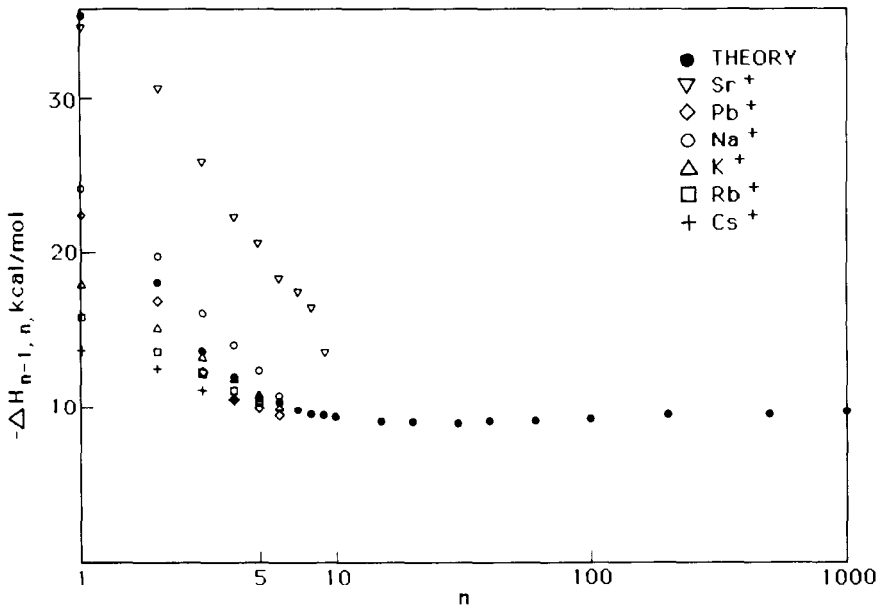

Fig 54 Gas-phase enthalpies of hydration of several positive ions, $M^+(H_2O)_n$, where $n = 1, 2, 3$ The theoretical and experimental values are obtained as described by Castleman [234]

Br^-, F^-, etc. Some representative data are shown in fig. 54. The interaction energies can be described surprisingly well by point-charge/dipole interactions, together with a hydrogen-bonding contribution (in the case of the negative ions). The heat of formation is 100 kJ/mol for $Na^+(H_2O)$ and 96 kJ/mol for $F^-(H_2O)$ [234]; these are stronger than the heats of adsorption of H_2O on many surfaces! Kistenmacher et al. [78] compute the expected molecular structures for a series of such complexes (fig. 55 [78]) and show that, in general, the H_2O molecules are oriented with O atoms closest to positive ions and H atoms closest to electronegative ions. The hydration sphere, which is related to the number of H_2O molecules bonded to a particular ion, varies with ionic size. For $n \approx 4$ in $Na^+(H_2O)_n$, the data show that the binding energy of the next H_2O molecule is close to the heat of sublimation of H_2O [234,235]. In view of the influence of free ions on the structure and bonding of gaseous H_2O, it is not surprising that adsorbed electropositive and electronegative atoms can affect H_2O on surfaces.

In fact, *all* of the above models which relate to the interaction between additives and water lead to the conclusion that modifiers can strongly influence the surface structure and reactivity of adsorbed H_2O. The interaction of the polar H_2O with electronegative and electropositive additives should be quantitatively different, both energetically and structurally, due to electrostatic

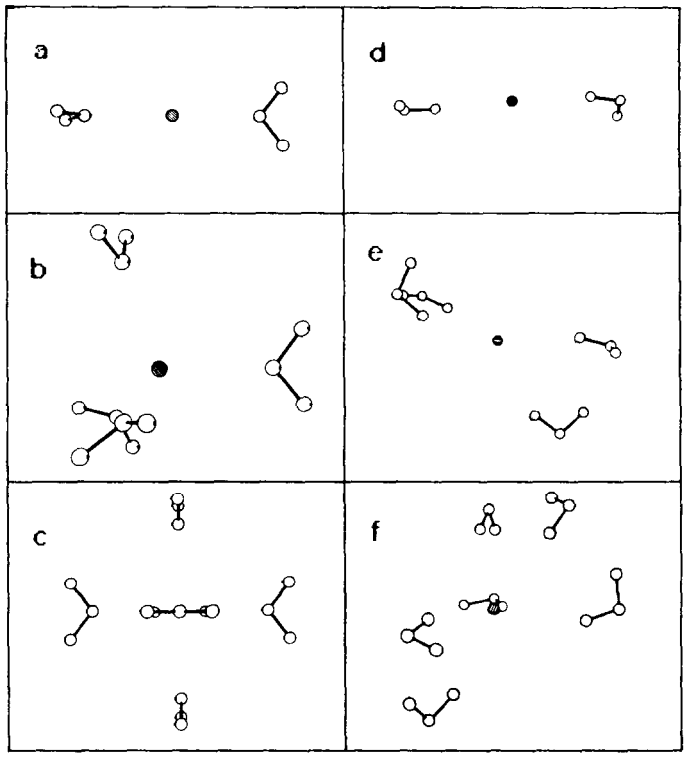

Fig. 55 Left (a–c): Clusters of $Na^+(H_2O)_2$, $Na^+(H_2O)_4$, and $Na^+(H_2O)_6$ The Na^+ ion is darkened. Note that in the $Na^+(H_2O)_6$ cluster the ion is masked by a water molecule Right (d–f)· Clusters of $Cl^-(H_2O)_2$, $Cl^-(H_2O)_4$, and $Cl^-(H_2O)_6$ corresponding to minimal energy structures. The Cl^- ion is darkened. Taken from Kistenmacher et al. [78].

and other electronic effects. Finally the chemistry of adsorbed H_2O (associative versus dissociative adsorption) is, not unexpectedly, influenced markedly by additives.

6.2. Influence of additives on surface chemistry and bonding

In the following discussion, we loosely divide the interaction of H_2O with additive-dosed surfaces into two classes: (a) substrate–additive systems on which H_2O adsorbs and desorbs in molecular form, and (b) substrate–additive systems for which the adsorption of H_2O is dissociative even though adsorption is largely molecular on the *clean* substrate. This division is useful but somewhat artificial, since often both molecular species and dissociation fragments coexist. A further useful division involves electronegative and electropositive additives, for which the chemistry is rather different. An

interesting and somewhat surprising generalization which is drawn from all these studies is that there is *no additive-doped metal surface on which water is reported to adsorb in molecular form at room temperature in ultrahigh vacuum.* A possible exception involving a modified nickel powder is discussed below. Invariably, the desorption of H_2O which is seen at higher temperatures is due to a surface reaction involving H, O, and/or OH which are formed from H_2O adsorbed *at* lower temperature.

6.2.1 Electronegative additives: adsorption without dissociation of H_2O

The most widely-studied electronegative additive in H_2O surface chemistry is adsorbed atomic oxygen. In most cases fractional monolayers of oxygen promote H_2O dissociation; these are discussed in section 6.2.2. There are specific cases where H_2O dissociation does *not* occur in the presence of oxygen. These cases are addressed in the present section, along with data involving other electronegative additives. For the sake of this discussion, we classify H_a and CO_a as electronegative additives as well, since they generally cause the surface work function to increase

Some of the weakest water–additive interactions are reported by Peebles and White [115] for the coadsorption of D_2O with CO_a and D_a on Ni(100). CO precoverages up to ~ 0.3 monolayers cause the D_2O TDS peak temperature to increase from 183 to 206 K, and the authors attribute this to hydrogen bonding between H_2O and CO [115] Higher CO coverages (0.66 monolayers) result in a weakening of the D_2O–substrate interaction, with a decrease of the TDS peak temperature to 173 K. Predosing with > 1.6 monolayers of D_2O blocks CO adsorption. Other authors also report a general sensitivity of water desorption to the presence of CO [60,127]. Tornquist and Griffin [149] report infrared studies with conclusions rather similar to those of Peebles and White [115], except that low coverages of CO are completely displaced from the preferred linear binding site on Pt(111) by coadsorbed water A saturated layer of CO, on the other hand is *not* significantly perturbed by H_2O, which forms clusters on top of the CO layer [149]. For increasing precoverages of atomic D on Ni(100), a monotonic decrease in the D_2O TDS temperature from 186 to 172 K is observed for the range $0.4 < \theta_D \leq 1.0$ monolayers [115]. On Rh(111), a monolayer of atomic hydrogen also reduces the binding energy of adsorbed H_2O, so that only the "multilayer" TDS peak is seen [127]. In contrast, studies of the desorption of water from Pt(111) dosed with hydrogen indicate that the desorption peak temperature is approximately independent of coverage [146]. On polycrystalline Pt, Peng and Dawson [163] report measurable but incomplete isotopic mixing between H_a and a thin layer of D_2O. This concurs with early work reviewed by Bond [237], where isotopic scrambling between gaseous H_2O and D_2 is catalyzed by polycrystalline Pt but cannot be reconciled with a kinetic model involving H_2O dissociation. On Ru(001), however, there is no observable exchange between bilayer H_2O_a and D_a [60]. In all these

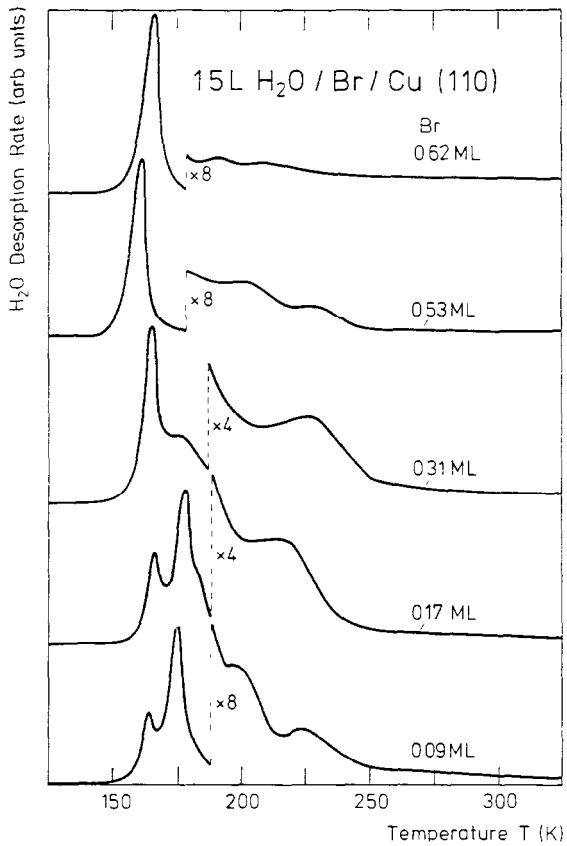

Fig. 56 Thermal desorption spectra of water on bromine-covered Cu(110) The bromine coverages are shown in units of monolayers (ML). The peaks at ~165 K and 175 K are characteristic of H_2O on clean Cu(110), the higher-temperature features are bromine-induced. From Sass et al [231]

studies, it appears that the interaction between H_2O and CO_a or H_a is relatively weak, and that dissociation of H_2O is not enhanced by the coadsorbate; if anything, dissociation of a small fraction of the H_2O layer is actually inhibited on Ni(100) [115].

Interactions stronger than those described above are reported for the coadsorption of H_2O with Br on Cu(110) and Cu(111) [120,231], and Br on Ag(110) [136]. In an electrochemical "double layer simulation" experiment [120], a Cu(110) surface is first dosed with a fractional monolayer of Br, then exposed to H_2O; reversal of the adsorption sequence produces essentially the same results. Fig. 56 [120,231] shows a series of TDS spectra of $\gtrsim 1$ monolayer of H_2O for various Br coverages. The two peaks at ~165 K and ~175

K indicate desorption from the multilayer state and the clean surface, respectively. A certain amount of water desorbs at higher temperatures ($\gtrsim$ 190 K) in the presence of Br, and is interpreted as surface hydration water From the areas under the desorption spectra, the number of H_2O molecules interacting with each adsorbed Br ion is one, up to $\theta_{Br} \simeq 0.3$, after which the H_2O/Br ratio drops. There is no evidence for dissociation of H_2O at any Br coverage, in particular, no OH is formed [120,231]. This is verified using UPS as well as TDS; if OH is present, a desorption peak of H_2O would be expected at ~ 275 K [118].

The spatial distribution of Br and water are deduced from LEED patterns observed for the coadsorption layers. Over a wide range of Br coverage, dosing with H_2O results in a sharp and intense (3×2) LEED pattern. An arrangement of bromine and water in a composite surface layer consistent with the observed (3×2) LEED pattern and the 1 1 coverage ratio determined by TDS is shown in fig. 57 [231]. The LEED data demonstrate clearly that islands having such a possible real space structure grow on the surface so as to maintain the 1 : 1 ratio, and fully cover the surface at a Br coverage of 0.33.

Information about the local orientation of H_2O molecules in the bromine-induced adsorption states may be obtained from work function measurements as a function of H_2O coverage and Br coverage. Fig. 58 [120] shows the perpendicular component of the initial dipole moment per adsorbed water molecule, $\mu_\perp$, as a function of Br coverage on Cu(110) and Cu(111). For low Br coverages, the value of $\mu_\perp$ is initially higher than on the clean surfaces; the authors [120] conclude that the interaction with the Br causes the H_2O molecules to tilt into configurations with the dipole moments more closely perpendicular to the surface. More direct evidence that Br induces preferred orientations in adsorbed H_2O is seen from ESDIAD measurements of H_2O + Br on another fcc(110) surface, Ag(110) [136]. Fig. 59 [136,181] contains H^+ ESDIAD patterns which provide evidence for the orientations induced in H_2O_a by coadsorption with Br.

Since the TDS and LEED behavior for H_2O + Br on Ag(110) are similar to those on Cu(110) [120,136,231] we conclude that the structure and chemistry of H_2O on both of these halogen-doped metal surfaces are similar. In particular, H_2O remains molecular at all Br coverages at $T \approx 90$ K, and the stronger Br–H_2O interaction overpowers the weaker H_2O–H_2O hydrogen bonds to form new ordered two-dimensional structures which have both preferred molecular orientations and long-range (LEED) order; these differ in detail for the two substrates, however. The layers are not stable above ~ 250 K, however, where desorption of H_2O is complete.

In recent years, there have been extensive discussions in the electrochemistry community concerning the use of electrode emersion techniques to characterize the electrochemical interface. These measurements, which have been pioneered by Kolb and his colleagues in Berlin [238], are based on the